REPORT DOCUMENTATION PAGE

Form Approved OMB No. 0704-0188

1. REPORT DATE *(DD-MM-YYYY)*	2. REPORT TYPE	3. DATES COVERED *(From – To)*
05-02-2010	Final Report	12-Jun-07 - 15-Jul-10

4. TITLE AND SUBTITLE

Development of methods and facilities for radio-wave UHF diagnostics of plane-layered dielectric structures

5a. CONTRACT NUMBER
STCU Registration No: P-281

5b. GRANT NUMBER

5c. PROGRAM ELEMENT NUMBER

6. AUTHOR(S)

Dr. Dozyslav Bohdanovych Kuryliak

5d. PROJECT NUMBER

5d. TASK NUMBER

5e. WORK UNIT NUMBER

7. PERFORMING ORGANIZATION NAME(S) AND ADDRESS(ES)

Karpenko Physico-mechanical Institute
5 Naukova St.
Lviv 79601
Ukraine

8. PERFORMING ORGANIZATION REPORT NUMBER

N/A

9. SPONSORING/MONITORING AGENCY NAME(S) AND ADDRESS(ES)

EOARD
Unit 4515 BOX 14
APO AE 09421

10. SPONSOR/MONITOR'S ACRONYM(S)

11. SPONSOR/MONITOR'S REPORT NUMBER(S)
STCU 06-8011

12. DISTRIBUTION/AVAILABILITY STATEMENT

Approved for public release; distribution is unlimited.

13. SUPPLEMENTARY NOTES

14. ABSTRACT

This report results from a contract tasking Karpenko Physico-mechanical Institute as follows: This project will propose a new approach to the creation of the up-to-date technology for non-destructive testing and diagnostics of plane-layered dielectric materials. The approach is based on the following: (1) employment of the electromagnetic UHF sounding for the plane-layered structures; (2) measuring of the complex reflection coefficient by the different frequencies; (3) theoretical estimation of the reflection coefficient by these frequencies; and (4) employment of the methods of inverse problems' solutions for estimation of the unknown parameters of plane-layered structures using the experimental and theoretical results. Based on this approach a non-destructive testing system will be proposed that has the ability to operate as a defectoscopic, defectometric, and diagnostic system, which also does not imply strong restrictions on electro-physical and geometrical parameters of the plane layers.

15. SUBJECT TERMS
EOARD, Materials, Miscellaneous Materials

16. SECURITY CLASSIFICATION OF:			17. LIMITATION OF ABSTRACT	18, NUMBER OF PAGES	19a. NAME OF RESPONSIBLE PERSON
a. REPORT	b. ABSTRACT	c. THIS PAGE			WYNN SANDERS, Maj, USAF
UNCLAS	UNCLAS	UNCLAS	UL	83	19b. TELEPHONE NUMBER *(Include area code)* +44 (0)1895 616 007

Development of methods and facilities for radio-wave UHF diagnostics of plane-layered dielectric structures

Manager of the Project: **Dozyslav Kuryliak,** Ph.D. & D .Sc., IEEE member, head of the department
Tel*:* (0322) 63-32-00, Fax (0322) 63-32-00, E-mail : dkuryliak@ipm.lviv.ua;
kulynych@ipm.lviv.ua
Karpenko Physico-Mechanical Institute of National Academy of the Sciences of Ukraine
Project starting: 01.06.2007; Project ending: 01.06.2009 p.
Financing parties: The United States of America
Project's code acourding to the scientific-technical area: industrial technologies.

COMPLETE REPORT

Summary

The non-destructive control systems with electromagnetic UHF probe of plane-layered structures are mainly used for the estimation of the location of defect. As a rule they work by a given frequency and cannot determine neither the depth of the defect location, nor its proportions. Thus, these are only defectoscopes aimed at locating defects. There also exist systems oriented at the estimation of plane-layered dielectric structures' parameters, but within a very narrow diapason of their change. The existing systems do not ensure the control and diagnostics (defectoscopy and defectometria) of multi-layered constructions in the wide diapason of the change of their geometrical and electro-physical parameters.

In this report we propose a technique, which allows estimating the amplitude and the phase of the complex reflection coefficient for various frequencies. At the beginning stage of the location of defect the device operates by a given frequency, similar to defectoscope. Under such working conditions the zone on the surface of the plain-layered structure, under which the defect is possibly located, is found. Next, the mode of multi-frequency sounding of the given area comes into operation. That is, in the area where the defect is located the device estimates the complex reflection coefficient by various frequencies (these coefficients bear the information about the dielectric structure with a defect.) The information about the value of complex reflection coefficient is saved in the memory of the computer. After that, the mathematical technology comes into operation. It serves for the estimation of the parameters of the defect (the depth of the location of the defect and its thickness). The model of interaction of the electromagnetic wave with the multi-layered structure plays the important role in this approach. Using such model the complex coefficients of reflection by the necessary frequencies are estimated by means of the mathematical procedures. Next, the functional are built, which ,compare experimental and theoretical complex reflection coefficients in such a way that the values of parameters, that ensure reaching of the global minimum of this functional, are equal to the values of the parameters of the defect or of the parameters of the layers in the structure.

Here we give the complete report, which includes the methodology of resumption of parameters of plane-layered dielectric structure basing on the comparison of the theoretical and experimental data. The designing of the radio-wave NDT device for dielectric structures has finished. Frequency range, sensitivity, measurement precision, models of measuring system and interaction of probing field with dielectric flat-layered environment, as well as methods for solution of inverse problems would allow solving a wide range of practical problems of non-destructive testing.

I. DEVELOPMENT OF THE MATHEMATICAL MODEL FOR FIELD CALCULATION IN THE ANTENNA'S APERTURE, WHICH TAKES THE ANTENNA'S GEOMETRY INTO ACCOUNT

1. Introduction

Contemporary high-quality analysis of the field of horn antennae in the radiation zone is based on the usage of the solutions of problems of electromagnetic excitation of semi-infinite perfectly conducting cones. The solutions of the wave diffraction problem by the semi infinite cone are well known (see [1,2]). However, they do not take the diffraction effects on the edges of finite cone into account. These effects lead to the complication of field in the antenna's aperture and losses of energy because of the penetration of the field into the shadow zone. As the near field is important in our case, the consideration of these effects or their minimization is one of the key problems. The aim of the project at this stage is to show the possibility of minimization of edge effects by choosing the horn antenna parameters (radius of aperture, length of the cone's generate, source of excitation). The real field of horn antenna has of a complex character and is formed as a result of the modes' distribution, their transformation and interaction on the edges, caused by the vector character of electromagnetic field. To reach the goal at this stage of the project we considered the simplest case, in particular the formation of axially symmetric field. Thus, to reach the aim we will: firstly, solve the simplest axially symmetric problem of radiation field of the radial electric dipole from the finite conical horn antenna; secondly, we estimate the field of the adequate semi-infinite cone; thirdly, for every scatterer, for various combinations of their geometrical parameters and dipole locations, we find numerical distribution of the fields and their mode structure. The data obtained will be used for the formation of the principles for choosing of the parameters of horn antennae and the method of their excitation.

2. The field calculation technique

Let us consider the perfectly conducting conical horn antenna of finite length as

$$\mathbf{Q}:\{r\in[0,c];\,0\le\theta\le\gamma;\,\varphi\in[0,2\pi]\}, \tag{1}$$

where (r,θ,φ) is the spherical coordinate. The horn antenna (1) is excited by the radial electric dipole, which is located at the conical axis in the point with the coordinates $r=l<c,\ \theta=0$ (see Fig.1). In this case we have an axially symmetric electromagnetic field with nonzero field components E_r, E_θ, H_φ (axially symmetric TM- waves). The time dependence of the electromagnetic field takes as $\exp(-i\omega t)$ and is omitted in this paper.

Using the semi-inversion technique, the problem of the electromagnetic waves radiation from the horn antenna (1) is reduced to the solution of the set of linear algebraic equations of the second kind as in [3,4]

$$X = A^{-1}(A-A_1)X + A^{-1}F\,. \tag{2}$$

Here $X=\{x_n\}_{n=1}^{\infty}$ is the vector of unknown coefficients; A_1, A are the infinite matrices with elements:

$$a_{qn}^{(1)} = \frac{\rho_1 W\left[K_{z_n} I_{\xi_q}\right]_{\rho_1}}{(\xi_q^2 - z_n^2)K_{z_n}(\rho_1)I_{\xi_q}(\rho_1)}\,, \tag{3a}$$

$$a_{qn} = (\xi_q - z_n)^{-1} \tag{3b}$$

with $q,n=\overline{1,\infty}$; $I_\nu(\cdot)$, $K_\nu(\cdot)$ are the modified Bessel and Macdonald

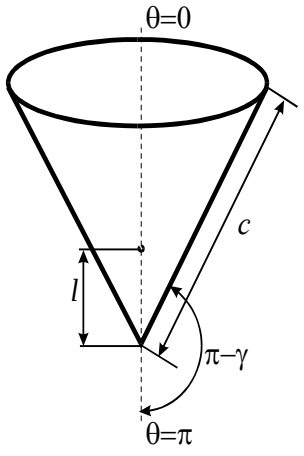

Fig. 1. Geometry of the problem

functions respectively; $\rho_1 = -ikc$, k is the wave number, c is the horn antenna's length; $z_n \in \{z_p\}_{p=1}^{\infty}$, $\xi_q \in \{\xi_p\}_{p=1}^{\infty}$ are the growing sequences of the positive simple zeros and poles of the meromorphic function

$$M(\nu) = \frac{\cos(\pi\nu)}{(\nu^2 - 0.25)P_{\nu-1/2}(\cos\gamma)P_{\nu-1/2}(-\cos\gamma)}, \tag{4}$$

$P_{\nu-1/2}(\cdot)$ is the Legandre function,

$$W[K_\nu I_\mu]_\rho = K_\nu(\rho)I'_\mu(\rho) - K'_\nu(\rho)I_\mu(\rho). \tag{5}$$

The matrix elements τ_{nq} for the inverse operator A^{-1} are defined as follows

$$\tau_{nq} = \left\langle \left\{[M_-(\xi_q)]^{-1}\right\}' \left[M_-(z_n)\right]' (z_n - \xi_q)\right\rangle^{-1}. \tag{6}$$

Here $[M_-(z)]' = d/d\nu\{M_-(\nu)\}_{\nu=z}$; $M_-(\nu)$ is the split function, which we obtain after the procedure of factorization of the function (4). The known vector $F = \{f_k\}_{k=1}^{\infty}$ is given as

$$f_k = -\frac{A_0\pi}{2\sqrt{\rho_0}} \frac{I_{\xi_k}(\rho_0)}{I_{\xi_k}(\rho_1)} \frac{(\xi_k^2 - 0.25)P_{\xi_k-1/2}(-\cos\gamma)}{\cos(\pi\xi_k)}, \tag{7}$$

where $A_0 = 2P_0 Z/l$; P_0 is the moment of the electric dipole, Z is the wave resistance of the medium, $\rho_0 = -ikl$.

Next we express the field radiated from the horn antenna through the solution of the equation (2) as follows

$$U(r,\theta) = \frac{1}{\sqrt{\rho}} \sum_{n=1}^{\infty} x_n \frac{P_{z_n-1/2}(\cos\theta)K_{z_n}(\rho)}{(z_n^2 - 0.25)P_{z_n-1/2}(\cos\gamma)K_{z_n}(\rho_1)}, \; r > c, \; \rho = -ikr. \tag{8}$$

The solution of the similar wave diffraction problem for semi infinite perfectly conducting cone we represents as

$$U(r,\theta) = \frac{A_0\pi}{\sqrt{\rho\rho_0}} \sum_{n=1}^{\infty} \frac{\eta_n P_{\eta_n-1/2}(\cos\theta)P_{\eta_n-1/2}(-\cos\gamma)}{\cos(\pi\eta_n)\frac{\partial}{\partial\eta}\left[P_{\eta-1/2}(\cos\gamma)\right]_{\eta=\eta_n}} \begin{cases} K_{\eta_n}(\rho)I_{\eta_n}(\rho_0) & r \geq l, \\ I_{\eta_n}(\rho)K_{\eta_n}(\rho_0) & r \leq l, \end{cases} \tag{9}$$

where η_n are the positive roots of the transcendental equation $P_{\eta-1/2}(\cos\gamma) = 0$; $0 \leq \theta \leq \gamma$.

The determination of the electromagnetic field components is based on the equations (8), (9) and differential operators as

$$\{E_r, E_\theta, H_\varphi\} = \left\{-\frac{1}{r\sin\theta}\frac{\partial}{\partial\theta}(\sin\theta\frac{\partial U}{\partial\theta}); \frac{1}{r}\frac{\partial^2}{\partial r\partial\theta}(rU); ikZ^{-1}\frac{\partial U}{\partial\theta}\right\}. \tag{10}$$

We have analysed numerically the near horn antenna fields as well as far radiated fields' pattern. The far fields' pattern characteristics were calculated by the formula

$$D(\theta) = \lim_{r\to\infty} |rH_\varphi e^{-ikr}|. \tag{11}$$

Due to axial symmetry of the problem, plots of diagrams are drawn in the angle range $0 \leq \theta \leq \pi$.

We also analysed the total and diffracted fields. The expression for diffracted field potential looks as fol-

lows

$$U^{(d)}(r,\theta) = U(r,\theta) - U^{(i)}(r,\theta), \tag{12}$$

where $U^{(i)}(r,\theta)$ is the incident field potential:

$$U^{(i)}(r,\theta) = \frac{A_0}{\sqrt{\rho\rho_0}} \sum_{n=1}^{\infty} z_n P_{z_n-1/2}(\cos\theta) \begin{cases} K_{z_n}(\rho) I_{z_n}(\rho_0) \\ I_{z_n}(\rho) K_{z_n}(\rho_0) \end{cases} \begin{matrix} r \ge l, \\ r \le l. \end{matrix} \tag{13}$$

The radiation power of horn antenna (dipole radiation resistor) was analysed using the formula

$$R = \frac{W}{W_0} = \frac{3\pi Z^{-2}}{8P_0^2 k^2} \sum_{n=1}^{\infty} \frac{|x_n|^2}{z_n(z_n^2 - 0.25)[P_{z_n-1/2}(\cos\gamma)]^2 \, |K_{z_n}(sc)|^2}, \tag{14}$$

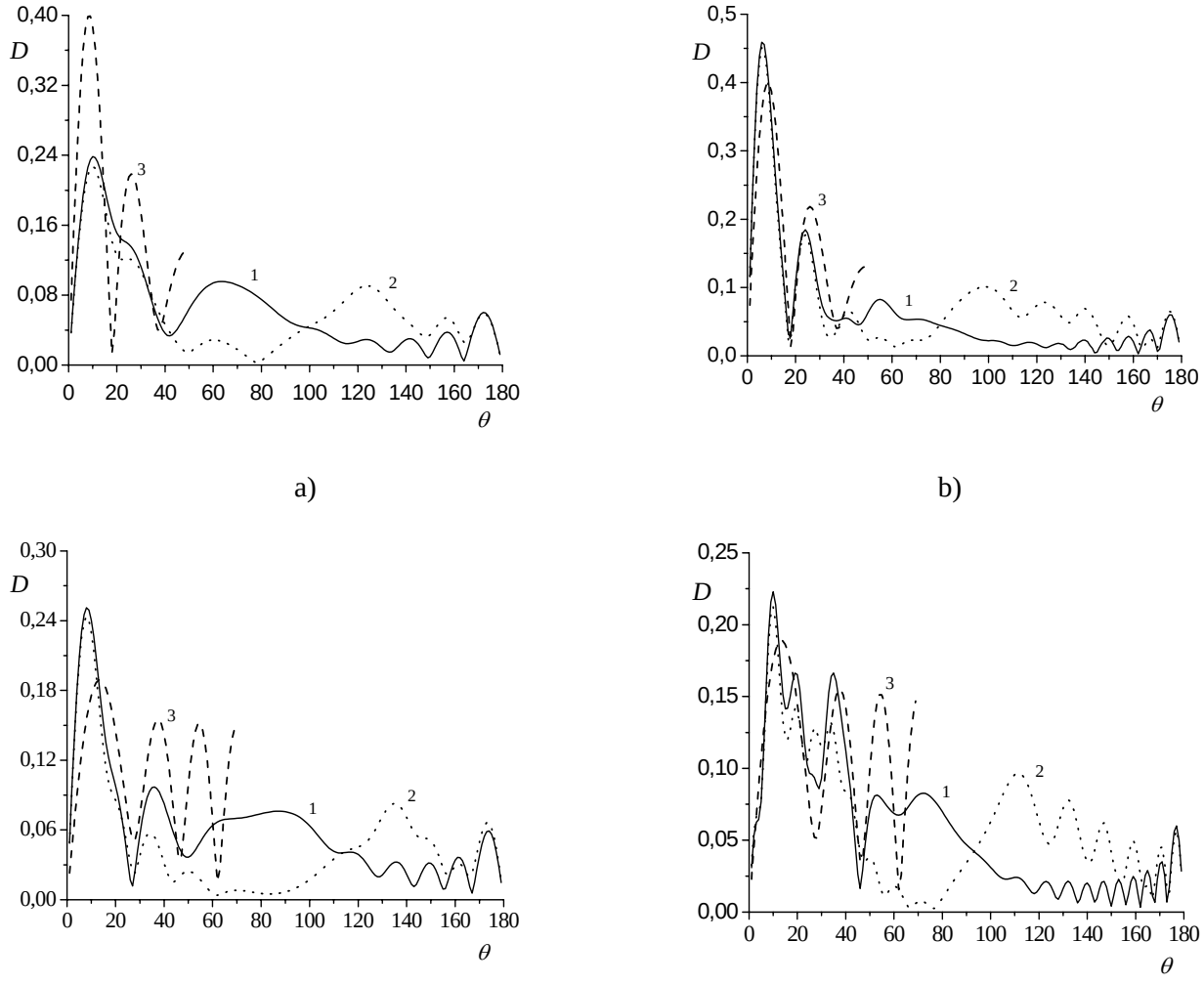

Fig. 2. Far field pattern for conical horn antenna at $kl = 12.5$: 1 – total field, 2 – diffracted field, 3 – field in the case of semi infinite cone (a) $\gamma = 50^\circ$, $kc = 18$; b) $\gamma = 50^\circ$, $kc = 30$; c) $\gamma = 70^\circ$, $kc = 18$; d) $\gamma = 70^\circ$, $kc = 35$).

where W , $W_0 = (4/3)\pi P_0^2 k^2 Z$ are powers, radiated by dipole in the presence of conical horn antenna and without it, respectively.

3. The results of the numerical analysis

3.1 Radiated field pattern

Plots in Fig. 2 illustrate converging forms of far field distribution in the radiation zone of finite and semi-infinite cones in lighted angular sector with the rise in the generatrix length of the finite cone. For calculations we assumed that $P_0 k = 1/(4\pi)$ [A], $Z = 1$ [Ohm]. Forms of these fields, as shown by studies, are defined by the number of modes, excited in semi-infinite cone. For example, the field distribution of semi-infinite cone, that correspond to curves 3 of Fig. 2a, b, is mainly contributed by three modes (second – fourth). The second peak is formed because of the third mode and a final correlation between amplitudes of the first and the second peaks is established owing to the fourth mode. In conical horn of finite length, which far field pattern corresponds to curve 1 in Fig. 2a, the third and fourth modes of semi-infinite cone are not formed completely yet. They appear with the rise in the length of finite conical horn. The second peak is formed only at $kc_1 > 28$ and further rise in horn length just weakly influences the shape of far field patterns in lighted sector. The rise in cones' aperture gives the increase of number of modes, excited in semi-infinite cone. So, the formation of the same field distribution by finite cone it is necessary to increase its length. This is confirmed by plots on Fig. 2c, d. Therefore, the use of fields, scattered by semi-infinite cones for analysis of far field patterns for finite horn antennae in the radiation sector is possible, when horn parameters and excitation conditions provide the excitation of modes that form field distribution for corresponding semi-infinite cones. This property, in its turn, allows regulate field mode composition of radiation from finite conical horn antennae with using the changes in its length. Let us try, with the help of finite conical horn antenna, to form the radiation distribution for the field with suppressed higher modes. In this respect we will study the change of shape for far field patterns from conical horn antenna with the decrease of its length, aperture angle and dipole position remaining fixed. The obtained results are shown in Fig. 3. As can be seen from plots in this Figure, the decrease in the cone length leads to approximation of shapes of the main lobes on far field pattern of finite conical horn antenna and the second mode of the semi-infinite cone. However, they still have substantial difference in amplitude, because of proximity of radiation source to the aperture.

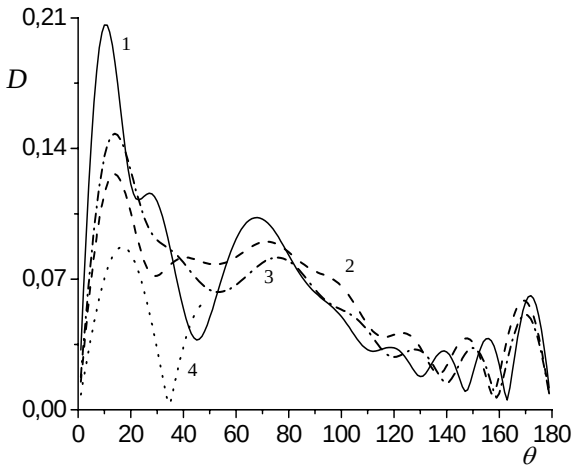

Fig. 3. Influence of horn generatrix length on directional diagrams at $\gamma_1 = 50^\circ$, $kl = 12{,}5$: 1 – $kc_1 = 17$; 2 – $kc_1 = 15$; 3 – $kc_1 = 13$; 4 – field distribution for second mode of semi-infinite cone.

3.2. Near field of conical horn antenna

For many technical problems the radiation characteristics of horn antennas are found basing on Huygens method. The application of this approach to finite conical horns is grounded on the assumption that the field in horn apertures can be approximated by the field of semi-infinite cone. Applicability of

such approximation was studied in the case of distribution of magnetic component of total field on spherical surfaces with a radius close to the length of the horn. The field calculations results, obtained from the solution of wave diffraction problems by finite and semi-infinite cones were analysed. Their comparison showed that upon approximation of source to the vertex the total field in aperture of finite horn antenna (i.e. on spherical segment embracing cone basis) became closer to the similar spherical segment of semi-infinite cone (safe in the region close to the edge). This is confirmed, for example, by plots in Fig. 4a, where even for substantially wide horn we see only small field oscillations in the aperture as related to the curve, corresponding to field distribution in semi-infinite cone. These oscillations are stipulated by wave diffraction on cone edge, and their amplitude increases with approximation to aperture boundary. The shift of the source toward the basis of horn leads to substantial difference in behavior of these fields, which is clearly seen in Fig.4b.

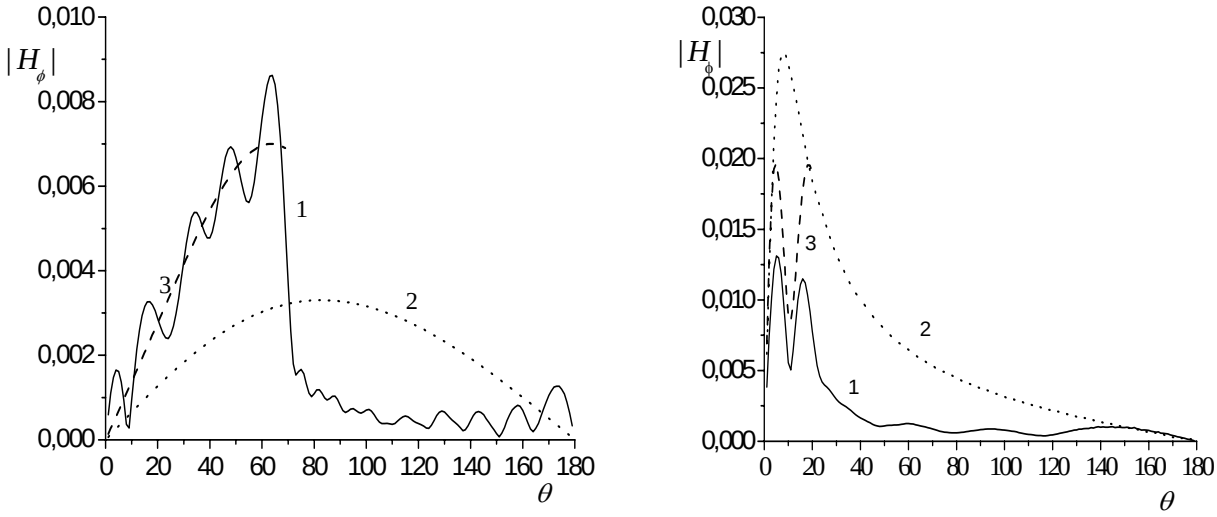

a) b)

Fig. 4. Distribution of H_φ – field components in vicinity of conical horn on a sphere of radius kr : 1 – whole field, 2 – primary field, 3 – field in semi-infinite come (a) $kc_1 = 24$; $kl = 1{,}5$; $\gamma_1 = 70^\circ$; $kr = 24{,}2$; b) $kc_1 = 12$; $kl = 10{,}5$; $\gamma_1 = 20^\circ$; $kr = 12{,}2$.

3.3. Field penetration into shadow region

Using the horn antennae as measuring elements it is important to study the effects, stipulated by field penetration into the shadow region. In order to study them we analyzed the dependence of far field patterns as a function of geometrical parameters of the finite cone and position of the source under the fixed values of angular parameter θ . Fig. 5a shows the character of oscillation and decay of field in the direction $\theta = \pi / 2$ under the increase of the horn length for different cone aperture angles, caused by wave diffraction on the edge of aperture. It is obvious that the screening effect should be increased with the decrease of angle near the vertex, which is confirmed by curves on Fig. 5a. Screening properties of conical horn antenna in other directions θ are illustrated on Fig. 5b, where dependences of the field in certain directions on the position of radiation source on the axis are shown. As can be seen from this Fig-

ure, the field level and span of oscillations extinguish with transfer of observation point into the shadow

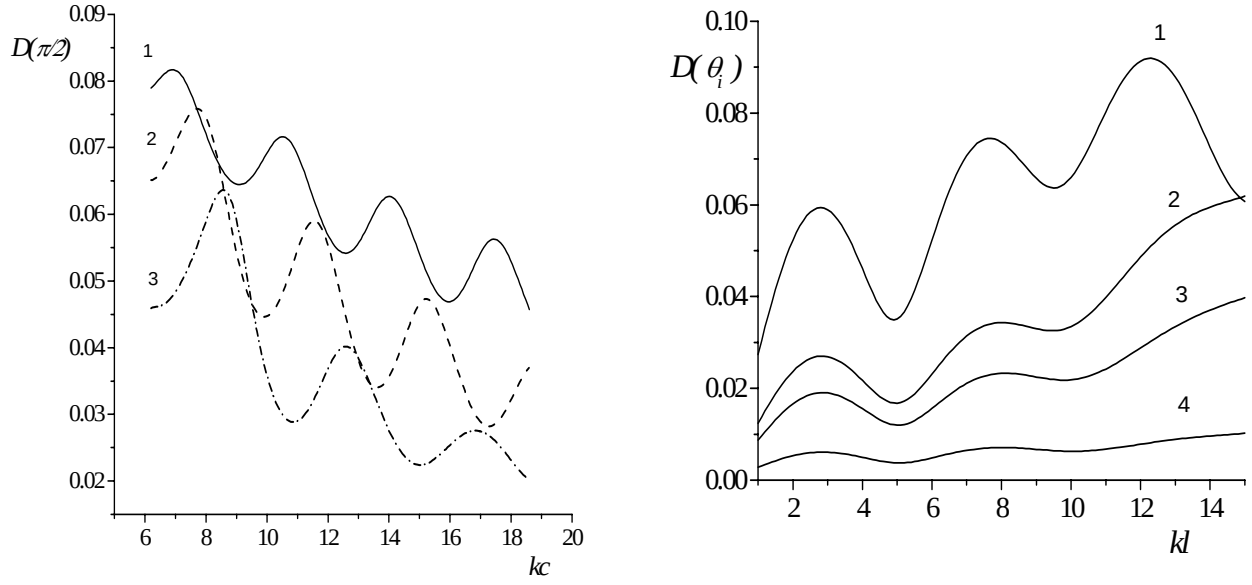

a) b)

Fig. 5. Dependence of $D(\theta)$ at fixed angle values $\theta = \theta_i$ on geometric parameters of cone and source positions; a) $\theta = \pi/2$, (1– $\gamma_1 = 70^\circ$; 2– $\gamma_1 = 59^\circ$; 3– $\gamma_1 = 50^\circ$); b) $kc_1 = 18$, $\gamma_1 = 50^\circ$ (1– $\theta_i = 70^\circ$; 2– $\theta_i = 90^\circ$; 3– $\theta_i = 110^\circ$; 4– $\theta_i = 150^\circ$).

region.

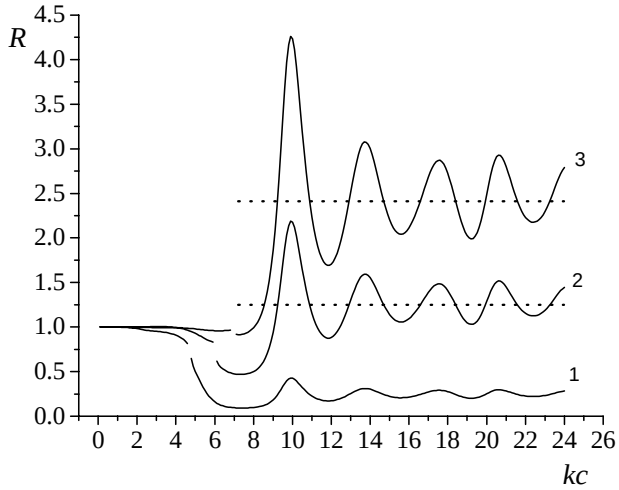

Fig. 6. Dipole radiation resistance in conical horn at $\gamma_1 = 20^\circ$; 1 - $kl = 4{,}7$; 2 - $kl = 6$; 3 - $kl = 7$.

3.4. Dipole radiation resister in conical horn antenna

Important characteristic of antennae, which gives an idea about their efficiency, is normalized radiation resistance. Its dependence on wave length of horn at different dipole positions on the axis is given on Fig.6. Curves on this figure were calculated using formula (14). As can be seen from this Figure, the level of oscillations decreases with parting of radiated source from aperture into the depth of the cone. The dashed lines on Fig. 6 correspond to normalized radiation resistance of radial electric dipole with $kl = 6$ and $kl = 7$ on the axis of semi-infinite cone with aperture angle $\gamma_1 = 20^\circ$. Therefore, oscillations of normalized radiation resistance on the axis of finite conical horn proceed in relation to the value of normalized radiation resistance of dipole on the axis of semi-infinite cone with the same aperture angle and extinguish with the rise in the length of the horn. This, in particular, explains the possibility of approximation of the field patterns of semi-infinite and finite horn antennae with the rise of the length of the latter.

Fig.6 shows that the resistance of radiation R has its distinct maximum at $kc = 9{,}96$ and tends to one if $kl > kc$ (this corresponds to the outlet of the radiation source outside of horn antenna). In Fig.7 we see the far field patterns of finite conical horns. The wave length of their generatrix takes a value that ensures maximal radiation resistance, and also two closest minimums of radiation resistance of dipole in cone at $kl = 7$, $\gamma = 20^\circ$ (see curve 3, Fig 6). As seen from Fig. 7, the curve 1 corresponds to maximal normalized radiation resistance and envelops the far field pattern of cones, that form minimal reflection resistance.

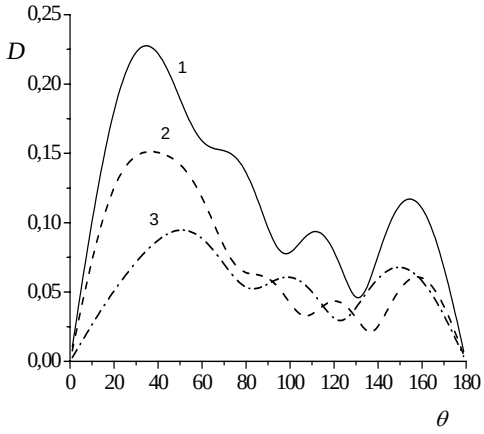

Fig. 7. Far field patterns of finite conical horn antenna at $kl = 7$, $\gamma = 20^\circ$: 1 – $kc = 9.96$; 2 – $kc = 11.8$; 3 – $kc = 8$.

4. Conclusions

1. The possibility of approximation of the reflection field of the finite conical horn in illuminated area by the field of semi-finite perfectly conducting cone, is shown using the example of axially symmetric excitation. The conditions on geometrical parameters of horn and the position of the effective radiation source, under which the improvement of the approximation may be reached, are formulated.

2. The physical principles of the formation of field in the horn antenna are formulated. It is shown that the best approximation is reached when dominant modes of the semi-infinite cone are formed in finite conical horn.

3. The losses of the field on radiation into the shadow area and the energetic characteristics of radiation of finite conical horn are evaluated.

These results will be taken as a basis for modeling of the behavior of the field in the diagnostic system under elaboration.

5. References

1. A.Z. Fradin “Antennae for high frequency waves”. Moscow. Sov. Radio, 1957, 647p.
2. Yu. P. Kelohlu, Yu. H. Kozulin, S.T. Maclovich Journal of technical Physics, 1978, **48**, №5, p. 894-904.

3. D.B. Kuryliak, Z.T. Nazarchuk "Analytical – Numerical Methods in the Theory of Wave Diffraction on the Conical and Wedge-Shape Surfaces. Kyiv, Naukova Dumka, 2006, 275p.
4. D.B. Kuryliak Izvestiya Vuzov. Radioelectronica. 1992, **35**, №3, p. 3-9.

II. ESTIMATION OF THE FIELD MODES AND FINDING THE INFLUENCE ON THE ANTENNA'S EDGE AND DIELECTRIC INFLUENCE FOR THE FIELD IN THE ANTENNA'S APERTURE

1. Introduction

The wide use of dielectric and composite materials and products requires creation of the methods for their non-destructive testing (NDT) and diagnostics, particularly for determination of electrophysical and geometric parameters. Classic methods of radio-wave NDT allow performing defectoscopy (flaw detection) and determining one-two parameters of materials in the narrow range of changes in these parameters. However, modern dielectric materials and products have a complex geometry and intrinsic structure. This complicates mathematic models and requires solving inverse problems of diagnostics, which, in its turn, puts forward new requirements for measuring systems and testing devices. One of the most informative parameters in radio-wave non-destructive testing is a complex reflection coefficient (CRC), since with the help of the given frequency dependence of the CRC of electromagnetic wave, which falls on the layered dielectric, the electrophysical parameters and thicknesses of its layers can be determined.

During the remote probing for the description of the interaction between electromagnetic field and the dielectric medium the model of the plane wave is widely used. This model allows building simple solutions of direct problems of probing, which, in its turn, strongly simplifies the solution of the inverse problem. However, the wave can be considered as a plane one only at substantial distance from the source (far-field region). In addition at large distances, the signal reflected from the tested object is weak. In order to solve the problem of measuring of CRC of layered dielectric structure and to determine their electrophysical parameters and thicknesses of layers, the measuring scheme on the basis of a doubled T-bridge and its mathematical model based on scattering matrices of independent modes have been used. The work is aimed at experimental determination of parameters for the model of the bench and study of their influence on measurements results.

During reporting period the following problems have been solved:

1. The method and software for automated calibration of the bench by frequency and extinction have been developed. The experiments on measuring of the length of electromagnetic wave in waveguide and calibration plots of the B-1182 wave-meter have been built, which allowed controlling the frequency with the error not exceeding 20 MHz in the 53…78 GHz range. The extinction of the standard Д3-38 attenuator in the 0…30 dB range has been measured and the calibration characteristics by extinction for all the frequency range has been built. The error in extinction measurements does not exceed 2%.

2. The algorithms and programs for pre-processing of measurements data have been developed. The spectrum of the digitalized U_x and U_y signals of panoramic extinction gauge has been analyzed. The algorithm for filtering and elimination of accidental and industrial interferences has been elaborated. The optimum step of frequency sampling has been chosen, the decimation (resampling down) algorithm of frequency sampling has been developed, which allowed, without decreasing the self-descriptiveness of measurements, shorten the volume of calculations on the stage of determination of extinction and CRC.

3. The experiments on the CRC determination for standard loadings have been carried out. The methodical and instrumental errors appearing on each stage of measurements have been analysed. On the basis of analysis of measurements' results a new mathematic model of interferometer has been proposed. This model deeper describes the properties of the bridge scheme, which allowed decreasing methodical errors of CRC measurement. The proposed method allows determining the module of the CRC with an error of 2% and a phase with an accuracy of 2° in 5-mm range of electromagnetic (e.m.) waves.

4. The calibration methods for the gauge system and for measuring CRC accounting the radiating-receiving aerial have been reviewed. The experiments on measuring of CRCs for "horn antenna – plane-layered medium" loading in the 62…65 GHz range for estimation of horn antennas parameters, have been performed. Such measurements were conducted for free space, metal plate screens and dielectric plates at

different distances from antenna aperture.

5. The algorithm for determination of scattering matrix of the radiating-receiving aerial on the basis of the measured CRCs of standard loadings, situated in free space is elaborated. The e.m. wave in plane-layered medium is modelled as a plane wave with normal incidence on the interface.

6. The full-scale and numerical experiments have been performed, scheme models for the aerial in "near-field" and "far-field" regions have been obtained. The measured CRCs of standard loadings have been compared with the theoretic ones. The dependence of modelling errors on the distance from the sample to the aperture of the aerial has been analyzed.

2. Structure and operation principles of the measuring bench.

Creation of new methods and means of radio-wave testing of multilayer dielectric materials with the use of inverse problems requires conducting precise experiments for verification of theoretical models of electromagnetic waves diffraction on the tested structures [2,3]. This needs the automated high accuracy measurement of CRC of electromagnetic field at multiple frequencies. From this point of view the bridge methods of the CRC measurement have a number of advantages: relative simplicity of realisation of measuring scheme, calibration simplicity, wide frequency range, high measurements' accuracy, which depends only from the accuracy of calibrated loading [5,6].

The laboratory automated bench for multifrequency measurements of scalar (voltage standing wave ratio (VSWR), extinction) and complex parameters (modulus and phase of reflection coefficient) has been created at the PhMI. This part of the work is aimed at refinement of the method of measurements data processing, minimization of errors in determination of CRC from the plane-layered structure (PLS).

The appearance of the automated test bench for radio waves diagnostics is shown in Fig. 1.

a)

b)

Fig. 1. Automated bench of radio-wave diagnostics, general view (a), SHF tract with an aerial and a sample (b)

The bench has been built on the basis of commercial panoramic gauge of voltage standing wave ratio (VSWR) and attenuation P2-69, which main blocks are sweep-frequency generator (2) (see Fig. 2), indicator unit (1) and SHF tract. Generator unit produces SHF oscillations of 53,57...78,33 GHz frequencies. The measurement of VSWR and extinction foresees separate measurement of power of incident wave and a wave, which reflected or passed though the structure. Measurement of SHF oscillations power in the tract is performed with the help of two directed bifurcators with detector sections (6,7). The detected signal of incident U_{inc} and reflected U_{ref} waves arrives at indicator unit Я2Р-67 (1), which forms the signal X, proportional to the frequency of the e.m. wave and $Y \sim U_{ref}/U_{inc}$. The indication and processing of information is performed by a computer (4), joined though the interface unit (IU) (3) with X and Y outputs of the indicator unit.

For the measurement of CRC the double T-bridge (8) is included into waveguide tract by the "passing" scheme. One of shoulders of the bridge is joined to the unknown loading (sample under testing) (10), and the other – to calibrated loading (5). The output signal of the bridge – "disbalance signal" D – is a mixture of a signal, reflected from the unknown loading and a reference wave, reflected from the cali-

brated loading. The calibrated loading is cascade of polarization attenuator and phase changer. The parameters of the model of the bridge scheme are determined with the use of standard loading – direct reading phase changer (movable short-circuitor with a 0.01 mm scale step).

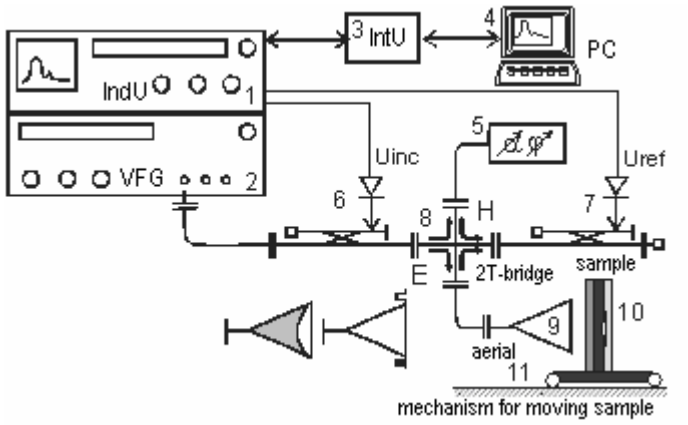

Fig. 2. Automated bench for multifrequency probing, flow chart:
1 – indicator unit; 2 – sweep-frequency generator; 3 – interface unit;
4 – computer; 5 – calibrated loading with module (α) and phase (φ) control; 6, 7 – directed detector sections; 8 – double T-bridge; 9 – horn-lens aerial; 10 – sample; 11 – mechanism for moving the sample.

3. Calibration of the bench by frequency and extinction

For frequency measurement of generated oscillation the waveguide tract contains the B-1182 wave-meter. This device has the extinction coefficient of about 0.1 dB in all frequency range, and absorbs the energy of electromagnetic field in the band <10 MHz. On the frequency dependence of the transmission coefficient (TC) wave-meter there is a “mark”, which position depends on the wave-meter’s scale (Fig. 3). The scale allows controlling frequency with the ~20 MHz accuracy. The software of the bench allows binding the measured signal X to the readings of the wave-meter scale and to frequency.

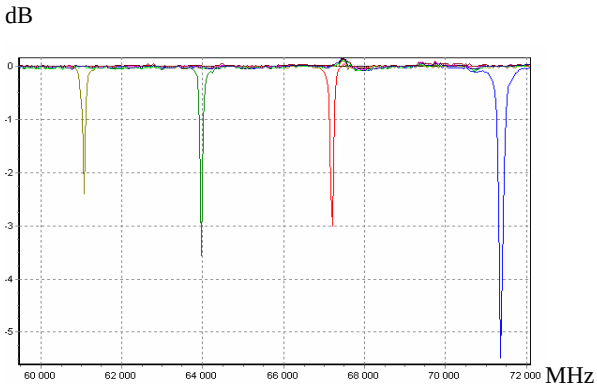

Fig. 3. Frequency dependences of the B11-82 wave-meter, s = 3.50; 3.00; 2.50; 2.00

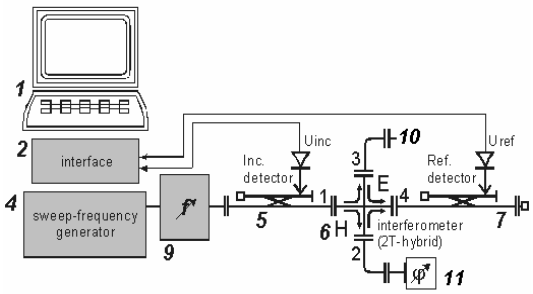

Fig. 4. Scheme of wave-meter calibration: 9 – wave-meter; 10 – short-circuitor; 11 – direct reading phase changer

In order to build the wave-meter calibration plot f [GHz] = f(s [mm]) we have used the bridge scheme (Fig. 4). One of shoulders of the bridge was joined to short-circuitor, and the other – to direct reading phase changer (movable short-circuitor). By changing position of movable short-circuitor and balanc-

ing the scheme the wavelength in waveguide was measured at fixed frequencies. The relative error of frequency determination in the middle of frequency range is ~0,07% ($\Delta\lambda$ = 0,005 mm at the wavelength in the waveguide of λ_a = 3,676 mm). The calibration plot of the wave-meter obtained by this way is shown in Fig. 5.

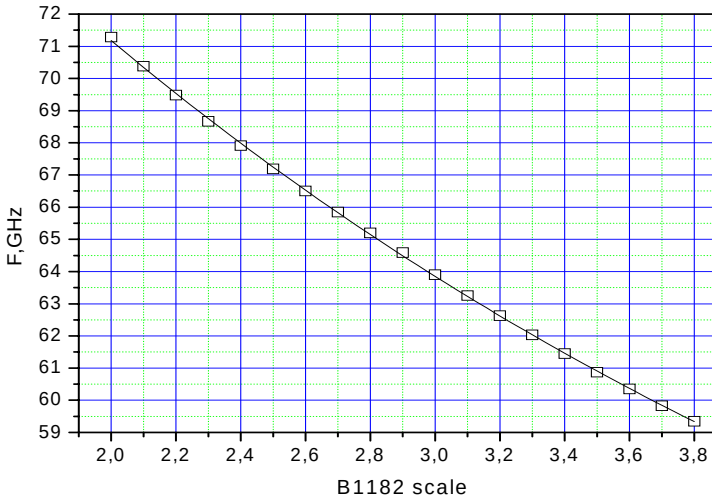

Fig. 5. Calibration plot of the B1182 wave-meter.

Measurement of the extinction $Y \sim U_{ref}/U_{inc}$ is performed in seven dynamic wavebands of the indicator unit (see. Fig. 2) with the 5 dB step. For wideband signals the logarithmic measurement regime is foreseen. The software of the bench allows automatic pre-processing of realizations Y(X), conversion into logarithmic presentation $A = 10\times\lg(Y/Y_0)$, where $Y_0(X)$ is a beforehand measured realization, corresponding to the extinction level of 0 dB.

The measuring tract was studied experimentally with the use of the Д3-38 polarization attenuator as an extinction standard. The measuring scheme is shown in Fig. 6. Fig. 7 illustrates the relative error of the measured TC, as well as the error of standard Д3-38 attenuator (according to device certificate, dashed line). On the basis of these data one can determine the relative error and the linear range of extinction measurement. The extinction calibration plot A[dB]=A[Y] has been built (Fig. 8).

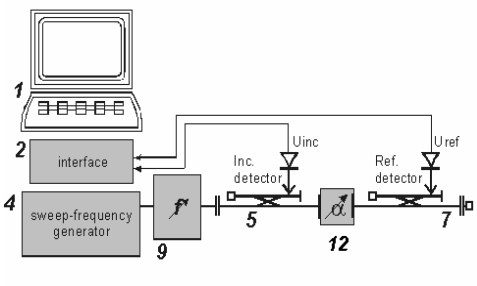

Fig. 6. Scheme of passing junction of attenuator: 12 – polarization attenuator

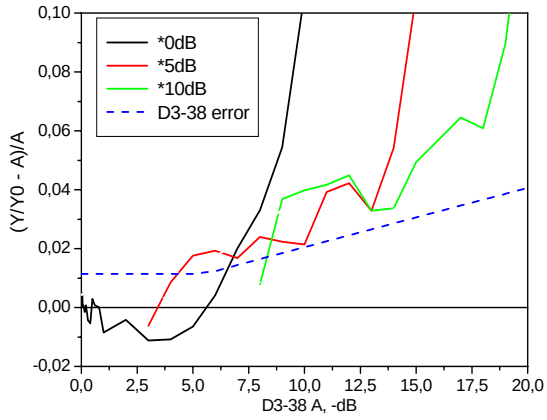

Fig. 7. Relative error of measured extinction coefficient.

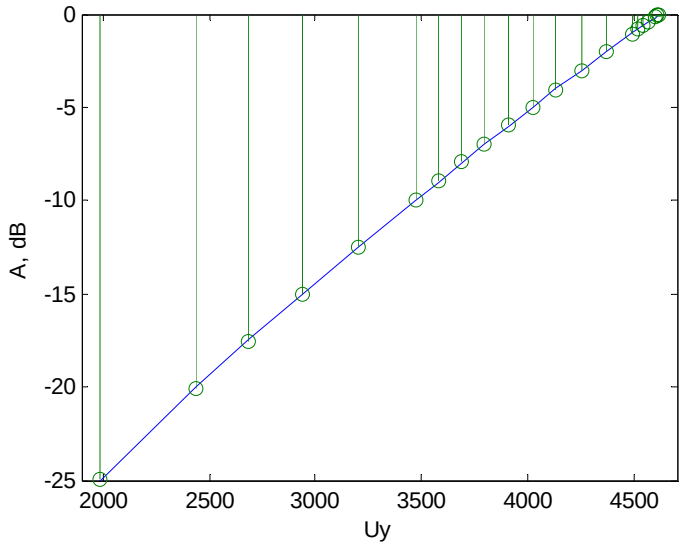

Fig. 8. Calibration plot by extinction.

The software of the bench allows us to process the measurements' results and present them in convenient form. The measurement and calculation data are stored in the PC memory and are accessible for visual observation as frequency and phase dependences. Fig. 9a illustrates the measured dependence of bridge disbalancing signal (in dB) as a function of the frequency (MHz). Fig. 9b shows the dependence of disbalancing signal on the phase of the reference signal at the same frequency.

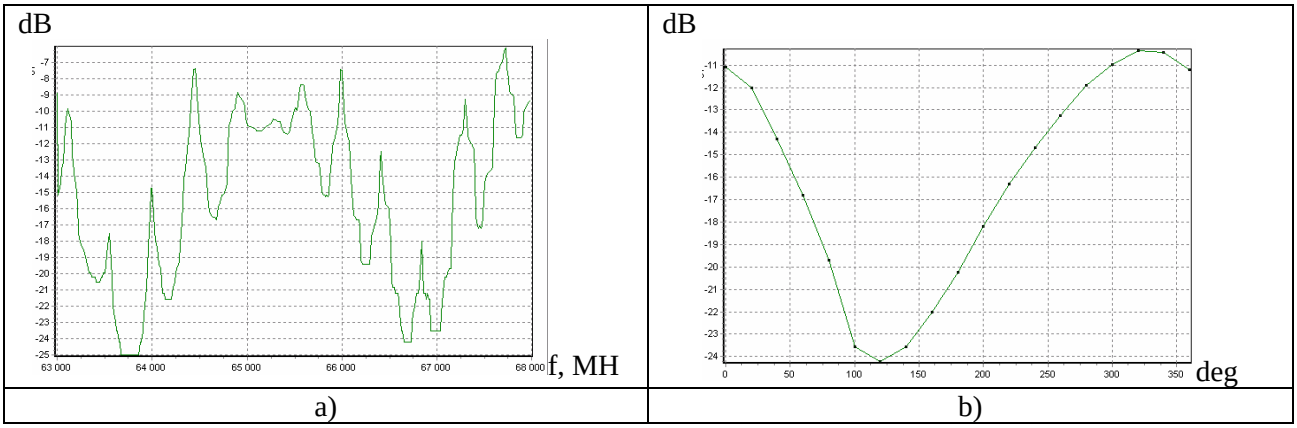

a) b)

Fig. 9. Frequency and phase dependences of the disbalancing signal of the bridge scheme.

4. Model of gauge on the basis of double T-bridge

Traditional approach to the measurements of the CRC by bridge method is in the balancing of bridge scheme – comparison of the unknown CRC and calibrated loading in shoulders of the bridge (see Fig. 2). The value of reflection coefficient (module α and phase φ) can be found directly from readings of the calibrated loading.

For the SHF range devices the precision calibrated loadings (polarization attenuators and phase changers) are mechanical devices, that is why the balancing of bridge scheme at each frequency is labour-consuming, and under full automation the use of precise electromechanical gears is needed.

The method for measuring of CRC with minimum (finite) number of manipulations with calibrated loading, aimed at automation and computer processing of measurements results is proposed.

This was salved by building a mathematic model of the device, joining the measured complex reflection coefficient V and calibrated loading $V_c(\alpha,\varphi)$ with disbalance signal of the bridge $D=U_{ref}/U_{inc}$:

$$D=D(V,V_c(\alpha,\varphi),\mathbf{S}). \quad (1)$$

Here **S** = **S**(f) is a complex scattering matrix of the double T-junction, dependent on frequency. The double T-junction is considered as a multiport. Shoulders 1 and 4 (see Fig. 10) are loaded on the coordinated units – detector of incident U_{inc} and reflected U_{ref} wave, respectively. Shoulder 3 is loaded on the unknown complex loading V(f), shoulder 2 – on calibrated controllable loading $V_c(\alpha,\varphi)$ (Fig. 10).

The T-joint is filled by dielectric (air), it is the reciprocal device, that is why the matrix **S**(f) is symmetric. Accounting also the symmetry of shoulder of the T-joint one can show that in this scheme the complex amplitudes of signals in shoulders 1 and 4 are bound by the relation:

$$\frac{A_4}{A_1} = S_{41} + S_{21}S_{42}\frac{V - V_c}{(1 - S_{33}\cdot V)\cdot(1 - S_{33}\cdot V_c) - S_{23}^2\cdot V\cdot V_c}. \quad (2)$$

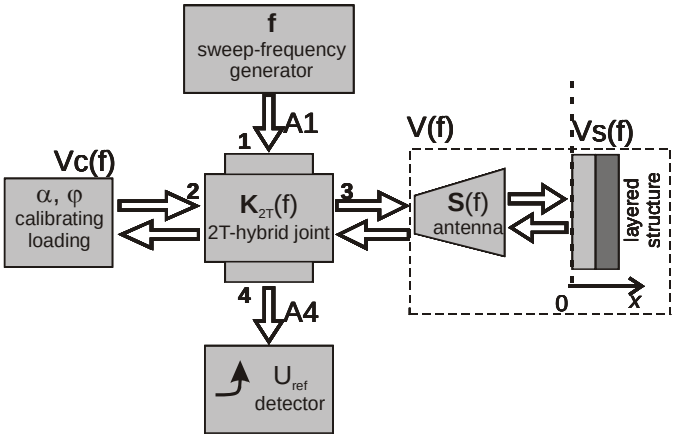

Fig. 10. Schematic model of the bench:
f – sweep-frequency generator;
U_{ref} – detector if the signal from the reflected wave;
V_c – CRC of calibrated loading;
$\mathbf{K}_{2T}$ – scattering matrix of double T-bridge;
V(f) – CRC of the loading under measurement;
S(f) – antenna;
$V_s(f)$ – CRC of plane-layered environment in a free space

The detected tensions of the incident and reflected waves are proportional to the signal power in the SHF tract $U \sim P \sim |A|^2$. Then the normalized signal of bridge disbalance can be written as:

$$D\left(\dot{V},\dot{V}_c(\alpha,\varphi),\dot{k}_0,\dot{k}_1,\dot{k}_2,\dot{k}_3\right) = \frac{U_{ref}}{U_{inc}} = \left|\dot{k}_0 + \dot{k}_1\cdot\frac{V - V_c}{(1-\dot{k}_3\cdot V)\cdot(1-\dot{k}_3\cdot V_c) - \dot{k}_2\cdot V\cdot V_c}\right|^2, \quad (3)$$

where $k_0(f)$,.. $k_3(f)$ are complex coefficients, dependent on the geometry of the 2T-bridge and the frequency. They describe properties of interferometer and can be determined on the basis of the full-scale experiment.

5. Experiment and numerical modelling

Calibration of measurement scheme consists in determination of bridge scheme parameters $k_0(f)$,.. $k_3(f)$ for all frequencies of measurement range. The dependence of D signal on the phase of calibrated loading φ for all frequencies of the range and the set of standard loadings (see Fig. 11) is conducted.

Coefficients of mathematic model of the bridge are determined by the following target function:

$$F_1\left(\dot{k}_0,..,\dot{k}_3\right) = \sum_{i=1}^{N_\varphi}\left(D_i - D\left(\dot{V}_{et},\dot{V}_c(\alpha_i,\varphi_i),\dot{k}_0,...,\dot{k}_3\right)\right)^2 \quad (4)$$

where D_i are measured values of disbalacing signal of the set of calibrated loadings $V_c(\alpha,\varphi)$ and the known standard loading V_{et}; N_φ ιs the number of fixed positions of the phase of calibrated loading. Optimal coef-

ficients values for the model are determined by the minimum of target function:

$$(\dot{k}_0,...,\dot{k}_3)^* = \inf_{|k_0|<1} F_1\left(\dot{k}_0,...,\dot{k}_3\right) . \quad (5)$$

The direct search was used as an optimization method.

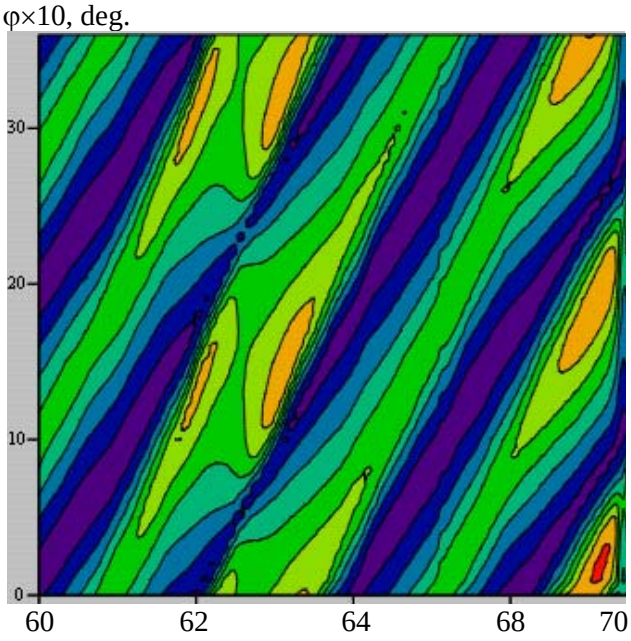

Fig. 11. Measured phase-frequency dependence of the disbalancing signal D of standard loading.

Fig. 12 shows experimental and modelled by formula (3) phase dependences of D for five standard loadings on the same frequency, for determination of $k_0(f)$,.. $k_3(f)$ three standard loadings having been used. As can be seen from the figure, this model accurately describes other phase dependences not used in the identification of model parameters.

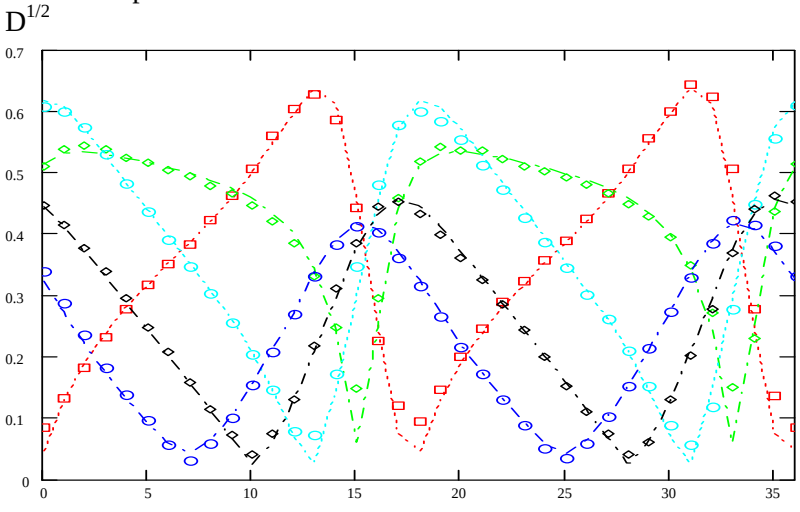

Fig. 12. Phase dependences D: ■ – experiment; ------ – numerical modelling $D\left(V_{et}, V_c(\alpha,\varphi), \dot{k}_0,...,\dot{k}_3\right)$.

Value of phase of standard loading depends on the choice of the reference plane – zero position of phase changer of the calibrated loading φ_0. The position of the standard short-circuitor at s_{sh} = 0 mm was chosen as a zero reference plane. Distance between two neighbouring positions of the standard short-

circuitor was Δs_{sh} = 0,5 mm. Phase of the CRC of standard loading φ_{sh} was determined through the wavelength in the waveguide λ_a by the formula

$$\varphi_{sh} = 2\pi \frac{2s_{sh}}{\lambda_a}, \text{ [rad].} \tag{6}$$

The CRC of the unknown loading is determined on the basis of measured $D_i(f)$ at different values of φ_i for the frequence spectrum; the sought CRC V*(f) is determined for each frequency by the minimum of the target function F_2:

$$F_2(\dot{V}) = \sum_{i=1}^{N_\varphi} \left(D_i - D(\dot{V}, \dot{V}_c(\alpha, \varphi_i), \dot{k}_0, ..., \dot{k}_3)\right)^2, \quad \dot{V}^* = \inf_{|V|<1} F_2(\dot{V}). \tag{7}$$

Fig. 13 shows frequency dependences of bridge scheme parameters $k_0(f)$,.. $k_3(f)$.

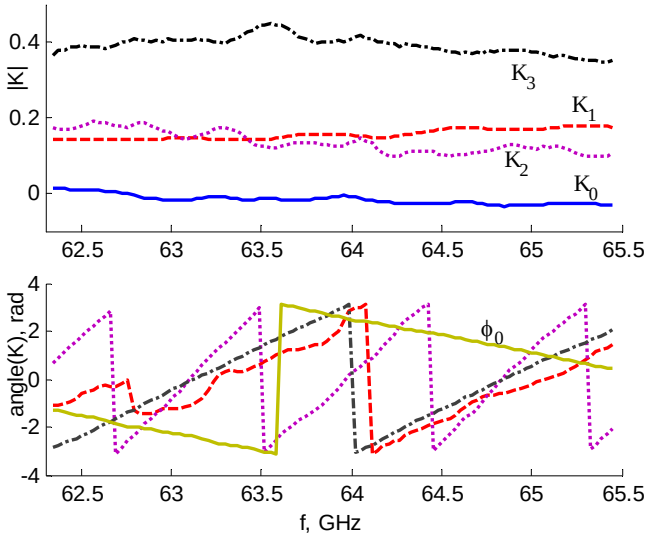

Fig. 13. Frequency dependence of complex parameters of the model of double T-bridge k_0..$k_3(f)$ and phase of zero plane

In order to verify this method the CRCs of the standard loadings (short-circuitor) have been measured. The average deviation of the module and phase along the range do not exceed 0.02 relative unit (r.u.) and 0.04 rad. The average deviation and dispersion of the optimal CRC V* from the standard value by module and phase in the 63...68 GHz range are presented in Table 1

.

Table 1.

Parameter	Value
$\lvert\dot{V}_{et}\rvert - \lvert\dot{V}^*\rvert$, relative unite (r.u.)	0.02
$\arg(\dot{V}_{et}) - \arg(\dot{V}^*)$, rad.	0.04
$\sigma(\lvert\dot{V}^*\rvert)$, r.u.	0.001
$\sigma(\arg\dot{V}^*)$, rad.	0.003

6. Model of antenna: experiment and numerical modelling

Let consider the antenna as a passing linear device (four-pole) with losses (Fig. 10). Let assume that in the free space there is a plane electromagnetic wave which falls perpendicularly onto infinite (M–1)-layered structure on the semi-infinite medium with flat interfaces, which CRC depends on the layer thickness and electrophysical parameters of materials [3,4]

$$V_s=V_s(f,h_1,..,h_{M-1},\varepsilon_1,..,\varepsilon_M,tg\delta_1,...,tg\delta_M). \quad (8)$$

Connection between the measured CRC V(f) and the CRC of the plane-layered medium $V_s(f)$ can be expressed as [5]

$$V = S_1 + \frac{S_2 V_S}{1 - S_3 V_S}, \text{ or } V_S = \frac{S_1 - V}{S_1 S_3 - S_2 - S_3 V}, \quad (9)$$

where $S_1,..,S_3$ are complex coefficients, determined by the elements of the scattering matrix of the antenna and can be determined experimentally.

In order to determine the antenna's parameters as the standard loading in the free space $V_{set}(f, x)$ the flat metal screen has been used, its position was changed from the zero plate x=0 to 20 mm with the Δx=0.2 mm step. Geometric parameters of the used antenna: distance from the aperture to the zero plane is 85 mm, antenna's aperture was 10×10 mm, length of the antenna from the mouth to aperture was 50 mm.

Fig. 14 shows the measured CRC of the "antenna – metal screen" structure for different positions of the screen $V_{et}(f, x)$.

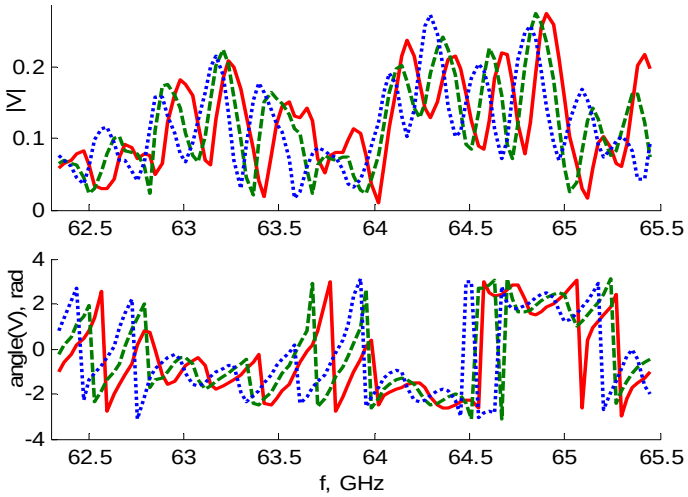

Fig. 14. Measured CRC of the antenna–metal screen system $V_{et}(f)$: ___, _ _ _ , ... movement of the screen by Δx=0.4 mm (different colours correspond to different positions of the screen)

Complex coefficients $S_1(f),..,S_3(f)$ for each frequency are determined with the use of experimentally measured values $V_{et}(f, x)$ and theoretic value of the CRC of the standard $V_{set\ th}(f, x)$.

$$(S_1, S_2, S_3)^* = \inf_{|S_i|<1} F_3(S_1, S_2, S_3);$$

$$F_3(S_1, S_2, S_3) = \sum_{i=0}^{Nx} \left| V_{et}(x_i) - V(S_1, S_2, S_3, V_{set\ th}(x_i)) \right|^2, \quad (10)$$

where $x_i=i\Delta x$. For metal screen it is assumed that

$$|V_{set\ th}| = 1, \ \arg(V_{set\ th}) = 2 \cdot 2\pi x/\lambda_0 + \pi, \quad (11)$$

where x is the position of the screen compared to the zero plane, λ_0 length of the electromagnetic wave in vacuum.

Fig. 15 and 16 show frequency dependences for coefficients of the antenna model $S_1(f),..,S_3(f)$ and CRC of the standard loading recalculated to the free space according to the aerial model $V_s(f)$ (9).

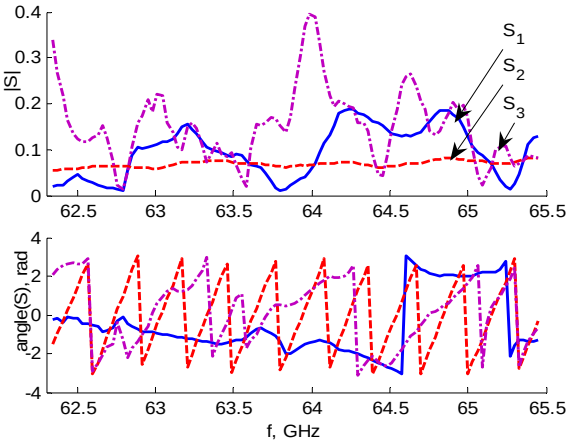

Fig. 15. Frequency dependence of parameters of the horn antenna model $S_{1..3}(f)$

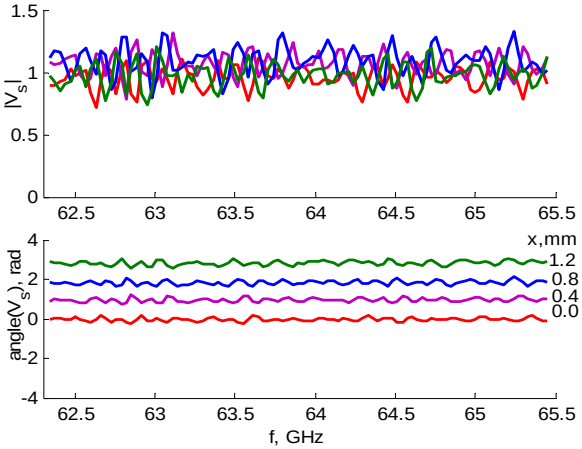

Fig. 16. Measured CRC of the metal screen recalculated for free space $V_{set}(f)$, screen movement by x=0.4 mm

Fig. 17 shows the measured and calculated by the model of the plane wave [4] CRC of the fluoroplastic plate with the following dimensions: h=8.0 mm; ε=2.07; tgδ=0.4×10^{-3}. As can be seen from Fig. 16 and 17, there exists the correlation between theoretical coefficient of reflection from the plane-layered structure and the calculated CRC accounting the influence of the antenna, the error being about 0.05 r.u. The measurement error can be stipulated by the error in modelling of measuring system, inadequacy of the plane wave approximation. The CRC in the free space can be affected by spurious reflections from the surrounding bodies. As can be seen from the character of the frequency dependence $V_s(t)$, the reliable interpretation of measurements' data according to the plane wave model, one should consider the maximum possible number of frequency points.

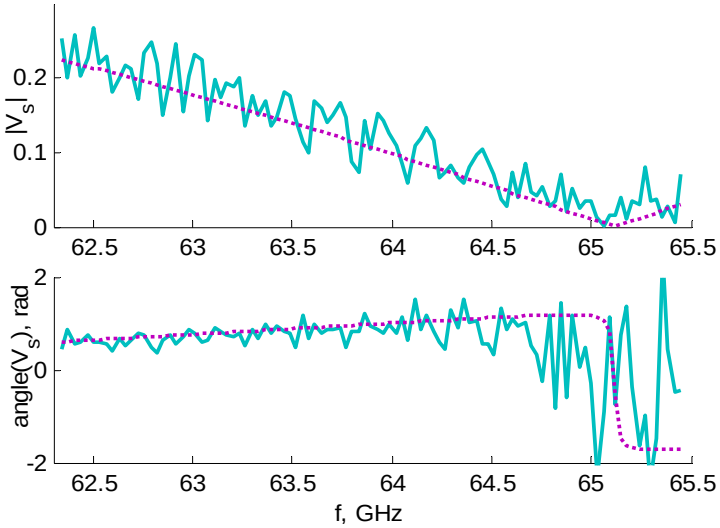

Fig. 17. CRC of fluoroplastic plate:
___ experiment; .... the CRC calculated for the plane e.m. wave

The dependence of the model error on the distance from the aperture of the horn antenna to the zero plane d has been studied, the results being presented in Fig. 18.

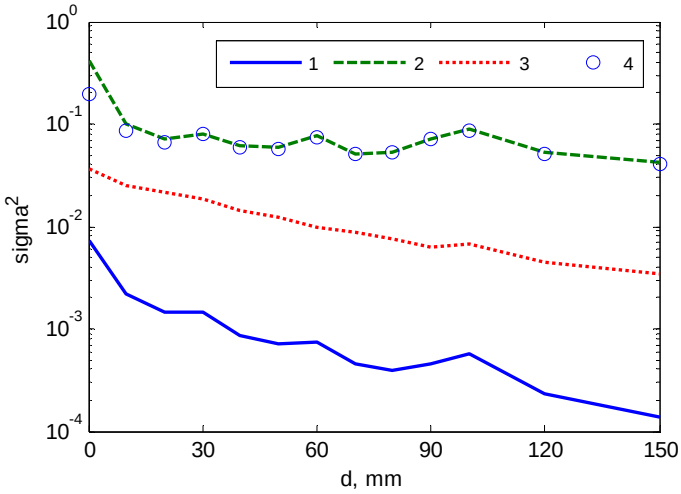

Fig. 18. Dependence of modelling errors (in r.u.) on the distance from the antenna's aperture to the plane of the sample d:

1 – $\sigma^2(V, V_{th})$ of the measured CRC of the "antenna–sample" system, $V_{th}=V(S_1(f),..,S_3(f),V_{sth})$;

2 – $\sigma^2(V_s, V_{sth})$ for the sample (Al) in free space V_s;

3 – $\sigma^2(V, V_b)$ power of the measured signal from the sample (Al), V_b – from the antenna in the free space;

4 – $\sigma^2(V, V_{th})/\sigma^2(V, V_b)$ deviation of the measured CRC V(f), normalized to the power of the measured signal.

It can be seen from the figure that:

1) with the rise of the distance the modelling error for the measured CRC V(f) (see plot 1) $\sigma^2(V, V_{th})$ decreases.

2) modelling error of the CRC of the structure in the free space with the rise in distance sharply decreases to d=20 mm, and then remains almost unchanged;

3) useful signal from the structure (plot 3) decreases with the distance;

4) modelling error of the measured CRC, normalized on the signal (plot 4) is very close to the plot 2, which, in the physical sense, is also normalised by energy CRC in a free space V_s, equal here to 1.

7. Conclusions.

Automated bench for radio-wave diagnostics allows measurements in the 56…78 GHz range, the accuracy of frequency determination is ±0.02 GHz, extinction coefficient is in the range of 0…30 dB with ±1% accuracy, complex reflection coefficient with the accuracy of 0.01 relative unite.

The error of measuring of CRC with the use of the plane wave model for the two simplest plane-layered structures (flat metal screen, dielectric plate, see Fig. 16, 17, 18) has been determined. This error was shown to be of $\approx 20\%$ in amplitude. In the case of sufficient frequency sampling the error of modelling, as can be seen from Fig. 16, 17, can be considered as an interference and for simple structure it should influence the diagnostics results only weakly.

In order to increase the accuracy of measurement of frequency dependence of CRC the use of more realistic models for the interaction of electromagnetic field with layered environment is needed, in particular they should take into account the change of the power of the reflected field and the influence of the finite dimensions of aperture.

These results will be taken as a basis for modeling of the behavior of the field in the diagnostic system under elaboration.

8. References

1. Nondestructive testing and diagnostics / V. V. Klyujev, F. R. Sosnin,… Mashinostrojenie, Moscow, 1995, 488 p.
2. Kolodiy B.I., Ljashchuk O.B. Direct and Inverse Problems of Electromagnetic Waves Reflection from the Anisotropic Dielectrics // Proc. VI International Conference on Mathematical Methods in Electromagnetic Theory (MMET'96) - Lviv. 1996. - P.453-456.
3. Kolodiy B. I., Ljashchuk O. B. Methematical models, methods, and algorithms used for the radio-wave diagnostics of multilayer dielectrics // Material Science, Vol. 33. No.5, 1999. – P. 639-649.
4. J.Wait, "Electromagnetic waves in stratified media", Pergamon Press, Oxford – etc., pp.608, 1970.
5. Kukush V. D. "Electro and radio measurements", Radio i sviaz, Moscow, 1985.
6. Volman V. I., Pimenov Yu. B. "Technical electrodynamics", Sviaz, Moscow, 1971.

III. ADAPTATION OF THE THEORY OF INVERSE PROBLEM SOLUTION TO ESTABLISH THE PARAMETERS OF THE MULTI-LAYERED STRUCTURE TAKING THE ANTENNA'S GEOMETRY INTO ACCOUNT

1. Introduction

The reliability enhancement in diagnostics of plane-layered dielectric materials with the help of UHF waveband electromagnetic field requires the enhancement of the experimental measurement data on the basis of solution of corresponding inverse problems. However, the elaboration of efficient mathematical methods for solution of inverse problems faces with the principle difficulties stipulated by their nonlinearity and incorrectness. One of the ways to solve inverse problems of probing of layered materials is to determine parameters of layered structure, for which the objective function for some fixed set of frequencies reaches the global minimum. However, despite of evident simplicity of such an approach, its efficiency substantially depends on the choice of the model, initial approximation, efficient minimization algorithm, preprocessing of measurements data. In addition, the objective function is multiextremal, and experimental data always have errors, which requires modification of existing algorithms of development of new ones, which would provide reliable estimation of structure parameters in solution of particular practical problems.

2. Direct problem of probing of flat-layered dielectric materials

2.1 Choice of physical model

The influence of interference on measurements results lead to errors in estimation of parameters of plane-layered structure. Let consider here interferences as a generalized influence of all possible factors on determination of the sought-for parameters. These could be both incorrectness in the theoretical model and measurement errors. At this stage of studies we remain within the model of the plane wave accounting that the deviation of real field of antenna from the field of plane wave can be accounted by introduction of some level of interference into the algorithm for solution of inverse problem. Such an assumption is acceptable at least for simple structures, which has been experimentally demonstrated in the previous report.

2.2 Initial correlations for calculation of reflection factor

Let us consider a layered structure S, which contains $n-1$ uniform isotropic dielectric layers with flat boundaries (Fig. 1), each of which is characterized by a thickness h_m, dielectric permeability ε_m and the tangent of wave reflection angle δ_m, ($m=1...,n-1$). Here we consider that magnetic permeability is equal of that of vacuum μ_0. Let assume that $E-$ a polarized plane wave with the $e^{-j\omega t}$ time dependence falls at the angle θ on the upper limit $z=0$ of the structure S. We should find an expression for reflection coefficients on the upper limit of the structure. For this purpose let find expressions for vectors of electromagnetic field in each of layers.

From the geometry of the problem it follows that the magnetic field has a single component $H_y^m = H_y^m(x,z)$ in each layer, which is normal to the plain of the figure, and the electric field has two components, related to the H_y^m by the following correlation:

$$E_x^m = \frac{1}{j\omega\dot{\varepsilon}_m}\frac{\partial H_y^m}{\partial z},\ E_z^m = -\frac{1}{j\omega\dot{\varepsilon}_m}\frac{\partial H_y^m}{\partial x},$$

where $\dot{\varepsilon}_m = \varepsilon_m(1+j\delta_m)$. The last equality appear from Maxwell equations.

Than we obtain that

$$\Delta H_y^m + k_m^2 H_y^m = 0,$$

where $k_m^2 = \omega^2 \dot{\varepsilon}_m \mu_0$, $\operatorname{Im} k_m > 0$.

In addition to the equality, the component of magnetic field satisfy the following boundary conditions on interfaces of uniform media

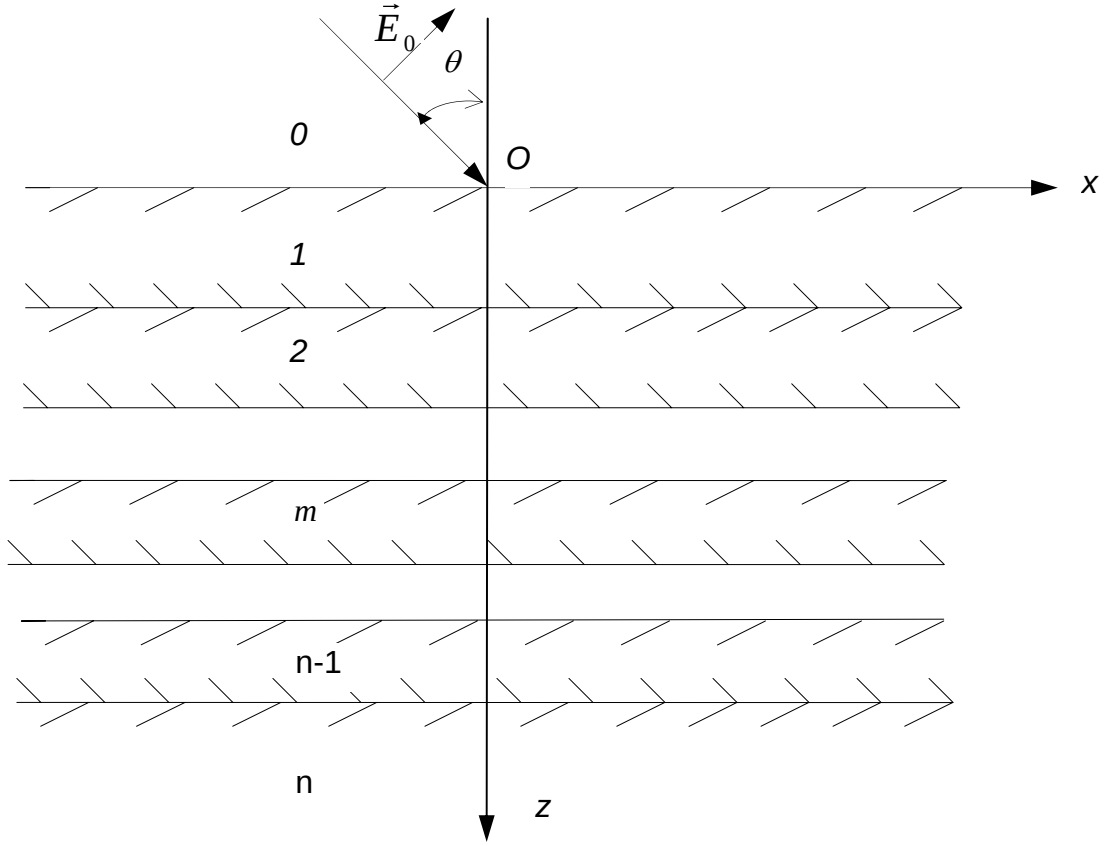

Figure 1 – Dielectric multylayer structure

$$\begin{cases} \left(H_y^0 + H_y^{inc}\right)\Big|_{z=0} = H_y^1\Big|_{z=0}, ..., H_y^m\Big|_{z=z_m} = H_y^{m+1}\Big|_{z=z_m}, ..., H_y^{n-1}\Big|_{z=z_{n-1}} = H_y^n\Big|_{z=z_{n-1}}; \\ \dfrac{1}{\dot{\varepsilon}_0}\dfrac{\partial\left(H_y^0 + H_y^{inc}\right)}{\partial z}\Big|_{z=0} = \dfrac{1}{\dot{\varepsilon}_1}\dfrac{\partial H_y^1}{\partial z}\Big|, ..., \dfrac{1}{\dot{\varepsilon}_m}\dfrac{\partial H_y^m}{\partial z}\Big|_{z=z_m} = \dfrac{1}{\dot{\varepsilon}_{m+1}}\dfrac{\partial H_y^{m+1}}{\partial z}\Big|_{z=z_m}, ..., \\ \dfrac{1}{\dot{\varepsilon}_{n-1}}\dfrac{\partial H_y^{n-1}}{\partial z}\Big|_{z=z_{n-1}} = \dfrac{1}{\dot{\varepsilon}_n}\dfrac{\partial H_y^n}{\partial z}\Big|_{z=z_{n-1}}. \end{cases}$$

and conditions of radiation on infinity [1]. Here $H_y^{inc} = H_0 e^{jk_0(z\cos\theta + x\sin\theta)}$ is an incident field, $z_m = \sum_{i=1}^{m} h_i$.

From these we obtain the following recurrence relation for finding complex reflection coefficient for r_0 on the surface of the structure S:

$$r_{m-1} = \frac{\beta_m + e^{\alpha_m} r_m}{1 + \beta_m e^{\alpha_m} r_m}, \qquad (1)$$

where $\beta_m = (1 - p_m)/(1 + p_m)$, $p_m = u_m \dot{\varepsilon}_{m-1} / u_{m-1} \dot{\varepsilon}_m$, $\alpha_m = -2u_m h_m$, $r_{n-1} = \beta_{n-1}$, $u_m^2 = \lambda^2 - k_m^2$, $\operatorname{Re} u_m > 0$, $m = 1, ..., n-1$.

Factors r_m – can be interpreted as reflection factors on the lower boundary of each layer. Only the r_0 factor is accessible for measurement.

As we can see from (1), the reflection factor r_0 is unambiguously defined by some combinations of physical and geometrical parameters $\varepsilon_m, \delta_m, h_m$. If the changes of these parameters the values of p_m and α_m remain constant, then the characteristics of the field r_0 is not changes as well. Thus, at certain value the r_0 corresponds to a certain set of real layered structures S. Let refer them as equivalent structures and parameters p_m and α_m – effective parameters.

Let us note that the choice of effective parameters is ambiguous. It is evident that the problem of uniqueness in determination of parameters of layered structure by the r_0 reflection factor can be considered only in relation to effective parameters. As a rule, at some additional information on a part of physical parameters we can reckon on unambiguous determination of the other part by effective parameters.

Let consider in details the case of normal incidence of electromagnetic wave, i.e. $\theta = 0$. Under these conditions we have $u_m = -jk_m$ and $p_m = k_m \dot{\varepsilon}_{m-1} / k_{m-1} \dot{\varepsilon}_m$, $\alpha_m = 2jk_m h_m$.

The values

$$\delta_m,\ \theta_m = \sqrt{\frac{\varepsilon_{m-1}}{\varepsilon_m}}\ ,\ \nu_m = \sqrt{\varepsilon_m \mu_m} h_m .$$

can be considered as effective parameters. Then $\alpha_m = 2j\omega\nu_m\sqrt{1+j\delta_m}$, $p_m = \theta_m \sqrt{\frac{1+j\delta_{m-1}}{1+j\delta_m}}$. These effective parameters are generalizations of parameters used in [2].

There is possible another way for introduction of effective parameters, which we shall use during further explanations:

$$\bar{\lambda}_m = 2h_m\sqrt{\varepsilon_m\mu_0}\ \mathrm{Re}\left(\sqrt{1+j\delta_m}\right),\ \bar{\gamma}_m = 2h_m\sqrt{\varepsilon_m\mu_0}\ \mathrm{Im}\left(\sqrt{1+j\delta_m}\right),\ \tau_m = \frac{h_m}{h_{m-1}}, \qquad (2)$$

where h_0 is some arbitrary length. It can be assumed equal to 1. We have $\alpha_m = \omega\left(j\bar{\lambda}_m - \bar{\gamma}_m\right)$ and $p_m = \tau_m \frac{j\bar{\lambda}_{m-1} - \bar{\gamma}_{m-1}}{j\bar{\lambda}_m - \bar{\gamma}_m}$. Let us note that $\bar{\lambda}_m$ and $\bar{\gamma}_m$ are dimensional parameters: $[\lambda_m]$, $[\gamma_m]$ = sec. Therefore for correct mathematical problem definition let introduce dimensionless in the following way

$$\lambda_m = \omega_0 \bar{\lambda}_m,\ \gamma_m = \omega_0 \bar{\gamma}_m, \qquad (3)$$

where ω_0 is some fixed circular frequency. Then

$$p_m = \tau_m \frac{j\lambda_{m-1} - \gamma_{m-1}}{j\lambda_m - \gamma_m}\ \alpha_m = \tilde{\omega}\left(j\lambda_m - \gamma_m\right), \qquad (4)$$

where $\tilde{\omega} = \omega / \omega_0$. For simplicity sake further we shall omit "~".

In other words, each set of equivalent structures, which is unambiguously described by a vector

$$p = \{\lambda_0, ..., \lambda_{n-1}, \gamma_0, ..., \gamma_{n-1}, \tau_1, ..., \tau_{n-1}\}$$

and a certain value of ω correspond to a concrete value of $r_0(\omega)$. In a compact form this can be written as an operator equation $A(\omega)[p] = r_0(\omega)$. For simplicity sake further we shall write this operator equation as

$$Ap = r_0 .$$

Operator A is called the operator of a direct problem. Let note that this operator is nonlinear and continuous. Its continuity is stipulated by fact that small variations in structure parameters correspond to small variation in parameters of electromagnetic field and, correspondingly, of reflection factor.

3. Inverse problem of probing of layered structures and methods of its solution

The problem of determination of effective parameters p of layered structures on the basis of

measured frequency dependence of reflection factor r_0 belongs to the class of inverse problems in mathematical physics, which in general case are incorrect. In mathematical aspect it means the solution of operator equation (5). It has been found that when in the equation (5) at a certain frequency range ω the precise values of r_0 are specified (for example, in the idealized numerical experiment), the inverse problem has a single solution [2].

Since the measured values of r_0 contain not only useful information, but as well interferences, then is such a case we can talk only about the approximated in a certain aspect solution of equation (5), which is stable for small changes of initial data r_0. For their construction one can use the additional information on the solution of equation (5). In our case the additional information, which has quantitative character, is determined by the range of changes of real thicknesses of structure layers and their electrophysical parameters and, correspondingly, effective parameters p.

For description of methods for solution of equation (5) in this case let us introduce the following symbols. Let put F for a set of possible values of effective parameters p, and R – for a set of possible dependences of reflection factor $r_0(\omega)$. Let assume that F and R are metric spaces (a certain metric specified on these sets), and M is a set of possible solution of values of effective parameters p of the structure under investigation ($M \in F$) and $N = AM$ is an image of the set M after its mapping with the help of operator A.

Under condition of $r_0(\omega) \in N$ there exists an element for which

$$p_a = A^{-1} r_0 . \qquad (6)$$

The most widely used method in calculation practice for finding p_a is a trial-and-error method. It means the following. Let build the sequence $\{p_n\}$, for which $\rho_R(Ap_n, r_0) \to 0$ under condition of $n \to \infty$. The p_n element is considered as some approximation of the solution p_0. In [3] it has been shown that $p_n \to p_a$, when M is compact.

Unfortunately there are no effective criteria, which would allow determine membership of the $r_0(\omega)$ element in the set N. As a rule, it is assumed a priori. In practical problems of diagnostics $r_0(\omega)$ can be not a member of the set N. In such a case we cannot build the approximate solution based on formula (6), since the $A^{-1} r_0$ can be senseless.

In this situation one should use generalization for the notion solution of equation (5) – quasisolution. According to [3] the quasisolution of the operator equation in the set M is an element $p_k \in M$, which minimizes the $\rho_R(Ap_k, r_0)$ functional:

$$\rho_R(Ap_k, r_0) = \inf_{p \in M} \rho_R(Ap, r_0) .$$

If M is a compact set, the quasisolution exists for arbitrary $r_0(\omega) \in R$ and when, in addition, $r_0(\omega) \in N$, then the quasisolution p_k coincides with the approximate solution $p_0 = A^{-1} r_0$. At approximation of the right side of (5) to precise value (interference in a metrics F tends to 0) the quasisolution p_k tends to precise solution p_0.

It is clear than in our case the set F coincides with the $3n$–dimensional space C^{3n}, and R – with the space $L_2(\omega_{\min}, \omega_{\max})$, if $r_0(\omega)$ is set in a range $[\omega_{\min}, \omega_{\max}]$. However, real measurements of reflection factors are performed on discrete mesh of frequencies

$$\omega_l = \omega_{\min} + (l-1)\Delta\omega, \qquad (l = 1, ..., m),$$

where $\Delta\omega$ is a sampling increment of frequency range. In such a case the set R coincides with complex m – dimensional space C^m. Then the problem of finding approximate quasi-solution is reduced to minimization of functional

$$f(p) = \sum_{l=1}^{m} \left| r_0(\omega_l; p) - r_e(\omega_l) \right|^2,$$

where $r_e(\omega_l)$ are measured values of reflection factor of electromagnetic field on the upper layer of the structure under investigation for frequency $\omega = \omega_l$. As was mentioned above, proceeding from natural limits for parameters of layered dielectric, one can define the range of changes in the p parameters as a certain limited region B_0 of the space C^{3n}, which is a compact set in C^{3n}. Then the inverse problem of probing of layered materials is the finding of the p_k as it is

$$f(p_k) = \inf_{p \in B_0} f(p). \qquad (7)$$

Since B_0 is compact, there exist a single solution for the problem (7).

Numerical experiments [7] indicate that the $f(p)$ function has a complicated topologic structure with a large number of local minimums with value of objective function close to the global minimum, the measure of attraction regions [11] of local minimum points is relatively small in comparison with the measure of the sought set. Despite of intensive studies [8–12], up to now there are no efficient algorithms for finding global minimum of linear functions.

Concerning the practical applications, it is very important to use systematic algorithms that guarantee finding of *ad lib* close approximations of solution to the finite, preset number of calculations. The main drawback of methods of this class is exponential [6,15,16] in relation to problem characteristics, estimation of number of calculations, which make their inefficiency for large scale problems or for seeking high precision solutions.

Therefore in practice one uses numerous stochastic and heuristic methods that provide solution of optimization problem only with certain probability or do not give any guarantee of it. As examples of such methods we can mention [5] cluster modifications [9,11] of random multistart [6], which combine methods of local minimization, some strategies for generation of random starting points and stochastic criteria of stopping [9,11].

Similar drawbacks are typical as well for other methods used for solution of inverse problems, particularly for genetic algorithms [6], algorithms of model quenching, neural nets [7], etc.

In the algorithm based on combination of the method of nets [11,12] with methods of local search, has been considered. It can be said that this method finds the point of global minimum only in the case of the choice of rather small meshwidth, which requires large array of calculations even for not many variables. Here the net is built without accounting the global model of behavior of the objective function [6], therefore the convergence of this algorithm cannot be guaranteed. The other drawbacks of the method is the absence of criteria for choosing necessary precision for finishing of the work of algorithm and estimation of error of the obtained solution in the case of incorrect input data.

4. Numerical solution of inverse problem of electromagnetic probing of layered dielectrics by the method of branches and limits

4.1 Presentation of results of mathematical interpretation

Characteristic peculiarity of mathematical theory for interpretation of data of radiowave probing of layered structures is the provision of uniqueness of the choice of the p_k element, which created the illusion of maximization of reliability of interpretation of results. During its choice in addition of the available (objective) a priori information, which is already accounted during building of the set B_0, on the basis of formal mathematical considerations, an additional attribute is introduced into consideration (subjectively), which allows making preferences to some of elements from the B_0, and call the choice optimal on this basis. In our case such a criterion is a minimum of misalignment between measured and theoretical values of reflection factor. The other option of criterion is possible; it includes the maximization of correlation func-

tion between precise and measured values of reflection factor.

Such a criterion for choosing optimum element provides convergence of the last to the precise solution under condition of tending of norm of interferences in the measured values to zero. Of course, if the convergence – as a possibility to estimate parameters of layered structures with the preset possible accuracy – would be realized in practice, there would be no doubts in the efficiency of the form of interpretation result presentation in the form of a single element.

However the assumption on tending of interferences to zero too much extent appropriate for solution of purely mathematical issues of the theory of inverse problems. In practice we always have interference. Therefore if to present the set of approximate solutions, which correspond to different levels of interference as a certain trajectory, then its behavior (in relation to the p_0 point) in vicinity of zero value of interference norm, in practice we are interested only in the part of this path than correspond to the range of really possible values of the interference norm.

The problem has as well the following explanation. An arbitrary set can be completely represented by one of its elements. This allows stating that arbitrary method for interpretation of radiowave probing, built on the basis of seeking of a single interpretation option from a set of possible ones, does not completely correspond to the main aim of interpretation theory – the obtaining of the maximum volume of reliable information, useful fro solution of a practical problem.

From the practical aspect presentation of interpretation results in terms of norm of difference of these elements

$$\|p_k - p_a\| < \varepsilon \qquad (8)$$

is more efficient since interpretation results and precise solution of inverse problems are elements of the same space. In other words, in addition to determination of approximate solution p_k, one should find the estimation of its error (the ε parameter).

The apparatus for solving direct and inverse problems is known to move from analytical methods to flexible numerical methods. Similarly, in the question of efficient estimation of reliability of interpretation results, the analytical methods should make the way to numerical ones. The reliability problem of presentation of results should be solved by algorithm way as a problem of computational mathematics, in the first turn this concerns constrained extremum problem in determination of the ε parameter on the basis of characteristics of interference.

Therefore for finding the point of the global minimum in the problem (7) the modification of the method of branches and limits [8-12] based on the use of interval analysis [4,8,9] has been used.

The advantages of this method, in comparison with those described above, is that it belongs to the class of systematic method, which allows estimating errors of the obtained solution in the case of inaccurate input data because of the use of interval arithmetic [4].

4.2 Interval function of inclusion of objective function for inexact values of reflection factor

Before starting the explanation of algorithm for realization of this idea let set some definitions, which will be used further on. A set

$$X = \{x \in R^n \mid -\infty < a_i \le x_i \le b_i < +\infty,\ i = 1,...,n\},$$

where R^n is n-dimensional Euclid space, $a, b \in R^n$, we shall refer to as real n–dimensional interval. Let put I^n for the set of n–dimensional intervals; let consider $X[i] \in I^1, i \in \{1,...,n\}$ to be the ith component of the interval $X \in I^n$. For an arbitrary interval $T = [x_1, x_2] \in I^1$, $-\infty < x_1 \le x_2 < \infty$ let mark $\underline{T} = x_1$, $\overline{T} = x_2$. Let call the set

$$Z = X + iY = \{x + iy \mid x \in X, y \in Y\}, \text{ where } X, Y \in I^n.$$

the complex n-dimensional interval. Let put C_I^n for a set of n–dimensional complex intervals.

Let $\varphi(x)$ is an arbitrary limited function defined on some interval $X \in I^n$. The interval inclusion

function [8,10] of the function $\varphi(x)$ on X we call mapping $\Phi: I^n \to I^1$, for which $\varphi(x) \in \Phi(Y)$ for arbitrary range $Y \subseteq X$ and arbitrary $x \in Y$. Similarly to differentiated function we can designate interval inclusion functions for partial derivatives of corresponding order. As we can see the interval inclusion function is not single.

The first stage in building algorithm for solution of inverse problem of probing of layered dielectrics and estimation of error of the obtained solution is building of inclusion function for $f(p)$. Let consider the simplest option of its construction with the help of complex interval arithmetic [4]. The ways of numerical realization of arithmetic interval operations with real and complex intervals, as well the construction of interval inclusion functions for elementary functions are extensively elucidated in literature [4,8,10], therefore we shall not describe them in details.

Let assume that we know the absolute measuring error of $r_0(\omega_l)$ $\delta(\omega_l) = \mathrm{Re}\,\delta(\omega_l) + i\,\mathrm{Im}\,\delta(\omega_l)$, values, where $\mathrm{Re}\,\delta(\omega_k) > 0, \mathrm{Im}\,\delta(\omega_k) > 0$ and some their approximate values $r_e(\omega_l)$. It is clear that this yields to $r_0(\omega_l) \in R_e(\omega_l) \in I_C^1$, where

$$R_e(\omega_l) = \left[r_e(\omega_l) - \delta(\omega_l), r_e(\omega_l) + \delta(\omega_l)\right] \in I_C^1 .$$

Let consider, instead of the $h_n, \varepsilon_n, \delta_n \in R^1$ values their interval analogues $H_n, E_n, \Delta_n \in I^1$ and perform sequentially all operation (1)– (4) by the rules of interval arithmetic. Then we obtain:

$$\Lambda_m = 2\omega_0 H_m \sqrt{E_m \mu_0}\ \mathrm{Re}\left(\sqrt{1 + j\Delta_m}\right),\ \mathrm{M}_m = 2\omega_0 H_m \sqrt{E_m \mu_0}\ \mathrm{Im}\left(\sqrt{1 + j\Delta_m}\right),\ \mathrm{T}_m = \frac{H_m}{H_{m-1}};$$

$$P_m = \mathrm{T}_m \frac{j\Lambda_{m-1} - \Lambda_{m-1}}{j\Lambda_m - \Lambda_m}\ \mathrm{A}_m = \tilde{\omega}\left(j\Lambda_m - \mathrm{M}_m\right),\ \mathrm{B}_m = \left(1 - P_m\right)/\left(1 + P_m\right); R_{m-1} = \frac{\mathrm{B}_m + e^{\Lambda_m} R_m}{1 + \mathrm{B}_m e^{\Lambda_m} R_m},\ R_{n-1} = \mathrm{B}_{n-1}.$$

Then interval inclusion function for objective function can be written as

$$F(P) = \sum_{l=1}^{m} \left| R_0(\omega_l; P) - R_e\left(\omega_l\right) \right|^2 .$$

It allows obtaining the lower and upper estimations of values of objective function (2) on the arbitrary interval $P \subset B_0$: $f(p) \in \left[\underline{F}(P), \overline{F}(P)\right]$ for arbitrary $p \in P$ and error $\delta(\omega_k)$.

4.3 Algorithm for solution of inverse problem of probing of layered structures

Let introduce some auxiliary symbols. Let consider sets of elements in the form $e = (B, \alpha, \beta)$, where $B \in I^{3n}$, $\alpha, \beta \in R$ are lower and upper limits of estimation of the $f(p)$ function at the B interval, respectively. Let put L for a set of such elements, for which in intervals B there is not yet a decision on possible location of problem solution in them, and G – for a set of such elements, that $\|B\| \le \Delta_0$, where $0 < \Delta_0 < 1$ is an arbitrary constant, $\|B\| = \max_i \overline{B[i]} - \underline{B[i]}$, $B \in I^n$. Let mark the upper estimation of the possible value of the objective function on B_0 as z. Algorithm contains the following steps:

0. Set $0 < \Delta_0 < 1,\ 0 < q < 1$. Assume $G = \varnothing$. Calculate $F(B_0)$, assume $y = \underline{F}(B_0)$, $z = \overline{F}(B_0)$, $L = \{(B_0, y, z)\}$.
1. If $L = \varnothing$, then go to the step 7, otherwise find an arbitrary element $e = (B, \alpha, \beta)$ within L with the minimum value of α. Assume $L = L \setminus \{e\}$.
2. If $\alpha > z$, then exclude element e from consideration and go to step 1.
3. If $\|B\| \le \Delta_0$, then assume $G = G \cup \{e\}$ and go to step 1 1.
4. If $(\overline{F}(mid\ B) - z)/z > q$, then go to step 5, otherwise find some point of local minimum $x^* \in B$ of the

function $f(p\}$. Calculate $f^* = \bar{F}(x^*)$. Assume $z = min\{z, f^*\}$.

5. Split the interval B into two – B_1 and B_2 by the largest coordinate: $B = B_1 \cup B_2,\ B_1 \cap B_2 = \varnothing$.
6. Calculate $F(B_1), F(B_2)$; assume $\alpha_i = \underline{F}(B_i), \beta_i = \overline{F}(B_i), i \in \{1,2\}$; $z = min\ \{ z, \beta_1, \beta_2 \}$. Assume $L = L \cup \{(B_i, \alpha_i, \beta_i)\}$, $i \in \{1,2\}$. Go to step 1.
7. Build such an interval $P^* \in I^{3n}$, that $P^*[i] = [\min\limits_{e \in G} \underline{e[i]}, \max\limits_{e \in G} \overline{e[i]}],\ i = 1,...,3n$.
8. The end of algorithm.

The q parameters, used in step 4, serve for controlling of the number of application of the local minimization method. The method of local minimization is applied in an interval B only when the upper limit of inclusion function in the central point of this interval is smaller or comparable with z.

Proof of convergence of the proposed algorithm is similar to the proof of convergence of the interval method of branches and limits [8,10,12].

For analysis of the algorithm we have performed the numerical experiment for determination of thickness of layers in dielectric structures with the following parameters: a) $h_1 = 0.02$, $\varepsilon_1 = 3.9$, $\delta_1 = 0.01$; b) $h_1 = 0.01, h_2 = 0.02$, $\varepsilon_1 = 3.9, \varepsilon_2 = 2.5$, $\delta_1 = \delta_2 = 0.01$. The values of reflection factor, calculated by formula $r_e(\omega_l) = r_0(\omega_l)\ (1 + \hat{\delta}\delta/100)$, where $\hat{\delta}$ is evenly distributed on $[-1,+1]$ arbitrary value, δ is relative error in percent, in the range of relative frequencies from $\omega_{\min} = 0.5$ to $\omega_{\max} = 4.1$, which at $\omega_0 = 420.0$ corresponds to the frequency range from 10 to 82 GHz, was assumed to be the measured ones.

During numerical experiment we studied the dependence of the error of the obtained solution by the argument Δ_X on the number of probing frequencies N and relative error δ of input data. We accepted the following values of parameters: $q = 10^{-6}$ and $\Delta_0 = 10^{-5}$. The table provides the averaged values of errors (after 50 trials).

	Structure a)				Structure b)			
N / δ, %	10	20	30	40	10	20	30	40
0	9.8E-6	9.8E-6	9.8E-6	9.8E-6	1.5E-5	2.2E-5	2.2E-5	2.2E-5
2.5	3.0E-5	4.7E-5	2.9E-5	3.1E-5	1.9E-4	1.8E-4	1.7E-4	1.7E-4
5	5.9E-5	7.9E-5	5.9E-5	5.9E-5	3.5E-4	3.3E-4	3.2E-4	3.2E-4
10	1.1E-4	1.5E-4	1.2E-4	1.1E-4	1.8E-2	6.4E-4	9.1E-3	6.5E-4
15	1.8E-4	2.3 E-4	1.8E-4	1.8E-4	2.9E-2	2.55E-2	2.32E-2	2.02E-2
20	8.5E-3	3.1E-4	2.4E-4	2.4E-4	3.4E-2	3.1E-2	3.1E-2	3.1E-2

The presented results confirm the conclusion on the efficiency of application of interval method of branches and limits for practical solution of problems in electromagnetic diagnostics of layered dielectrics for not many unknown parameters and insubstantial errors in input data.

Preliminary analysis of results of numerical modeling shows that the field of application of this method can be substantially widened (structures with larger number of layers, decrease in requirements to the accuracy of input data) by the following way.

First, this is the application of e inclusion functions built with the help of centered forms [4,12]; second, for quick finding the value of objective function, close to the global minimum, one can use the tunnel algorithms [4,8] based on tunnel functions (filling functions).

Then, elements of the set G obtained as a result of the work of algorithm, are located in vicinity of the point of the global minimum, forming the so-called cluster [8]. Accounting large number of such elements, particularly in the case of inaccurate measurement data, it would be promising to use the modified

method of branches and limits by the strategy on isolation of points of local minimum [8].

5. Conclusions

The theoretic study of direct and inverse problems of electromagnetic probing of multilayered structures has been performed.

It has been found that on the basis of frequency dependence of reflection factor it is possible to determine only effective parameters, than describe some set of real layered structures (equivalent structures).

The problem of determination of effective parameters of layered structures is reduced to the solution of inverse problem, which requires the minimization of misalignment functional (objective function) measured and theoretically calculated reflection factors on the surface of structure.

It has been shown that in the presence of interferences in addition to determination of approximate solution one should find the estimation of its error. For solution of this problem a numerical method based on a new algorithm for global minimization of objective function, which is the combination of interval method of branches and limits with methods of local search.

6. References

1. *Colton D., Kress R.* Inverse Acoustic and Electromagnetic Scattering. – Berlin, Heidelberg New York: Springer Verlag, 1997. – 334 p.
2. *Glasko, V. B.* Inverse problems of mathematical physics. – New York, American Institute of Physics, 1988. – 99 p.
3. Tikhonov A. N., Arsenin V. Ya. Metody resheniya nekorrektnykh zadach (Methods of Solution of Ill-posed Problems). – Nauka, Moscow, 1979. – 287 p.
4. Alefeld G., Herzberger Yu. Introduction to interval computation. 1983
5. *Gutman S.* Identification of multilayered particles from scattering data by a clustering method // J. Comp. Phys.–2000.–№163.–P.529–546.
6. *Xiaodong Li, Yong Fan, Tianzi Jiang.* Solving the Inverse Scattering Problem Using Global Optimization Methods // Proc. 12-th International Conf. on Biomagnetism. Helsinki, Finland, 2000.
7. *Caorsi S., Massa A., Pastorino M.* A computational technique based on a real-coded genetic algorithm for microwave imaging purposes // *IEEE Trans.Geosci.Remote Sensing.*–2000.– 38, №.4.–P.1697–1708.
8. *Hansen E. R.* Global Optimization using Interval Analysis. –Springer-Verlag, Berlin, 1993.–230p.
9. *Rinnooy A.H.G. Kan and G.T. Timmer.* Stochastic methods for global optimization //American J. of Mathematical and Management Sciences.–1984.–№4.–P.7.– 4.
10. *Kearfott R..B.* An interval branch and bound algorithm for bound constrained optimization problems // J. of Global Optimization.–1992.– №2.– P.259.–280.
11. *Torn A., Zilinskas A.*Global Optimization. Lecture Notes in Computer Science. Springer-Verlag, Berlin, 1989.–190p.
12. *Pinter J.* Global Optimization in Action. .– Kluwer Academic Publishers, 1996.– 478 p.

IV. MODIFICATION OF THE SOFTWARE FOR THE SOLUTION OF THE INVERSE PROBLEM

Branches and limits method [8-12] and its application for study of multiextremal mathematical models have been widely spread during recent decades. It is one of a few systematic methods, applicable for solution of a wide spectrum of continuous and discrete optimization problems under relatively simple assumptions concerning an objective function and a search-set.

Principle idea of the method is a step-by-step search-set partition of the initial problem into several subsets with subsequent exclusion of subsets, which do not contain the global minimum and continuation of search in subsets considered as "perspective" in scopes of possible finding in them the solution under certain criterion.

The substantial drawback of the method of branches and limits is an exponentional growth of the amount of calculations in relation of problem characteristics. Let note, that such a pessimistic estimation is typical of all systematic methods. However, if to apply interval analysis and means to accelerate the convergence for the method of branches and limits, numerical experiments confirm the possibility of it efficient realization [4,8,9] for optimization problems.

Let enter for convenience sake some designations. The set $X = \{x \in R^n \mid -\infty < a_i \le x_i \le b_i < +\infty,\ i = 1,...,n\}$, where $a, b \in R^n$ are some vectors, let refer to as n-dimensional interval. The set of all n-dimension intervals by I^n, and consider $X[i] \in I^1, i \in \{1,...,n\}$ as the i[th] component of the interval X. For arbitrary single-dimension interval $T = [x_1, x_2] \in I^1,\ -\infty < x_1 \le x_2 < \infty$ identify $\underline{T} = x_1$, $\overline{T} = x_2$ 1.

Let $\varphi(x)$ is an arbitrary bounded function, defined on a certain interval $X \in I^n$. Then the interval inclusion function of the function $\varphi(x)$ on X we consider such an image $\Phi : I^n \to I^1$ that $\varphi(x) \in \Phi(Y)$ for arbitrary interval $Y \subseteq X$ and arbitrary $x \in Y$. Similarly, for differentiated function we can denote interval inclusion functions for partial derivatives of corresponding order.

Interval inclusion functions are widely used in modifications of the method of branches and limits for solution of optimization problems, since by definition they allow easy determining upper and lower limits for objective functions and its derivatives.

There is substantial obstacle on the way of efficient application of the method of branches and limits for solution of applied problems, which is a cluster problem [8]. Its essence is that during the work of the method there appears the necessity to analyze a large number of subset with smaller, compared to the initial set, diameter (their aggregation is usually referred to as cluster), which are situated in vicinity of the global minimum point. Here the main part of the calculations work-time, performed by the method of branches and limits, is lost for exclusion of these subsets.

In the case of successful solution of the cluster problem we can hope to enhance the efficiency of the method concerning most of the applied problems.

It is clear, that there is now necessity of finding the point of the global minimum with high accuracy. This is stipulated by substantial errors in measurement data.

Then, in order to overcome the cluster problem, we shall use the algorithm in method of branches and limits, that allows finding points of local minimum and build some circles around them which contain local minimum. The method, in its turn, should be modified in the way that the partition of the search set would occur mostly outside the built circles. This idea is geometrically illustrated in Fig.1

Let $f(x) \in C^2(B_0)$, $B_0 \in I^n$ and all local minimum points of the $f(x)$ function on B_0 are internal. We should find such a point $x_{gl} \in B_0$ that

$$\mathrm{f}\left(x_{gl}\right) = \min_{x \in B_0} \mathrm{f}\left(x\right).$$

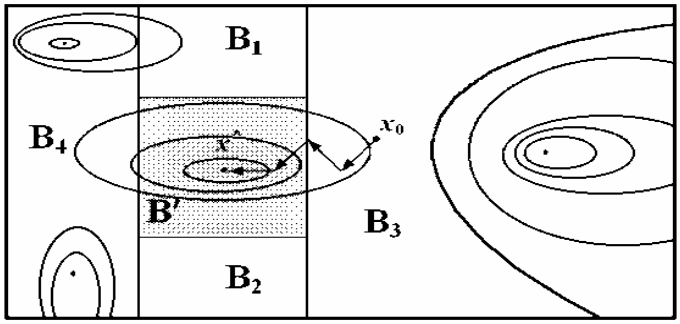

Fig. 1. Line of level for multiextremal function and strategy for solution of the cluster problem.

Realization of the proposed above idea of finding the point x_{gl} needs development of constructive and efficient method for solving such problems for arbitrary interval $B \in B_0$:

1) find a point $x^* \in B$ of the local minimum of the $f(x)$ function on B;
2) build a certain interval $B' \subset B$, that $x^* \in B$ and x^* would be a local minimum of $f(x)$ on B';
3) efficiently "cut out" the hyperinterval B' from B, i.e. build a set of subintervals $B_1, B_2, ..., B_m$, $m \geq 1$ for which $B_i \subset B,\ B = B' \bigcup B_i,\ i = 1,..,m.$

For solution of the Problem 1) one can use any globally convergent algorithm of conditional local minimization. For efficient accounting simple restriction $x \in B$ it worth to use quasi-Neuton modification of the linearization method [1-3].

Let consider the Problem 2). Let $X \in I^n$ is arbitrary hyperinterval (interval vector) and $wX = \max\limits_{1 \leq i \leq n} \left(\overline{T}_i - \underline{T}_i \right)$. In order to solve the problem it is enough to build the such a hyperinterval $B' \subset B$, that $x^* = midB'$ and $wB' = \Delta$, where $midX$ is the central point of hyperinterval X, and Δ is the preset precision of the solution by argument.

The algorithm A1 described below allows to find the solution of the problem 2).

0. Define intervals B, B'. Assume $S = \varnothing,\ i = 1$.
1. Suppose $T[i] = [\underline{B}[i]; \underline{B'}[i]],\ T[j] = B[j]$ for $j = 1,...,n,\ j \neq i$.
   Calculate $F(T)$ and suppose $\alpha = \underline{F}(T),\ \beta = \overline{F}(T)$.
2. Suppose $B = B \setminus \{T\},\ S = S \bigcup \{\ (T, \alpha, \beta)\ \}$.
3. Suppose $T[i] = [\overline{B'}[i]; \overline{B}[i]],\ T[j] = B[j]$ for $j = 1,...,n,\ j \neq i$. Calculate $F(T)$ and assume $\alpha = \underline{F}(T),\ \beta = \overline{F}(T)$.
4. Suppose $B = B \setminus \{T\},\ S = S \bigcup \{(T, \alpha, \beta)\}$.
5. If $i < n$, then assume $i = i + 1$ and go to step 1.
6. End of algorithm.

From the building of algorithm it is seen that as a result of its work the set S will contain not more than $2n$ elements, which allows to assume it efficient for large n.

1. Algorithm for solution of reverse problem of probing layered structures

The first stage in building the algorithm for solution of reverse problem of probing layered dielectrics and estimation of an error of the found solution is the construction of the inclusion function for the object function. Let consider the simplest case of its building with the help of complex interval arithmetic [4]. The methods for numerical realization of arithmetic interval operation with real and complex intervals,

as well as the building of interval function of inclusion for elementary functions are widely presented in literature [4], so we shall not describe them here.

Let assume that the absolute error of measurements of values of $r_0(\omega_l)$ $\delta(\omega_l) = \mathrm{Re}\,\delta(\omega_l) + i\,\mathrm{Im}\,\delta(\omega_l)$, where $\mathrm{Re}\,\delta(\omega_k) > 0, \mathrm{Im}\,\delta(\omega_k) > 0$ and some their approximates $r_e(\omega_l)$ are known. It is obvious that then $r_0(\omega_l) \in R_e(\omega_l) \in I_C^1$, where

$R_e(\omega_l) = \left[r_e(\omega_l) - \delta(\omega_l), r_e(\omega_l) + \delta(\omega_l)\right] \in I_C^1$.

Instead the $h_n, \varepsilon_n, \delta_n \in R^1$ values let consider their interval analogues $H_n, E_n, \Delta_n \in I^1$ and sequentially perform all operation in (1)– (4) (see the T03 report) according to rules of interval arithmetic. Then we obtain:

$$\Lambda_m = 2\omega_0 H_m \sqrt{E_m \mu_0}\ \mathrm{Re}\left(\sqrt{1 + j\Delta_m}\right),\ \mathrm{M}_m = 2\omega_0 H_m \sqrt{E_m \mu_0}\ \mathrm{Im}\left(\sqrt{1 + j\Delta_m}\right),\ \mathrm{T}_m = \frac{H_m}{H_{m-1}};$$

$$P_m = \mathrm{T}_m \frac{j\Lambda_{m-1} - \Lambda_{m-1}}{j\Lambda_m - \Lambda_m}\ \mathrm{A}_m = \tilde{\omega}\left(j\Lambda_m - \mathrm{M}_m\right),\ \mathrm{B}_m = \left(1 - P_m\right)/\left(1 + P_m\right);\ R_{m-1} = \frac{\mathrm{B}_m + e^{\Lambda_m} R_m}{1 + \mathrm{B}_m e^{\Lambda_m} R_m},\ R_{n-1} = \mathrm{B}_{n-1}.$$

Then interval inclusion function for the object function will look like [5-7]

$$F(P) = \sum_{l=1}^{m} \left| R_0(\omega_l; P) - R_e\left(\omega_l\right) \right|^2.$$

It allows obtaining lower and upper estimations of the object function (2) on arbitrary interval $P \subset B_0$: $f(p) \in \left[\underline{F}(P), \overline{F}(P)\right]$ for arbitrary $p \in P$ and error $\delta(\omega_k)$.

Let introduce some auxiliary notations. We shall consider sets in the form $E = (B, \alpha, \beta)$, where $B \in I^{3n}, \alpha, \beta \in R$ is the lower and upper estimations of the value of the function $f(p)$ on the interval B, respectively. Let put L for a set of such elements, for which on intervals B there is still no decision on possible finding solution in them, and G for a set of intervals, which width is smaller than some small value $\varepsilon > 0$.

Together with these sets we consider the set C made of elements in the $E = (B, \alpha, \beta, x^*)$ form, where $x^* \in R^n$ is a certain point of the local minimum of empirical point function of objective function $\tilde{f}(x)$, $B \in I^n, \alpha, \beta \in R$ have the same sense.

Let denote the upper estimation of the minimum value of target function on B_0 as z. The algorithm has the following steps.

Description of algorithm parameters**.**

$\Delta > 0$ is a fixed solution precision by argument.

$0 < \gamma < 1$ is a fragmentation constant.

$0 < \varepsilon < 1$ is a limit of hyperinterval. During the performance of the algorithm the hyperinterval B shifts to the set G, if $wB \le \Delta$.

$0 < \varepsilon_0 < 1;\ \varepsilon_0 << \varepsilon$ – utter limit of partitioning of hyperinterval. The partitioning of hyperintervals is forbidden if $wB \le \varepsilon_0$.

Let consider that the problem is solved, if at certain step their is fulfilled condition

$wP \le \Delta,$

Where $P = (P_1, .., P_n) \in I^n,\ P_i = \left[\min_{X \in L \bigcup C \bigcup G} \underline{X}_i, \max_{X \in L \bigcup C \bigcup G} \overline{X}_i\right],\ i = 1, ..., n.$

Condition for the exclusion of sets from consideration takes the form: $F(X) > 0$ where $F(X)$ is any interval function of inclusion of object function.

The algorithm is the anti-cluster modification of interval method of branches and limits of the 0-order in-

cludes the following steps.

0. [initialization]. To chose values of $\Delta > 0,\ \varepsilon > 0, \varepsilon_0 > 0,\ 0 < q < 1,\ 0 < \gamma < 1$ parameters; calculate $F(B_0)$; assume $y = \underline{F}(B_0)$, $z = \overline{F}(B_0)$, $L = \{(B_0, y, z)\}$, $G = \varnothing$, $C = \varnothing$.
1. [test to achieve accuracy]. If $wP \le \Delta$, then go to step 10.
2. [refinement of clusters]. If $L = \varnothing$ та $C \ne \varnothing$ then go to step 9.
3. [refinement by accuracy]. If $L = \varnothing, C = \varnothing, G \ne \varnothing$ and $\varepsilon > \varepsilon_0$, then assume $\varepsilon = \varepsilon \cdot \gamma, L = G, G = \varnothing$ and go to step 1. Otherwise, go to step 11 .
4. [search of the perspective element]. Find in L an arbitrary element $E = (B, \alpha, \beta)$, for which $wE = \max\limits_{X \in L} wX$ (element of the maximal width). Assume $L = L \setminus \{E\}$.
5. [tolerance test] If $\alpha > 0$, then exclude the element E from further consideration and go to step 1.
6. [optimality test] If $wB < \varepsilon$, then assume $G = G \bigcup \{E\}$ and go to step 1.
7. [modified partitioning]
   7.1. [condition of modified partitioning]. If $(\overline{F}(B) - z)/z > q$, then go to step 8.
   7.2. Using the method of local minimization, find a point of local minimum $x^* \in B$ of the function $\tilde{f}(x)$. Calculate $f^* = \tilde{f}(x^*)$. Assume $z = min\{z, f^*\}$.
   7.3. Build an interval $B' \subset B$, $x^* = mid\ B'$, $wB' = \Delta$.
   7.4. If $\underline{F}(B') > 0$, then exclude B' .
   7.5. Using algorithm A1, build a partition S of the interval B. Assume $L = L \bigcup S$ and $C = C \bigcup \{B'\}$
   7.6. Go to step 1.
8. [standard partition]. To find index k for which $wB_k = \max\limits_{i \in 1,..,n} wB_i$. Divide the hyperinterval B into two hyperintervals by k^{th} coordinate: $B = B_1 \bigcup B_2$. Calculate $F(B_1), F(B_2)$; assume $\alpha_i = \underline{F}(B_i)$, $\beta_i = \overline{F}(B_i)$; $z = min\ \{z, \beta_1, \beta_2\}$, $L = L \bigcup \{(B_i, \alpha_i, \beta_i)\}$. Go to step 1.
9. [treatment of the set C]. If $C = \varnothing$, then go to step 1.
   9.1. Choose an arbitrary element $E = (B, \alpha, \beta, x^*) \in C$.
   9.2. If $\alpha > 0$, then go to step 9.7.
   9.3. If $wB < \varepsilon$, then assume $G = G \bigcup \{E\}$ and go to step 9.7.
   9.4. Build the interval $B' \subset B$, $x^* = mid\ B'$, $wB' = wB * \gamma$.
   9.5. Assume $B = B'$, $\alpha = \underline{F}(B)$, $\beta = \overline{F}(B)$, $z = min\ \{z, \beta_1, \beta_2\}$ and go to step 9.1.
   9.6. Using the algorithm **A2**, build a partition S of the interval B. Assume $L = L \bigcup S$.
   9.7. Assume $C = C \setminus \{E\}$ and go to step 9.
10. [precision is achieved]. Go to 12.
11. [precision is not achieved].
12. [end]. Print-out the hyper-rectangle P. End of algorithm.

Parameter q and checking at the step 7.1 serve for controlling the number of the applied modified partition. Modified partition in the algorithm is used for certain interval B only when the upper limit of the inclusion function on this interval is smaller or commensurable with z.

2. Program realization of the modification of interval method of branches and limits for solution of inverse problem of probing of layered structures

The described above algorithm is realized with the help of methods of object-oriented programming in C++ as a batch of application programs. Structurally the batch contains two parts: auxiliary program **DirTask** and main program **DielScan**.

The **DirTask** program serves for calculation and recording in the text file values of reflection factors and results of modeling of errors of their measurements for the preset structure and chosen frequency range (imitation of reflection factor measurements data). These data will be input data for the **DielScan** program. Graphical interface of the user of the **DirTask** program is shown in Fig. 2. It contains fields for input of parameters of dielectric structure for calculation of complex reflection factor and other auxiliary information.

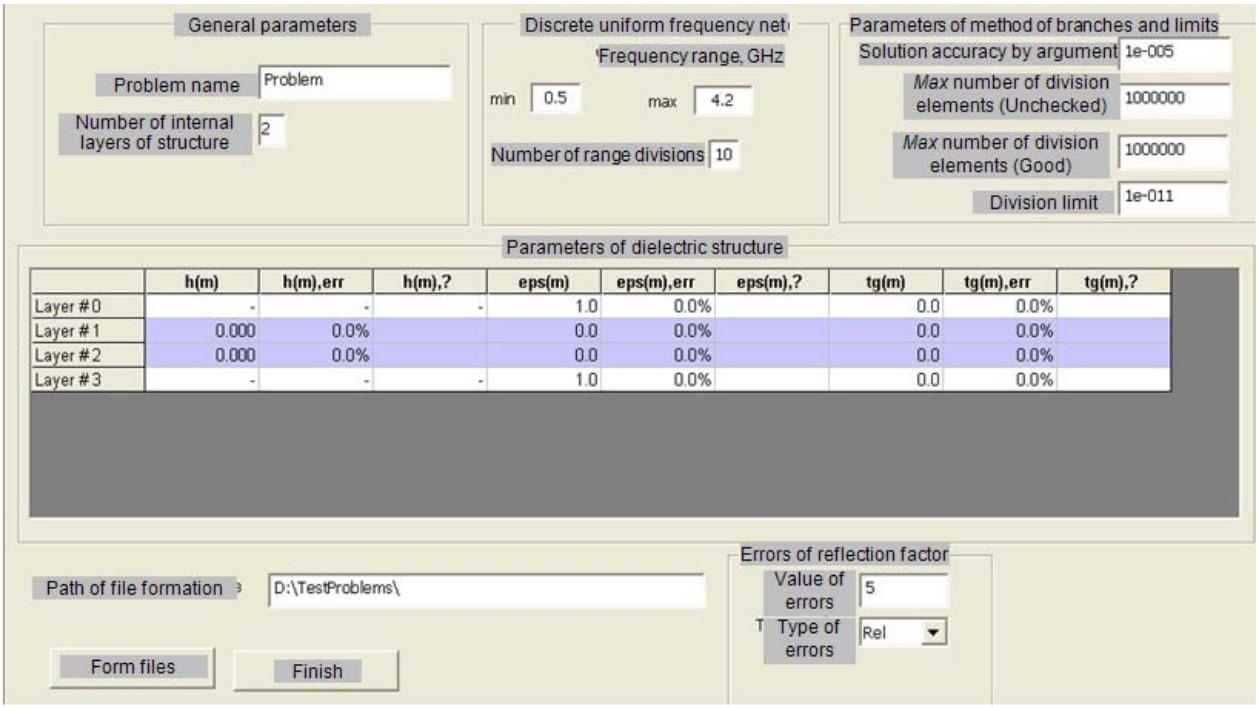

Fig.2. General outlook of the interface window of the **DirTask** program.

Parameters, which values are needed for the work of this program are divided into several groups. General parameters. Field «Problem name» contains the name of text file, in which the output information will be saved. The field «Number of internal layers in the structure» gives the number of layers.
Discrete uniform frequency net. The values of lower and upper limits of the chosen frequency range are put into the fields «min» and «max», respectively. The field «The number of range divisions» contains the number of intervals, into which the frequency range should be divided.

Parameters of the method of branches and limits. This group of fields is provided by necessary information for the methods of branches and limits. The value of Δ is given in the field «Solution accuracy by argument», and the value of the utter division limit ε_0 is put into the field «Division limit ». Numbers of maximum quantities of elements in L and G sets are contained by fields «Max quantity of division elements (Unchecked)» and «Max quantity of division elements (Good)», respectively.

Parameters of dielectric structure. Electrophysical (dielectric constant ε, dielectric dissipation $tg\delta$) and geometrical (layer thickness h) parameters for layers of structures and errors of their determination are provided through fields of the table in the central part of the window. In the same table parameters of structure, assumed to unknown should be marked by «?».

In the lower part of the window there should be filled a field «Path of file formation» with the subdirectory, in which the files with results of calculations by the **DirTask** program should be stored. Type of error in reflectivity factor is chosen from the floating list: «Rel» or «Abs», and its value is provided in the field «Value of the error».

The results of the work are created by pushing the button «Form files». The exit from the **DirTask** program is made by pushing the button «Finish».

DielScan software environment serve from solution of inversed problems of electromagnetic prob-

ing of dielectric structures. The Program has a standard graphic user interface for programs, working under Windows OS. Upon program start, there appears a interface window on the monitor, shown in Fig.3. This window contains several different components. In the upper part, immediately under the name of the window there is a line with a list of the main menu of the program. Below the line of main menu there is the main toolbar as a set of buttons, which duplicate the most frequent commands of the main menu.

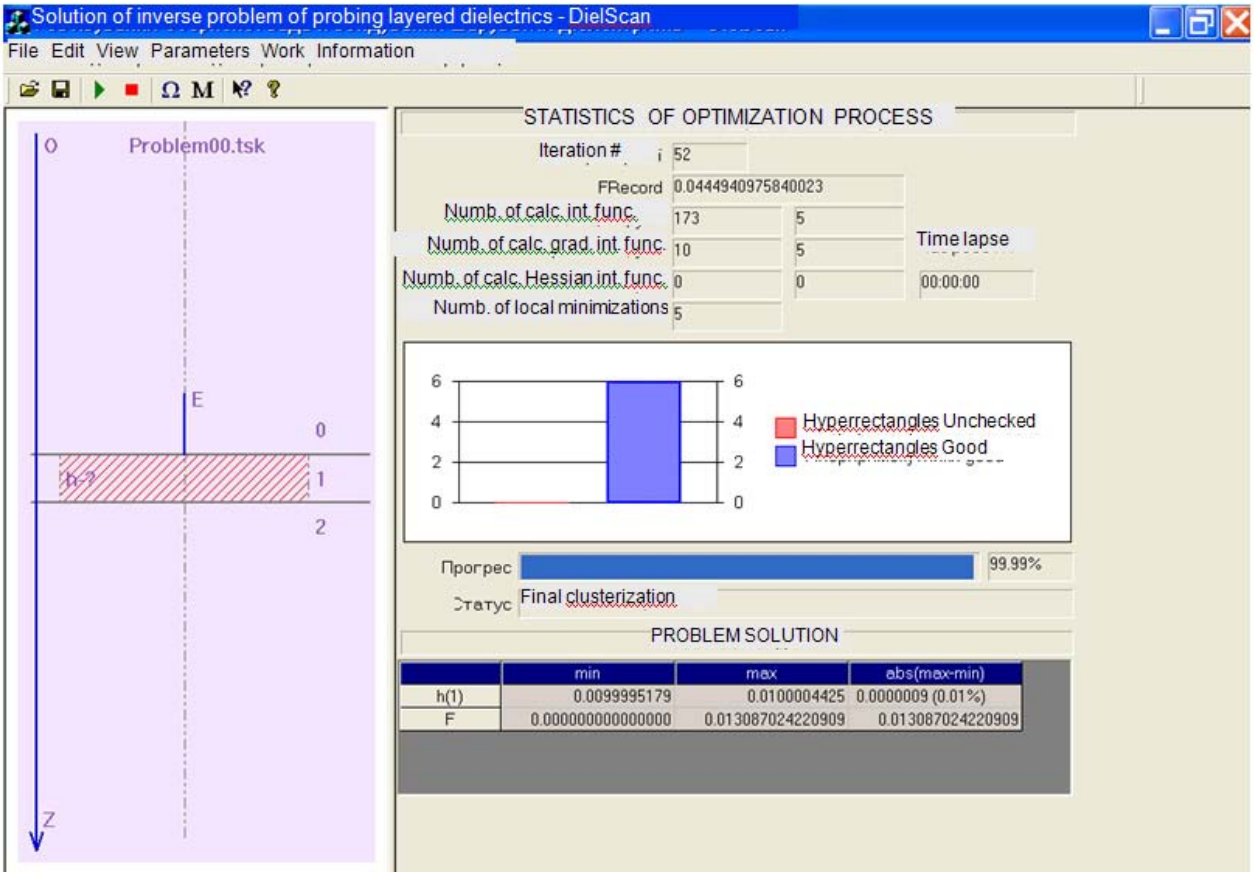

Fig.3. General outlook of the graphic interface of the **DielScan** program

In the lest part of the interface window there is schematic image of the studied structure, the upper part of which shows the name of file, in which the input data for the **DielScan** program are written. The right part of the interface window shows some parameters that describe the optimization process. After finishing program session, the results of calculation are output in the lower part of the window.

Commands of menu «File». Commands of this menu allow opening, saving and printing out input data for the **DielScan** program. Name of the file, containing the input data is provided by the command «Load task». In order save changes in input data, made with the help of other commands, the commands «Save task» and «Save As» are used. The first command saves changes in the same file, the second – in the file with another name. The command «Save As» opens a standard dialogue window for choice of the filename.

Commands of menu «Editor». Commands from this menu are temporary not available.

Commands of menu «View». Commands of this group are simple switch keys. They switch on or off display regime of the toolbar and status bar of the program.

Commands of menu «Parameters». Commands of this menu allow editing values of complex reflection factor. Upon performance of the command «Frequency parameters» there opens additional interface window, separated into tow parts (Fig. 4). In the upper part of the window there is a spreadsheet with real and imaginary approximate values of complex reflection factor and estimations of their precision for

the chosen range of frequency changes. Content of table cells (approximate values of reflection factor parameters) of can be edited with the use of standard Windows means. With the help of the button «Add frequency» and «Exclude frequency» the range of frequencies can be modified. In the lower part of the window there is graphic image of the dependence of reflection factor parameters on the frequency.

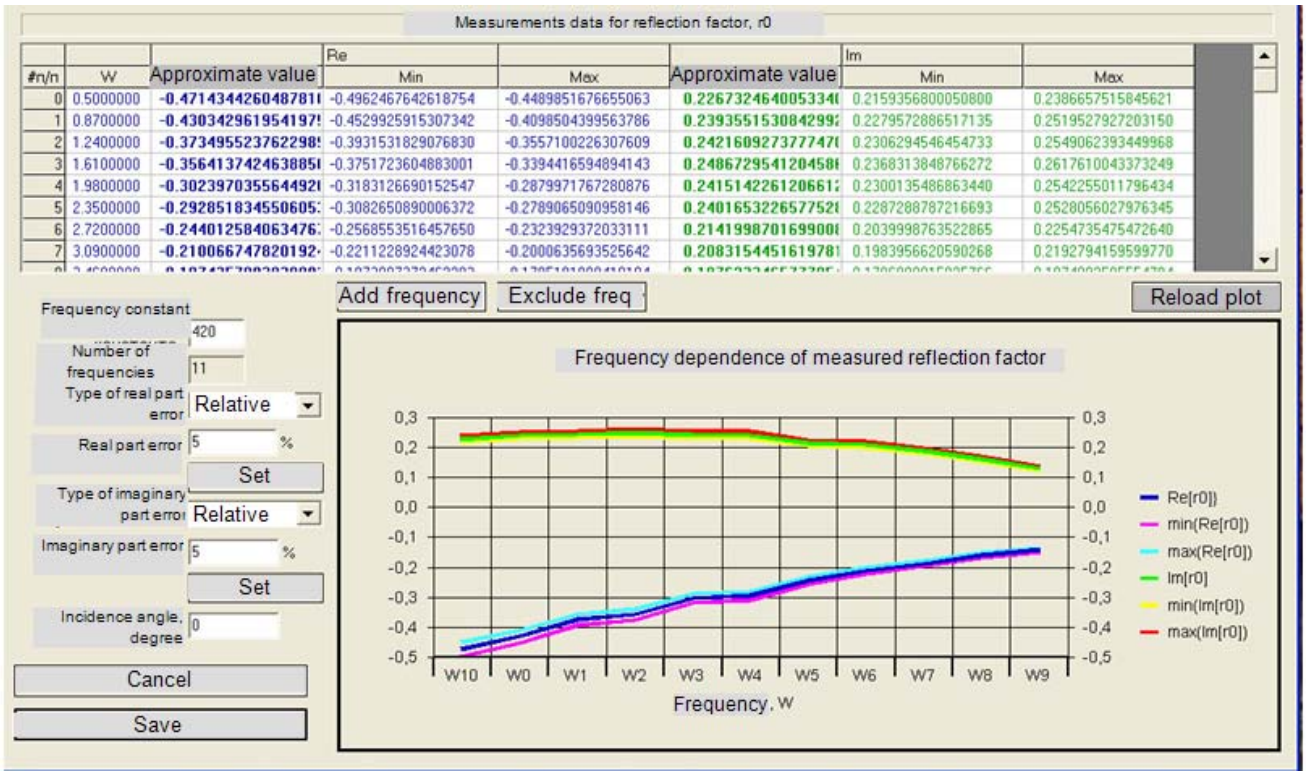

Fig.4. Outline of auxiliary graphical interface of the **DielScan** program

Commands of menu «Work» serve to control with work of the **DielScan** program.

3. Conclusions

In spite of a large number of modern global optimization algorithms [5-7] and their software implementations [13], the problem of development of universal software program for solution of inverse problems in very topical. This is stipulated by the fact that they do not account specific character of input data, which is its approximateness. The proposed interval method of branches and limits gives an possibility to account measurement errors, does not need additional numerical parameters, which determination is complicated (e.g. Liepschiz constant). Numerical experiments have shown the efficiency of **DielScan** software, which realizes this method for solution of inverse problem of dielectric structures probing. At the same time we should note the necessity of further updates and studies aimed on widening a spectrum of solvable problems and integration of this software with existing measuring complexes.

4. References

1. *Colton D., Kress R.* Inverse Acoustic and Electromagnetic Scattering. – Berlin, Heidelberg New York: Springer Verlag, 1997. – 334 p.

2. *Glasko, V. B.* Inverse problems of mathematical physics. – New York, American Institute of Physics, 1988. – 99 p.
3. Tikhonov A. N., Arsenin V. Ya. Metody resheniya nekorrektnykh zadach (Methods of Solution of Ill-posed Problems). – Nauka, Moscow, 1979. – 287 p.
4. Alefeld G., Herzberger Yu. Introduction to interval computation. 1983
5. *Gutman S.* Identification of multilayered particles from scattering data by a clustering method // J. Comp. Phys.–2000.–№163.–P.529–546.
6. *Xiaodong Li, Yong Fan, Tianzi Jiang.* Solving the Inverse Scattering Problem Using Global Optimization Methods // Proc. 12-th International Conf. on Biomagnetism. Helsinki, Finland, 2000.
7. *Caorsi S., Massa A., Pastorino M.* A computational technique based on a real-coded genetic algorithm for microwave imaging purposes // *IEEE Trans.Geosci.Remote Sensing.*–2000.– 38, №.4.–P.1697–1708.
8. *Hansen E. R.* Global Optimization using Interval Analysis. –Springer-Verlag, Berlin, 1993.–230p.
9. *Rinnooy A.H.G. Kan and G.T. Timmer*. Stochastic methods for global optimization //American J. of Mathematical and Management Sciences.–1984.–№4.–P.7.– 4.
10. *Kearfott R..B.* An interval branch and bound algorithm for bound constrained optimization problems // J. of Global Optimization.–1992.– №2.– P.259.–280.
11. *Torn A., Zilinskas A.*Global Optimization. Lecture Notes in Computer Science. Springer-Verlag, Berlin, 1989.–190p.
12. *Pinter J.* Global Optimization in Action. .– Kluwer Academic Publishers, 1996.– 478 p.
13. http://solon.cma.univie.ac.at/~neum/glopt/software_g.html.

V. ADAPTATION OF THE THEORY OF INVERSE PROBLEM SOLUTION TO ESTABLISH THE PARAMETERS OF THE MULTI-LAYERED STRUCTURE TAKING THE ANTENNA'S GEOMETRY INTO ACCOUNT

1. Improvement of processing of measured data at automated measuring bench of microwave diagnostics

Range of application and resolution capability of microwave method directly depend on precision and width of frequency range of measurement of complex reflection coefficient. Therefore we have made the work of improvement of ultrahigh-frequency path of the measuring test bench and algorithms for processing of measured data.

Thanking to the decrease of parasitic re-reflecting between components of UHF path (Fig. 1) we have succeeded to widen the measuring frequency range up to band of 18 GHz (58...76 GHz) without substantial loss in precision of the CRC measurement.

For a new frequency range we have built calibration graphs by extinction and frequency. The bridge circuit has been calibrated and parameters of doubled T-bridge have been determined. Frequency dependence of elements of dissipation matrix is shown in Fig. 2. Fig. 3 presents the root-mean-square deviations of measured signal from the modeled under reference terminations.

Let consider the antenna in the equivalent circuit of the test bench (Fig. 1) as a face-to-face linear quadrupole. If account all elements of antenna dissipation matrix, the relation between the measured CRC V(f) and CRC of flat-layered environment $V_s(f)$ (Fig. 1) can be written as

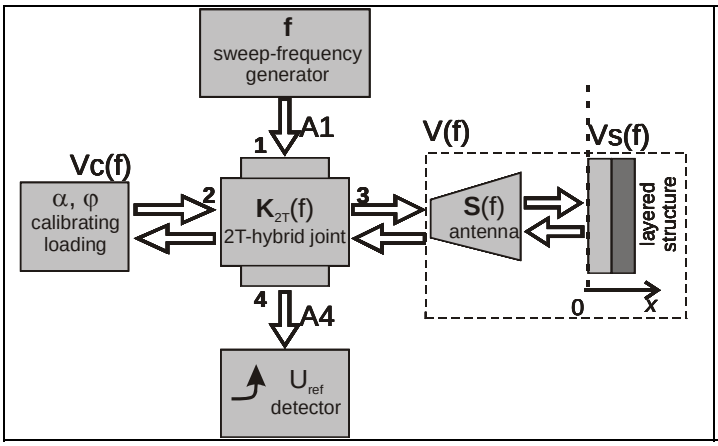

Fig. 1. Unit model of the test bench:
***f** – generation of oscillation frequency;*
U_{ref} – detector of the signal of reflected wave;
V_c *– CRC of calibrated load;*
***K_{2T}** – dissipation matrix of doubled T-bridge;*
V(f) *– CRC of the measured load;*
***S**(f) – antenna;*
V_s(f) *– CRC of flat-layered environment in free space*

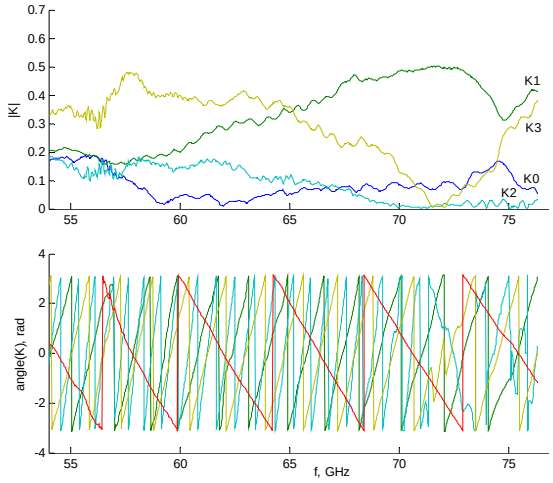

Fig. 2. Frequency dependence of components of dissipation matrix of the bridge scheme.

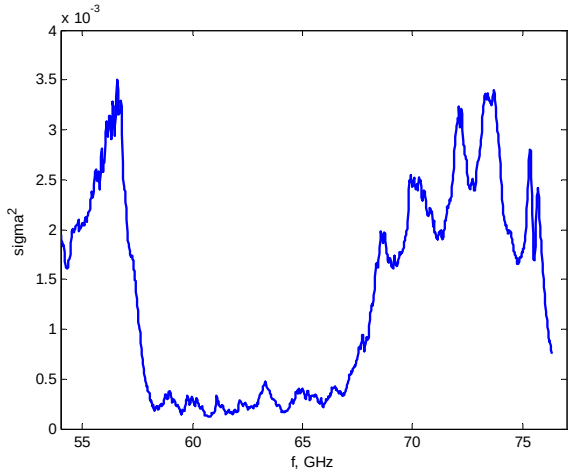

Fig. 3. The root-mean-square deviation of measured and modeled signals of the bridge scheme on the frequency.

$$V = S_1 + \frac{S_2 V_S}{1 - S_3 V_S}, \text{ or } V_S = \frac{S_1 - V}{S_1 S_3 - S_2 - S_3 V},$$

where S_1,..,S_3 are complex factors, which can be determined experimentally. The S_1 is the parameter of antenna CRC during its emission into free space, S_2 is a coefficient of transmission of the probing signal into environment, S_3 describes the re-reflecting of wave between antenna and environment.

In order to determine parameters of antenna, the plane metal screen has been used as a reference termination in free space $V_{Set}(f, x)$. The position of the screen was changed from zero plane x = 0 to 20 mm with a step of Δx=0.2 mm. On the basis of measured CRCs of reference termination of the „antenna–metal screen" system the frequency dependence of antenna parameters has been determined (Fig. 4). Fig. 5. shows the measured CRC of the screen $V_{Set}(f)$ for different positions x with accounting of antenna. Geometric parameters of antenna: distance from antenna aperture to zero plane 85 mm, aperture 25×25 mm, antenna length from nose to aperture is 65 mm.

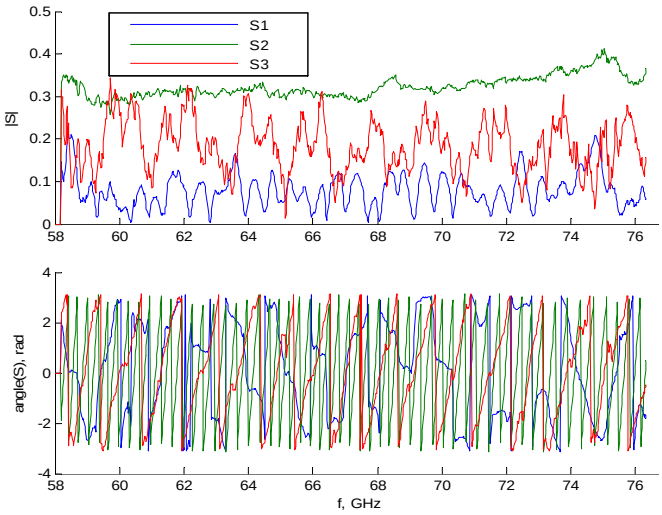

Fig. 4. Frequency parameters dependence of the model of horn antenna $S_{1...3}(f)$

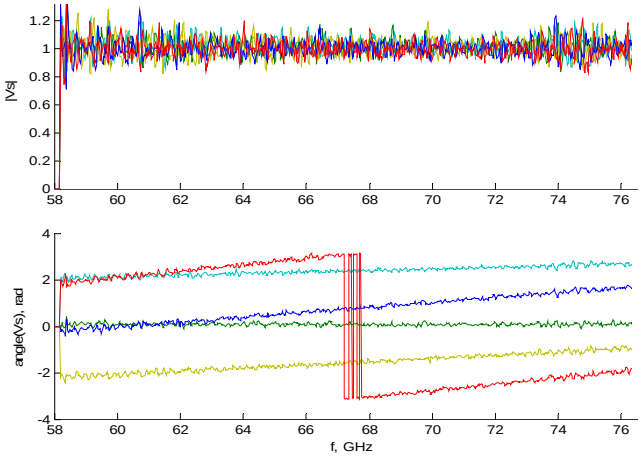

Fig. 5. Measured CRC of metal screen recalculated for free space $V_{Set}(f)$, drift of screen by $\Delta x=0.8$ mm

Let us consider the multi-layer dielectric structure and its reflection coefficient. Let assume that there is a plane electromagnetic wave propagating in the free space and it falls perpendicular onto the infinite (M–1)-layered environment on a semi-infinite substrate with flat interfaces, which CRC depends on the thickness of layers and electro-physical parameters of materials (Fig. 6).

$$V_s=V_s(f,h_1,..,h_{M-1},\varepsilon_1,..,\varepsilon_M,\mathrm{tg}\delta_1,...,\mathrm{tg}\delta_M).$$

where h_m, ε_m, $tg\delta_m$ are thickness, relative dielectric permeability and dielectric dissipation of the m^{th} layer, respectively. The CRC of flat-layered environment $V_s(f)$ is determined in the following way. The expression for the complex reflection coefficient can be written as [5]:

$$V_S = \frac{W_0 - Y_1}{W_0 + Y_1},$$

Here Y_1 is determined, depending on the number of layers, by recurrent relation:

$$Y_m = W_m \frac{Y_{m+1}(\exp q_m + 1) + W_m(\exp q_m - 1)}{W_m(\exp q_m + 1) + Y_{m+1}(\exp q_m - 1)}, \quad Y_M = W_M,$$

where $W_m = \sqrt{\varepsilon'_m / \mu_0}$; $q_m = 2j \cdot 2\pi f \cdot h_m \sqrt{\varepsilon'_m \mu_0 (1 - \sin^2\theta)}$; $\varepsilon'_m = \varepsilon_0 \varepsilon_m (1 - j \cdot \mathrm{tg}\,\delta_m)$ is complex dielectric permeability of the m^{th} layer; ε_0, μ_0 is absolute dielectric and magnetic permeability of vacuum.

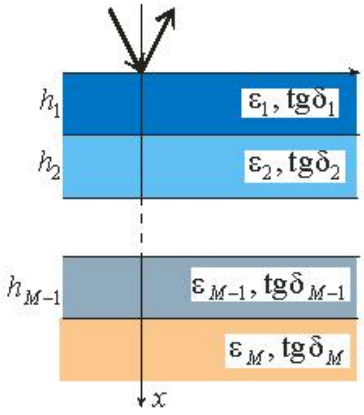

Fig. 6. Model of multi-layer dielectric structure.

Experiments on measuring of CRC of metal screen at different distances from the zero plane have been conducted. Fig. 7 shows the dependence of the module of measured CRC of metal screen $|V_s|$ at the distance to zero plane x. As results of energy losses due to dissipation beyond limits of the antenna aperture projection the efficient reflection coefficient, determined by the plane wave model, decreases with a distance. At the solution of inverse problem this would lead to incorrect interpretation of parameters of layered structure, particularly in the case of substantial length.

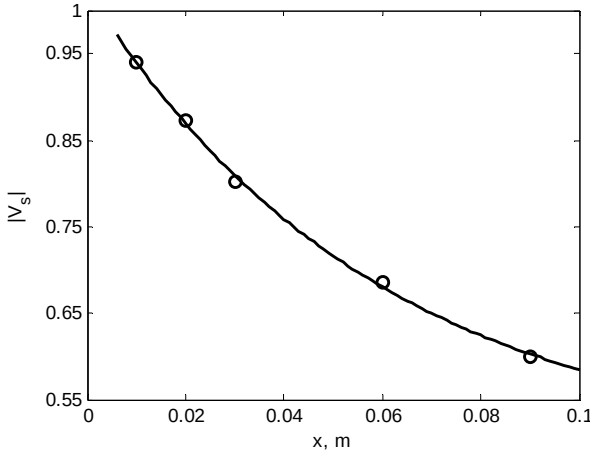

Fig. 7. Dependence of reflection coefficient model on the distance from the screen: ° experiment; — approximation $|V_s| \sim e^{-\alpha x}$.

It can be seen from Fig. 7, the change in reflection coefficient, and hence the wave amplitude can be approximately described by exponential dependence on the coordinate by the same law as for amplitude of plane wave in dielectric with losses. Thus, losses of energy for dissipation can be accounted in frames of plane wave by introduction of additional dimensionless parameter γ, which does not depend on coordinates and parameters of environment. For dielectric under condition of $\mathrm{tg}\delta_m << 1$, $\gamma << 1$ the dependence of progressive wave amplitude on coordinate with account of dissipation can be written as [1]:

$$|A_m| \sim \exp\left(-\frac{1}{2} \cdot 2\pi f \cdot \sqrt{\varepsilon_m \varepsilon_0 \mu_0} \cdot (\mathrm{tg}\,\delta_m + \gamma) \cdot x \right),$$

where ε_0, μ_0 are absolute dielectric and magnetic permeability of vacuum. Then the complex dielectric permeability of the m^{th} layer with account of losses for lateral dissipation:

$$\varepsilon'_m = \varepsilon_0 \varepsilon_m (1 - j \cdot (\mathrm{tg}\,\delta_m + \gamma)).$$

2. Experimental study of inverse problem for diagnostics of flat-layered dielectric

The inverse problem (IP) is to determine the vector of the sought-for parameters of flat-layered environment **p*** by the measured frequency dependence of the CRC [2,3] and can be solved by the method of functional minimization

$$\mathbf{p}^* = \inf_{\mathbf{p} \in \mathbf{P}} F(\mathbf{p}),\ F(\mathbf{p}) = \sum_{i=1}^{N_f} \left| V_S^{ex}(f_i) - V_S^{th}(\mathbf{p}, f_i) \right|^2,$$

where N_f is the number of frequency responses.

The CRC of fluoroplastic was determined and the inverse problem on parameters of flat-layered structure $\mathbf{p}=(h_1, h_2, \varepsilon_2, \mathrm{tg}\delta_2)$, where h_1 is a distance to the plate, h_2, ε_2, $\mathrm{tg}\delta_2$ – are thickness and electrophysical parameters of fluoroplastic. Fig. 8 shows measured and calculated by the plane wave model CRC

for fluoroplastic plate. The γ parameter has been estimated experimentally. If to account the γ dissipation parameter, parameters of dielectric are much closer to reference data that those determined by the plane wave model (see Table 1).

Fig. 9 shows the particular case of IP, namely the objective function for determination of geometric parameters of structure – position and thickness of the plane $F(h_1, h_2)$. Fig. 10 presents the objective function from dielectric permeability and thickness of the plate $F(h_2, \varepsilon_2)$. It can be seen from the figure, that the objective function is multiextremal, therefore methods of global minimization should be used in order to solve it.

Table 1. Estimation of dielectric (fluoroplastic) parameters

Environment parameter	Model of plane wave	Model accounting the dissipation	Additional data
γ	–	$(4.7\pm0.1)\times10^{-3}$	–
h_2, *mm*	*7.78*	8.193 ± 0.005	–
ε_2	*2.110*	2.068 ± 0.01	*2.07*
$tg\delta_2$	5.18×10^{-3}	$(0.48 \pm 0.1)\times10^{-3}$	0.4×10^{-3}

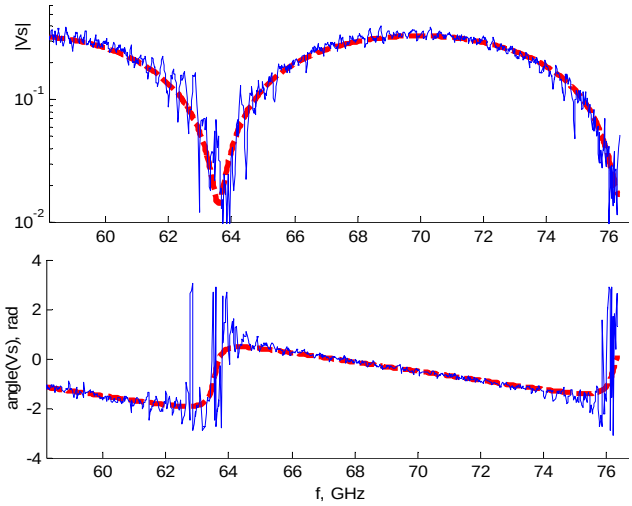

Fig. 8. CRC of fluoroplastic plate:
— experiment; "" the calculated CRC for plane wave.

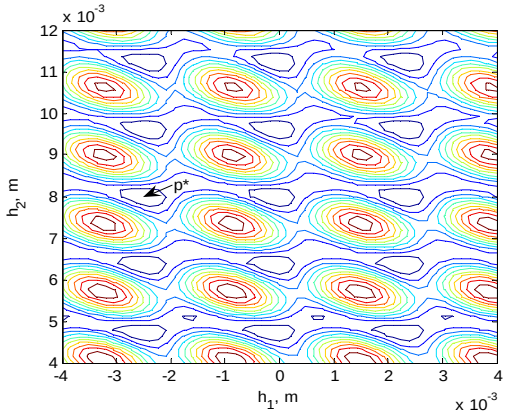

Fig. 9. Objective function of the IP for determination of location and thickness of the plate $F(h_1, h_2)$, $\boldsymbol{p}^*$=(-0.00249; 0.00819).

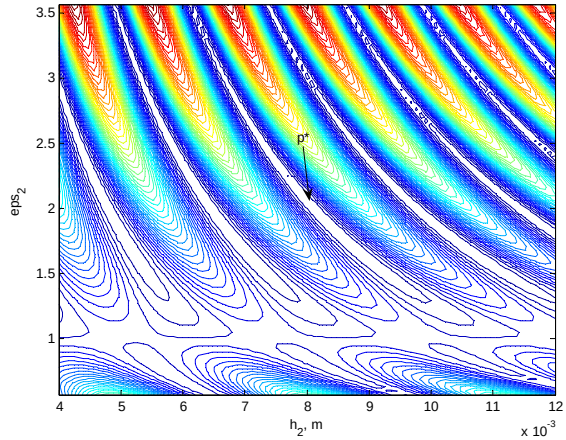

Fig. 10. Objective function of the inverse problem for determination of parameters of dielectric plate $F(h_2, \varepsilon_2)$, global minimum $p^*=(0.00819, 2.07)$.

3. Estimation of the influence of different factors on results of microwave diagnostics

Experimental studies of the influence of interfering factors on result of diagnostics of layered structures have been conducted. One of such factors is the deviation of antenna axis from the normal to the surface. Fig. 11. presents the CRC of metal screen in the case of 1.8° axis deviation.

Fig. 12 shows the range average reflection coefficient and dispersion in relation to model signal depending on the angle between the normal to the surface and the antenna axis.

It can be seen from figures, the change of angle between normal and antenna axis causes the decrease of the power of the sensed signal, at angles below 1° the influence is insignificant, and then it grows substantially. However such a deviation is detected by sight and can be removed without additional measurements.

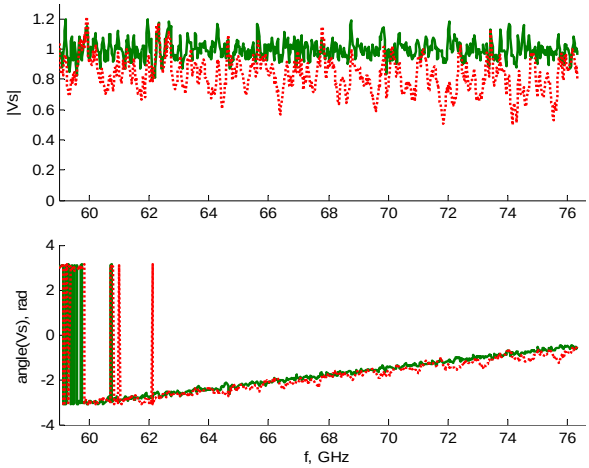

Fig. 11. CRC of the screen in the case of deviation of antenna axis by 1.8° from the normal.

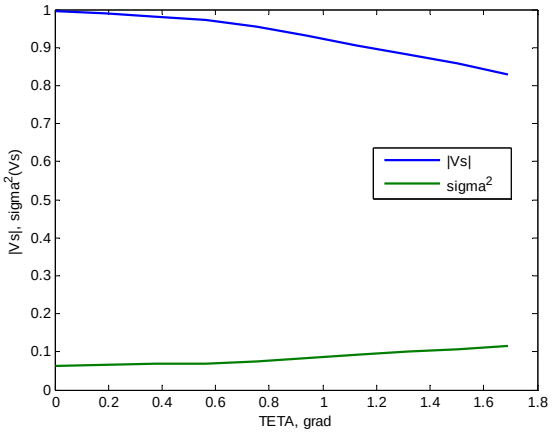

Fig. 12a. RC and dispersion for the metal screen in the case of tilt distortion

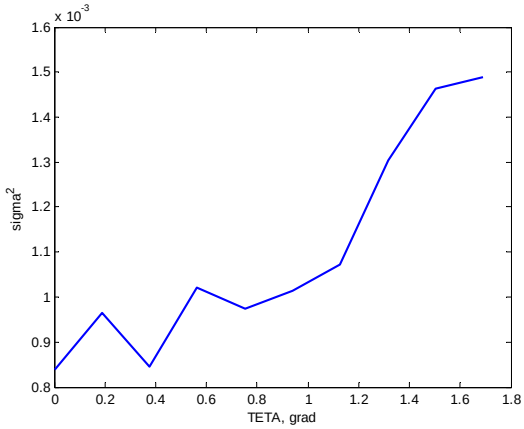

Fig. 12b. Dispersion for dielectric plate in the case of tilt distortion.

Let consider now the influence of edges of the structure on measurements results. Fig. 13 presents changes of the CRC during the drift of the screen relatively to the aperture projection, Fig. 14 shows the averaged module of the RC of the screen long the range during its drift.

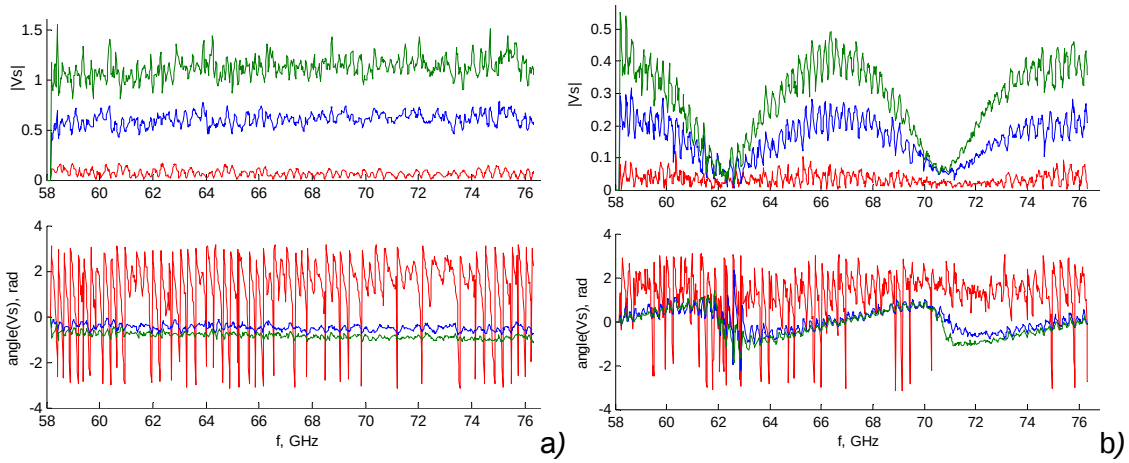

Fig. 13. Reflection coefficients from metal screen (a) and dielectric plane (b), moving over the antenna: red – screen on the edge of aperture projection, blue – screed half-shields the aperture projection, green – screen completely shields the aperture projection.

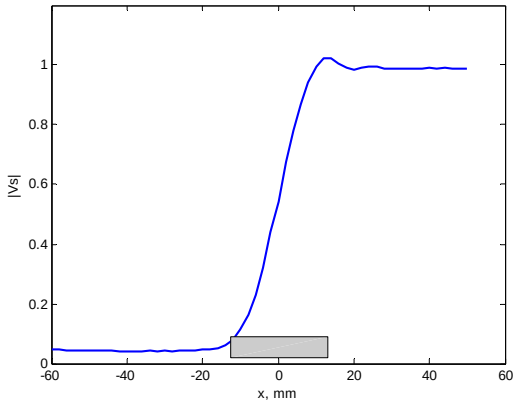

Fig. 14. Dependence of RC module on the position of screed related to the axis of antenna aperture.

It can be seen from figures, the signal substantially changes, when projection of aperture crosses the edge of screen, during approaching of antenna to the edge of the structure the influence of edge can be neglected. Conclusions are related only to the far-field region *(d>A/4λ),* for the near-field region additional studies are needed.

4. Modernization of the portable microwave NDT device

As was noted before, the range of application and resolution capacity of microwave method directly depends on the width of frequency range for measurement of complex reflection coefficient. That is why we analyzed possibilities to widen frequency range of the HK device. During the preliminary stage of the project we made a decision to change technical design of the controlled generator of the 3-mm wavelength range. New design foresees the use of wide-band generator controlled by voltage on the Gunn diode in the 8-mm range and frequency multiplier for transition into the 3-mm range. This approach would provide much wider (at least 5 times) frequency readjustment band, than the available solid state oscillators in this frequency range.

The model of the generator has been assembled and tested. Fig. 15 illustrates appearance of the model of generator with frequency readjustment.

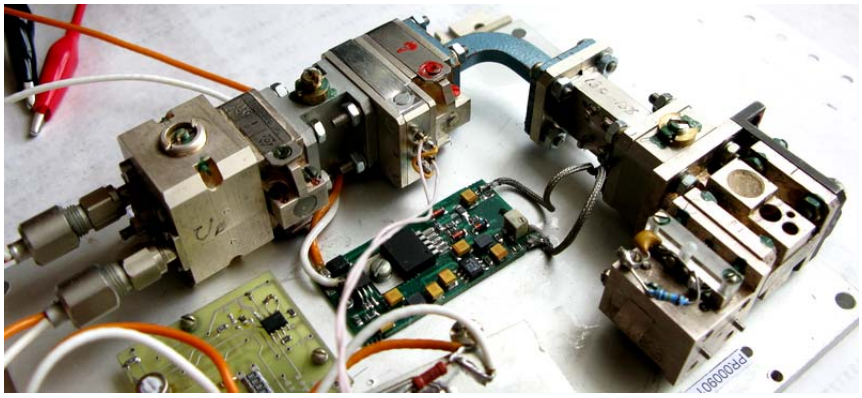

Fig. 15. Model of the unit for generation of 3-mm range.

The structural scheme of the generator is presented in Fig. 16. Here the voltage-controlled generator (**VCG**) is the waveguide structure with the 7.2×3.4 mm cross-section of the waveguide. In the middle of waveguide chamber, perpendicular to the axis of the waveguide there are Gunn diode and varactor diode. Both diodes are in cases. From one side of the chamber there is the short circuitor, from the output side there is an iris. At the exit from generator in order to decrease the influence of the outside load and provide stability of regime of soft agitation of generator the ferrite isolator (FI1) is installed.

Current of Gunn diode in working regime is ~1.2 A, feeding voltage is ~3.6 V. Voltage, supplied to the varactor diode, changes in the range +0.5 V ... 20 V. In such a case frequency of generator changes in the range of 31....33 GHz under output power of 20...35 mW.

Since the changes in environment temperatures change the current of Gunn diode, geometric dimension of waveguide chamber and parameters of varactor diode, under constant controlling voltage the frequency of the output signal will be changed on varactor diode. In Table 2 and Fig. 17 we provide dependencies of signal frequency from generator at different environment temperatures (it was measured by thermal sensor on the case of generator). In can be seen from figures, the changes of frequency $\Delta f \approx 30$ MHz at $\Delta T = 50°C$ ($U_{var} = 10$ V). It is also seen that the decrease of U_{var} the temperature instability of generator frequency increases.

After the ferrite isolator on generator waveguide attenuator (AT) with fixed attenuation, after that follows attenuator-modulator. The structure made of p-and-n diodes installed inside the waveguide section is used as controlling element of the modulator. It is used for modulation of generator signal (modulation depth is of ~3 dB and installed during adjustment of detectors unit).

The signal comes to the power amplifier (УМ). The fixed attenuator (AT) is used for setting the level of output power of driving oscillator at the entrance of amplified. The optimal power level at the entrance of amplifier is in the range 1.5...2.5 mW. The amplifier uses the МИС СНА3093а transistor microassembly (K= 18…20 dB, P_{-1} = 20…22 dBm, power supply ~ 350 mW, supply voltage +3.5 V). With the help of the second attenuator (AT) the level of the output power at the entrance of frequency multiplier (FM), P_{in}= 100...130 mW is provided (see Table 2).

Frequency multiplier "×3" (FM) is the waveguide structure of „overlapping cross". Along the axis of waveguides intersection there is a compound coaxial concordance structure, which serves as a filter as well. From one side of the coaxial structure there is a diode with Schottky barrier of honeycomb structure. The contact with the diode is provided with the help of tungsten needle. Agreement of multiplier at entrance and exit (wavelength channel of 2.4×1.2 mm^2) is performed with the help of short-circuitor pistons.

As a results of tuning of the FM under conditions of the maximum bandwidth we obtained levels of output power P_{out} > 1 mW, the output signal frequencies changing in the range of 92.4...98.5 GHz (Table 3, Fig. 18).

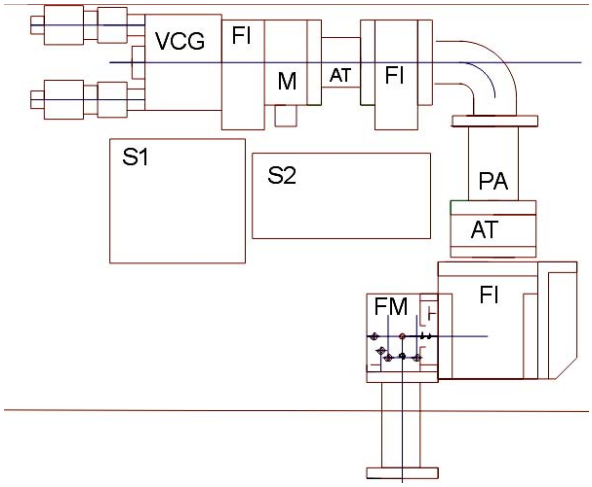

Fig. 16. Overall and functional scheme of the voltage-controlled generator block:
VCG – generator on the Gunn diode; FI – ferrite isolator; AT – fixed attenuator; M – attenuator-modulator; PA – power amplifier; FI – ferrite circulator (isolator); FM – frequency multiplier; S1 – power source for Gunn oscillator (+12 V, 1.5 A, controlling voltage U_{var}=0.5...20 V); S2 – power source for power amplifier (+5 V, 0.35 A).

Table 2. Dependence of output frequency and Gunn oscillator power on control voltage U_{var} and temperature.

U_{var}, V	0°C		20°C		50°C		P (PA), mW
	f, GHz	P, mW	f, GHz	P, mW	f, GHz	P, mW	
0.5	30.923	169	30.795	162	30.651	153	101
1	30.965	170	30.848	165	30.726	154	104
2	31.080	173	30.955	168	30.869	160	109
3	31.163	176	31.124	172	31.079	164	115
4	31.291	173	31.255	171	31.227	164	119
5	31.463	162	31.408	162	31.401	156	121
6	31.625	164	31.597	160	31.567	152	122
7	31.790	170	31.758	165	31.729	156	128
8	31.914	175	31.891	170	31.875	161	131
9	32.050	177	32.037	172	32.009	161	130
10	32.180	180	32.164	175	32.151	159	129
11	32.302	180	32.275	174	32.264	154	129
12	32.428	180	32.401	173	32.363	148	130
13	32.539	175	32.518	167	32.484	146	130

14	32.609	167	32.596	156	32.574	134	129
15	32.717	171	32.701	158	32.676	132	129
16	32.787	160	32.768	150	32.758	125	125
17	32.870	167	32.852	150	32.835	123	126
18	32.918	174	32.918	162	32.897	140	132
19	32.974	178	32.964	168	32.948	150	134
20	33.020	180	33.009	172	32.993	158	137

Table 3. Dependence of generator frequency and power on control voltage U_{var}.

U_{var}, V	20 ℃	
	f. GHz	*P. mW*
00.5	92.40	1.7
01	92.55	1.7
02	92.85	2.3
03	93.36	3.9
04	93.75	4.4
05	93.42	4.2
06	94.80	5.7
07	95.27	5.7
08	95.70	7.1
09	96.11	6.1
10	96.49	5.5
11	96.82	5.5
12	97.20	5.5
13	97.55	5.3
14	97.79	3.9
15	98.10	2.9
16	98.30	1.2
17	98.55	0.56
18	98.75	0.42
19	98.90	0.35
20	99.03	0.31

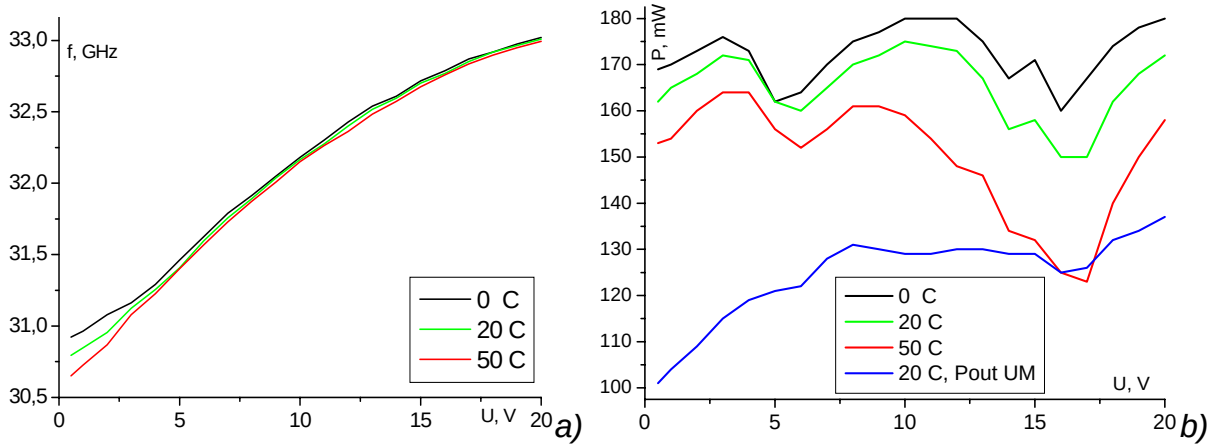

Fig. 17. Output frequency (a) and power (b) of Gunn oscillator at different temperatures of environment.

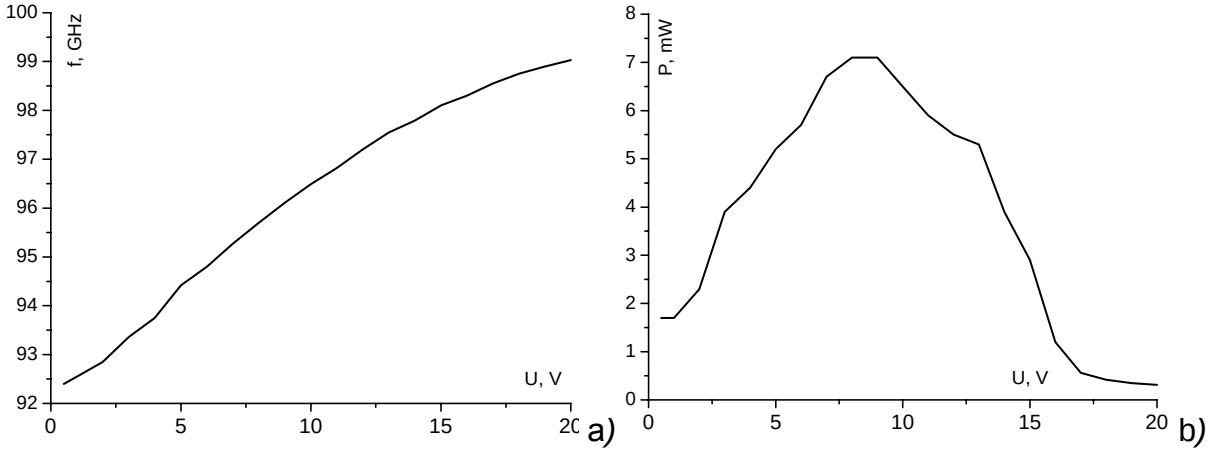

Fig. 18. Output frequency (a) and power of generator set (b).

5. Conclusions.

By improvements in the UHF path on the automated test bench of microwave NDT we succeeded in widening of the CRC measuring range up to 18 GHz (f = 56..78 GHz), precision of frequency determination ±0.02 GHz, extinction coefficient in range 0..30 dB with a precision of ±1%, complex reflection coefficient is determined with the precision of 0.01 a. u.

The model for probing of layered environment has been built. It accounts a complete antenna dissipation matrix as a path-through quadrupole, which accounts the availability of re-reflections of proving signal between antenna and environment. An additional parameter is introduced into the model of interaction between the probing field and flat-layered structure which describes the amplitude decrease of the proving field with a distance because of energy losses for radiation outside antenna aperture. This is shown to increase reliability of solution of inverse problem on determination of parameters of single-layer dielectric.

The influence of such interfering factors as the tilt of antenna axis and edge of the structure during measurements in the far-field zone on results of diagnostics has been checked experimentally.

The model for the generator module of the NDT device has been assembled, its frequency range, power and temperature instability have been determined. Under maximum bandwidth during changes of output signal frequency in the range 92.4...98.5 GHz the levels of output power $P_{out} > 1$ mW have been obtained.

6. References

1. Nondestructive testing and diagnostics / V. V. Klyujev, F. R. Sosnin,… Mashinostrojenie, Moscow, 1995, 488 p.
2. Kolodiy B.I., Ljashchuk O.B. Direct and Inverse Problems of Electromagnetic Waves Reflection from the Anisotropic Dielectrics // Proc. VI International Conference on Mathematical Methods in Electromagnetic Theory (MMET'96) - Lviv. 1996. - P.453-456.
3. Kolodiy B. I., Ljashchuk O. B. Methematical models, methods, and algorithms used for the radiowave diagnostics of multilayer dielectrics // Material Science, Vol. 33. No.5, 1999. – P. 639-649.
4. J.Wait, "Electromagnetic waves in stratified media", Pergamon Press, Oxford – etc., pp.608, 1970.
5. Kukush V. D. "Electro and radio measurements", Radio i svyaz, Moscow, 1985.
6. Volman V. I., Pimenov Yu. B. "Technical electrodynamics", Svyaz, Moscow, 1971.

VI. CONDUCTING OF THE PRECISE PHYSICAL EXPERIMENTS

1. Experiment description

The sketch scheme of experimental devise is provided in Fig. 1. Automated test bench allows measuring CRF of loadings in the 58...76 GHz frequency range. The test bench works as an interferometer on the basis of double T-bridge. The unknown loading V (specimen under control) is joined to one of shoulders of this bridge, the calibrated loading V_C – into the other. The output signal of the bridge– "unbalance signal" – is measured and on the basis of the bridge scheme model the complex reflection factor of the unknown loading is determined.

Loading is the successively joint transmitting-receiving horn antenna and a structure, which CRF V_S is to be determined. In the test bench model the antenna is considered as feed through linear quadruple, described by a complex scattering matrix.

The relation between the measured V(f) loading CRF and flat-layered environment CRF $V_S(f)$ (Fig. 1) can be written as

$$V_S = \frac{S_1 - V}{S_1 S_3 - S_2 - S_3 V},$$

where $S_1,..,S_3$ are complex factors, which can be experimentally determined. Parameters of bridge circuit and antenna have been determined during previous stages.

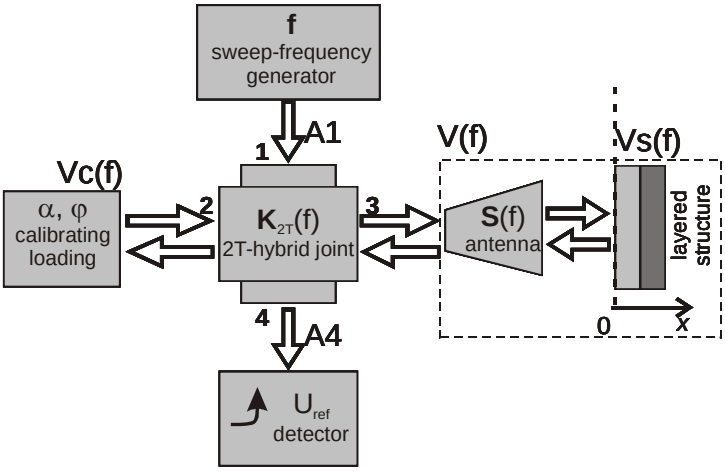

Fig. 1. Schematic model of the test bench:
f is oscillation frequency generator; U_{ref} is detector of the reflected wave signal; V_c is the CRF of the calibrated loading; $\mathbf{K}_{2T}$ is dissipation matrix of the doubled T-bridge; V(f) is CRF of loading under measurement; **S**(f) is antenna; $V_S(f)$ is CRF of flat-layered environment in free space.

Fig. 2 shows the scheme of experiment on diagnostics of exfoliation in dielectric plate. Exfoliation was modeled by a gap between two dielectric plates. Paper sheets of the 0.09±0.01 mm thickness were positioned between plates, so the gap thickness was changed in the 0…0.5 mm range.

The plexiglass was chosen and materials for layers of model structure. This material is cheep and available. Its optical transparency allows controlling the experiment process. The drawback of this materials is a large dispersion of electrophysical parameters between different samples due to different chemical

composition. Therefore before modeling multilayer structure parameters of each sample should be determined.

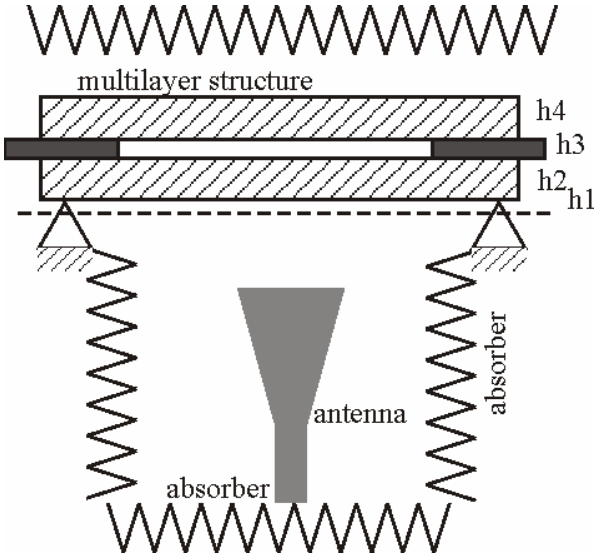

Fig. 2. Modeling of exfoliation in dielectric layer, scheme of experiment

Let consider the model of interaction between the probing field and the structure under control. Let assume, that a flat electromagnetic wave is spread in free space and falls perpendicularly onto infinite (M–1)-layered environment on semi-infinite support with flat interfaces, which CRF depends on thicknesses of layers and electrophysical parameters of materials.

$$V_S=V_S(f;\, h_1,..,h_{M-1},\varepsilon_1,..,\varepsilon_M,\mathrm{tg}\delta_1,...,\mathrm{tg}\delta_M). \qquad (1)$$

where h_m, ε_m, $tg\delta_m$ are thickness, relative dielectric permeability and tangent of loss angle of m-th layer, respectively. The model also accounts energy loss for scattering beyond the antenna aperture.

Let model dielectric plate with exfoliation by M–1=4–layered structure, where the layers are:

1) air gap between zero plane and structure, thickness of the layer h_1 can be negative, air ($\varepsilon_1=1$, $tg\delta_1=0$, fixed parameters);

2) first dielectric layer, thickness h_2 and parameters ε_2, $tg\delta_2$ can be unknown or fixed, depending on the purpose of experiment.

3) exfoliation, thickness h_3 is unknown, parameters depend on filling and correspond to either air ($\varepsilon_3=1$, $tg\delta_3=0$, fixed parameters) or paper (parameters should be determined);

4) the second dielectric layer, thickness h_4 and parameters ε_4, $tg\delta_4$ can be unknown or fixed, depending on the purpose of experiment.

The fifth semi-infinite slab is air.

The inverse problem (IP) for diagnostics of structure consists in determination of the vector of sought parameters **p*** by the measured frequency dependence of CRF and can be solved by minimization of functional

$$\mathbf{p}^* = \inf_{\mathbf{p}\in\mathbf{P}} F(\mathbf{p}),\ F(\mathbf{p}) = \sum_{i=1}^{N_f} \left| V_S^{ex}(f_i) - V_S^{th}(\mathbf{p}, f_i) \right|^2, \qquad (2)$$

where N_f is the number of frequency readings. The special software for solution of the operatore equation (2) has been developed. It includes effective algorithm for solution of direct problem (1) and minimization of objective function $F(\mathbf{p})$ with the use of global minimization method. The program allows the researchers to choose the vector of sought parameters and fix known parameters.

2. Estimation of dielectric plate parameters

Before studying multilayered structures the plate material parameters should be determined.

The CRF of the plexiglass plate was measured and the inverse problem for determination of flat-layered structure $\boldsymbol{p}=(h_1, h_2, \varepsilon_2, tg\delta_2)$, where h_1 is the distance to the plate, h_2, ε_2, $tg\delta_2$ are thickness and electrophysical parameters of plexiglass, has been solved. Fig. 3 shows the CRF of the plate, measured and calculated by the model of plane wave. Experimentally measured CRF of the plate is shown by solid line; the model approximation resulted from the IP solution is shown by dashed line.

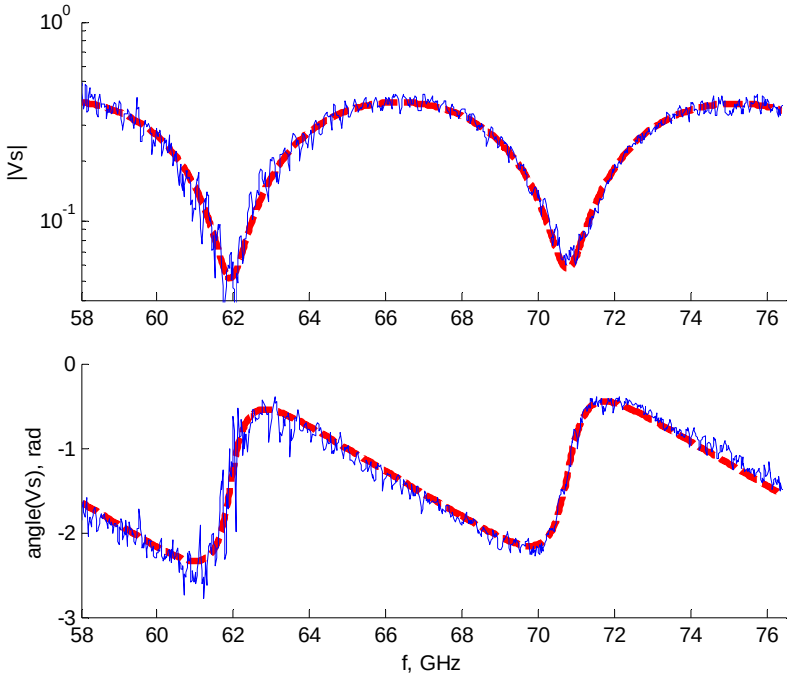

Fig. 3. Evaluation of the plexiglass plate parameters: h_1*=–0.358 mm,* h_2*=10.561 mm,* ε_2*=2.574,* $tg\delta_2=6.31\times10^{-3}$.

3. Experimental study on diagnostics of exfoliation in dielectric structures

In order to study the sensitivity of radio-wave method to parameters of dielectric structures we have measured the frequency dependences of CRF of model structures. Dependences of CRF on thickness and material of filling for exfoliation in the plate have been studied.

Fig. 4 illustrates experimentally measured frequency dependences of CRF of model structures with different gap thicknesses. Fig. 5 shows CRF for gaps of the same thickness but with different filling (air and paper). It can be seen from Figures, that radio-wave method in far zone is sensitive to the thickness and filling of exfoliation in dielectric. The CRF of structure with exfoliation between dielectric and metal screen (Fig. 6) has been studied as well.

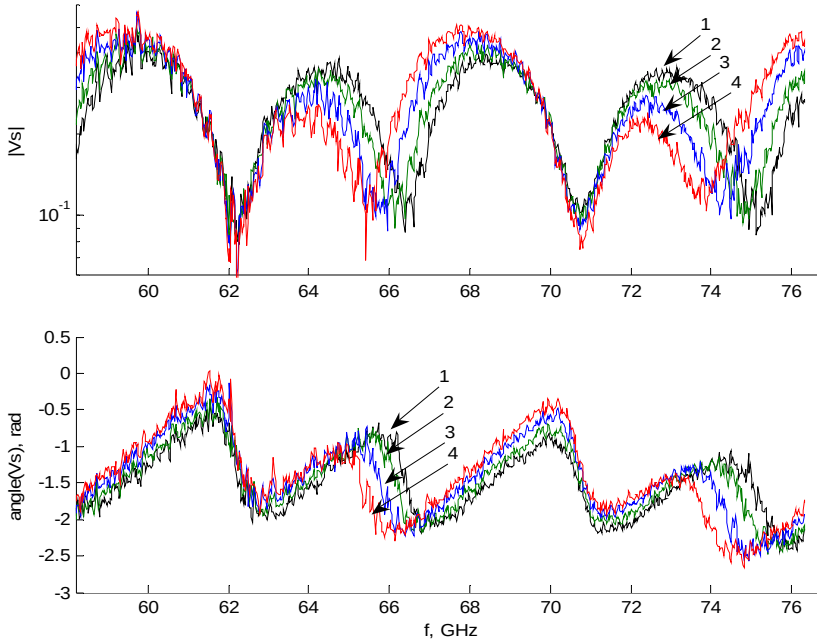

Fig. 4. Modeling of exfoliation in dielectric plate.
Two plexiglass plates of 10,5 mm thickness, air gap, filled by paper sheets:
1 – without exfoliation, 2 – 1 sheet exfoliation, 3 – 2 sheet exfoliation;
4 – 3 sheet exfoliation.

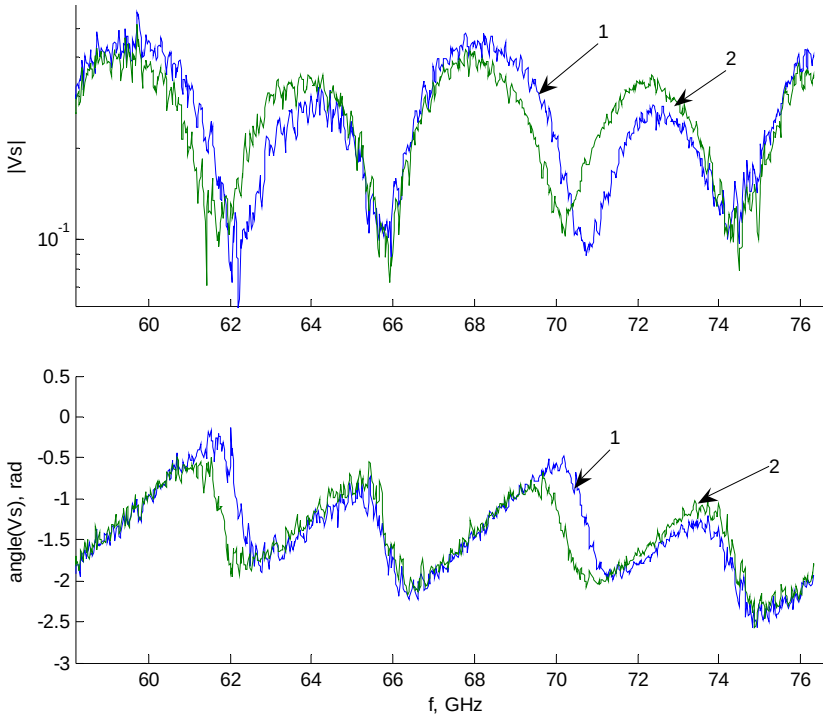

Fig. 5. Modeling of exfoliation in plate. Two plexiglass plates 10,5 mm, 1 – exfoliation of 3-sheet thickness with air; 2 – exfoliation with 2 sheets of paper.

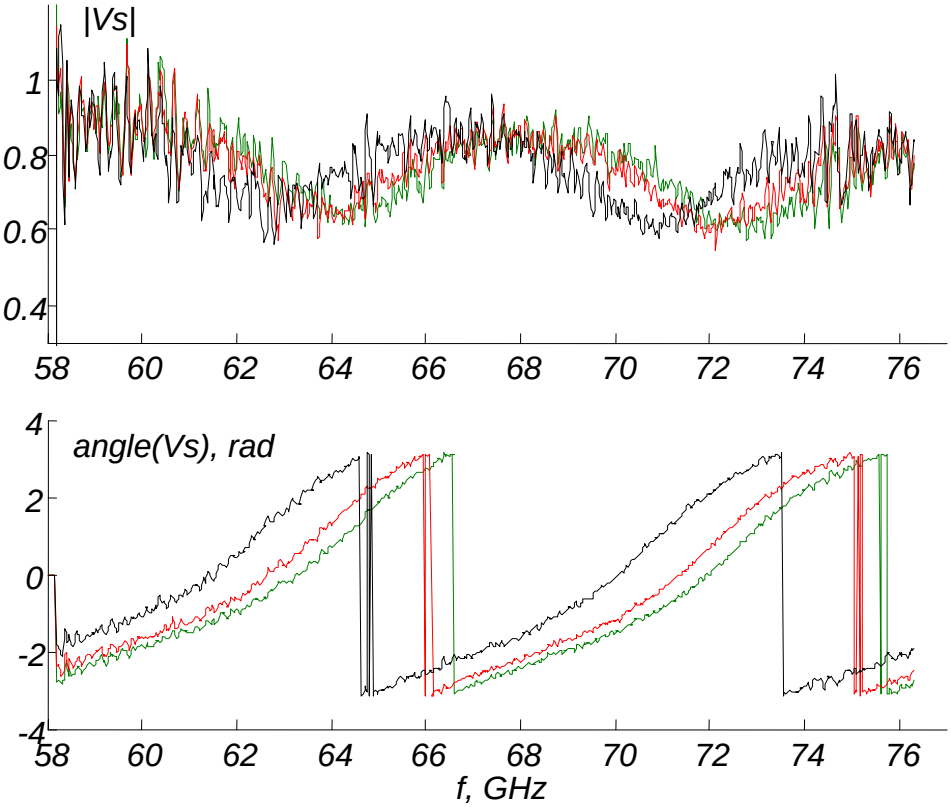

Fig. 6. Modeling of exfoliation between dielectric and metal, plexiglass plate 10,5 mm, Al screen; green – without exfoliation, red – exfoliation of 2 sheets, black– exfoliation of 6 sheets.

4. Study of the inverse problem for diagnostics of exfoliation in dielectric

Let consider the inverse problem for determination of parameters in the structure with exfoliation. Fig. 7…9 present experimental and theoretically approximated dependences of CRF for structures with different exfoliation depth (h_3). The measured dependence of CRF $V_S^{ex}(f)$ is shown by solid line, modeled dependence of CRF пунктиром – модельовану $V_S^{th}(f)$, obtained from the solution of inverse problem is shown by dash line. We can see that the proposed model for reflection factor describes the experimental data rather good.

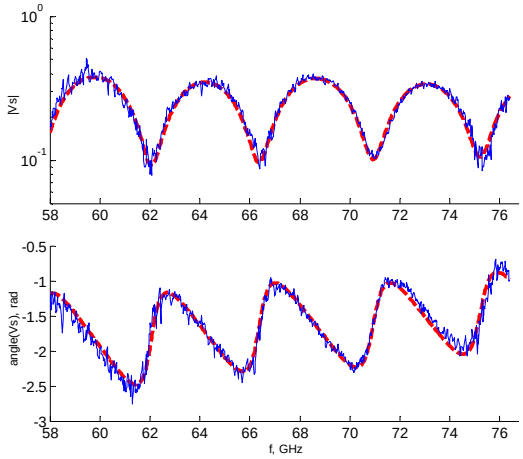

Fig. 7. Two plexiglass plates without a gap

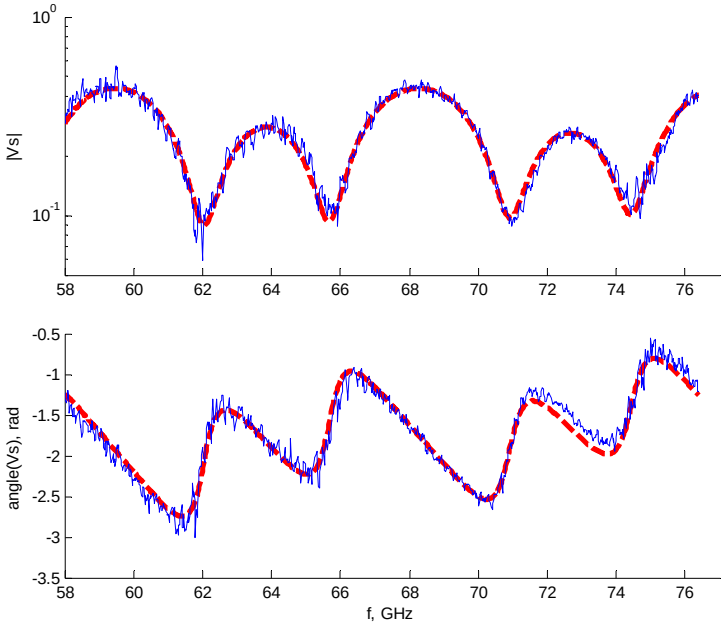

Fig. 8. Two plexiglass plates, gap of 2 sheets

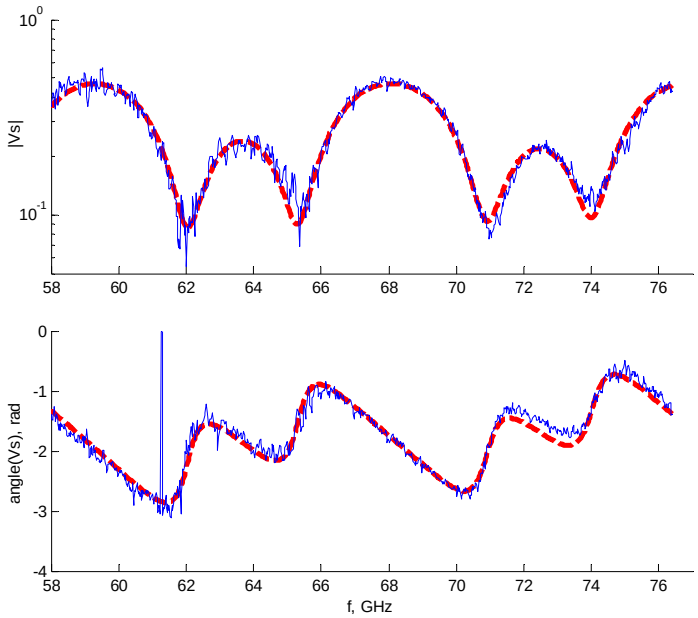

Fig. 9. Two plexiglass plates, gap of 3 sheets

Several options of the inverse diagnostics problems have been considered:
1) determination of structure position, thickness and dielectric permeability of exfoliation: **p**=(h_1, h_3, ε_3);
2) determination of structure position, thickness of the first layer and exfoliation **p**=(h_1, h_2, h_3);
3) determination of structure position, thickness of the first layer and exfoliation and the third layer: **p**=(h_1, h_2, h_3, h_4).

Thickness of exfoliation was changed from 0 to 6 sheets of paper with 0,09±0,01 mm thickness. Results of diagnostics are compiled in Tables 1..3. The average values and dispersion of estimated parameters of structures are provided as well. The thickness of exfoliation can differ from the thickness of inset since sheets can have own curvature. Therefore we consider as a parameter the changes of the determined gap thickness after adding one sheet Δh_3, which corresponds to the thickness of one paper sheet, used for reaching exfoliation thickness.

Table 1. Solution of IP for **p**=(h_1, h_3, ε_3).

Exfoliation, number of paper sheets (~0,09 mm)	0	1	2	3…	Average (from 1..6)	σ
h_1*, mm	-0,5293	-0,5111	-0,4935	-0,4856	–	–
h_3*, mm	7,7e-10	0,060	0,155	0,245	–	–
Δh_3*, mm	–	0,0601	0,0950	0,0902	0,0915	0,003
ε_3*	–	0,380	0,678	0,807	0,923	0,065

Table 2. Solution of IP for **p**=(h_1, h_2, h_3).

Exfoliation, number of paper sheets (~0,09 mm)	0	1	2	3…	Average (from 1..6)	σ
h_1, mm*	*-0,5245*	*-0,5080*	*-0,4911*	*-0,4852*	–	–
h_2, mm*	*10,519*	*10,528*	*10,542*	*10,549*	*10,540*	*0,007*
h_3*, mm	0,027	0,0881	0,1743	0,2590	–	
Δh_3*, mm	–	0,0613	0,0862	0,0846	0,0854	0,0008

Table 3. Solution of IP for **p**=(h_1, h_2, h_3, h_4).

Exfoliation, number of paper sheets (~0,09 mm)	0	1	2	3…	Average (from 1..6)	σ
h_1*, mm	-0,5245	-0,5079	-0,4911	-0,4849	–	–
h_2*, mm	10,664	10,586	10,570	10,564	10,573	0,008
h_3*, mm	0,03559	0,0961	0,1854	0,2736	–	–
Δh_3*, mm	–	0,0604	0,0893	0,0883	0,0888	0,0005
h_4*, mm	10,407	10,490	10,510	10,513	10,504	0,009

Fig. 10 displays the dependence of CRF for the structure with exfoliation filled by paper. The inverse problem on determination of structure position, thickness of exfoliation and its dielectric permeability has been solved. It can be seen that the solution for the thickness of exfoliation is close to the thickness of two sheets of paper.

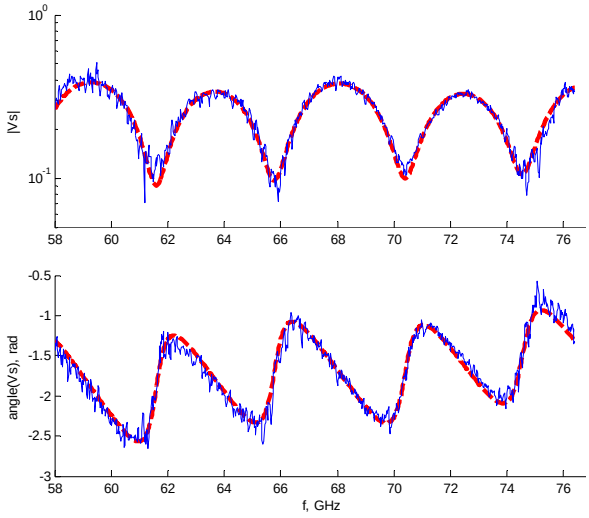

Fig. 10. Two plexiglass plates, зазор 2 листи, заповнення папір, h_3*=0,179 mm, ε_3*=3,066.

Fig. 11 illustrates the CRF from plexiglass plates and metal screen, between which the exfoliation of different width is created. The position of the plate and the thickness of exfoliation have been determined.

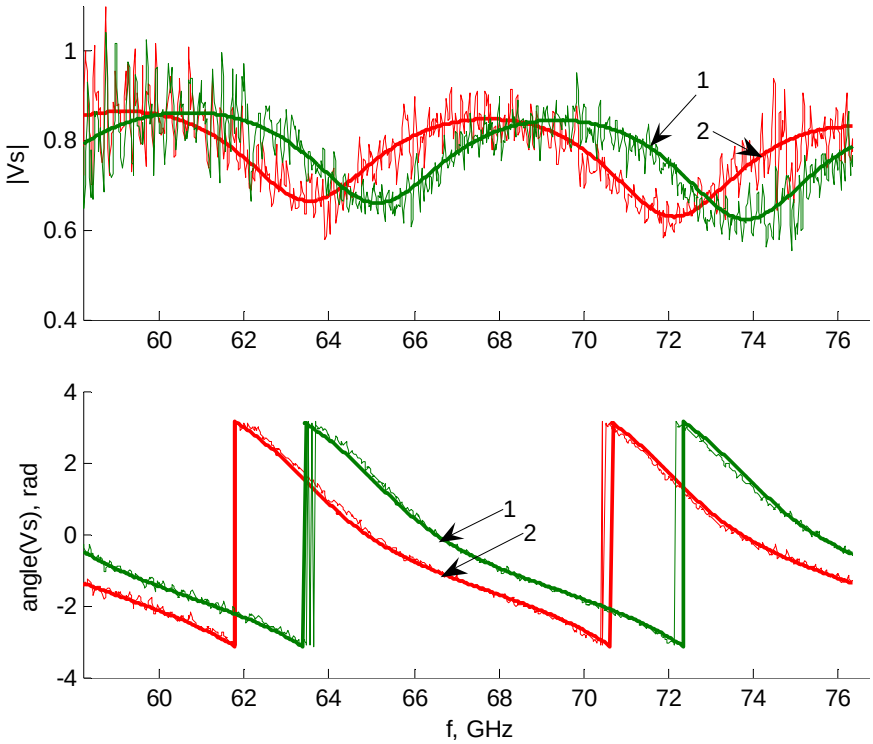

Fig. 11. Plate made of plexiglass, gap and Al screen:
1 – h_3*=0,021 mm (without exfoliation); 2 – h_3*=0,593 mm (6 plates).

5. Conclusions

For different setups of inverse problem of diagnostics the estimated structure parameters are somewhat different. This is related to errors in measurements, deviation of actual geometric and electrophysical parameters from the set, and by errors of the model, which describes the interaction between field and environment. In most cases these discrepancies are within limits of errors of conventional thickness measurements, e.g. by micrometer.

For the first problem (see Table 1) the estimated dielectric permeability of exfoliation ε_3* differs from physically possible, however, with the rise of the gap it approaches to the real one (ε=1 for air). Similarly, the geometric thickness of the gap in the case #1 differs from experiments #2 and #3. This can be explained by the fact that the thickness and dielectric permeability in the direct problem are related parameters. It has been shown experimentally, that the thinner is the layer, the more difficult is to determine simultaneously its thickness and dielectric permeability.

Radio-wave method in far irradiation zone with multifrequency probing, measurement of CRF and solution of IP allows measuring thicknesses of separate layers of structure and their electrophysical parameters with precision, sufficient for practical application. It is sensitive to changes in thickness of structure of 0.01 mm range and exfoliations in dielectric plate of 0.1 mm range of thickness.

VII. INVESTIGATION OF THE REAL DIELECTRIC STRUCTURES AND THE DEVELOPMENT OF THE DIAGNOSTICS TECHNIQUE.

1. Development of the method for testing flat-layered dielectric structure for apparatus of non-destructive testing.

On the previous stages of the project we have considered the method of NDT of layered dielectric structures, based on the determination of complex reflection factor (CRF) from the structure accounting properties of measuring tract, antenna and the use of model of interaction between probing wave and environment. The CRF is an important informative parameter for study of the interaction between the probing field and the object under control. Such an approach allows observe illustratively the connection between parameters of structure and electromagnetic field, estimate adequacy of the model and sensitivity of the method to the changes of environment parameters. Measurement of the CRF is the main mean for building of mathematical model of measuring tract and transceiver antenna.

However, for calculation of the CRF by the proposed method one should measure output signal of the bridge scheme at several different (not less than three) values of the phase of the reference signal, so the calibrated phase-twister should be readjusted during measurements. This complicates the procedure, which is not acceptable for the NDT device.

Therefore we propose to use to use the output signal of the bridge scheme on many frequencies as informative parameters and on the basis of the model of this signal to determine parameters of dielectric structure.

Let remind the model of output signal, described in the previous report. Fig. 1 presents the model of the bridge scheme.

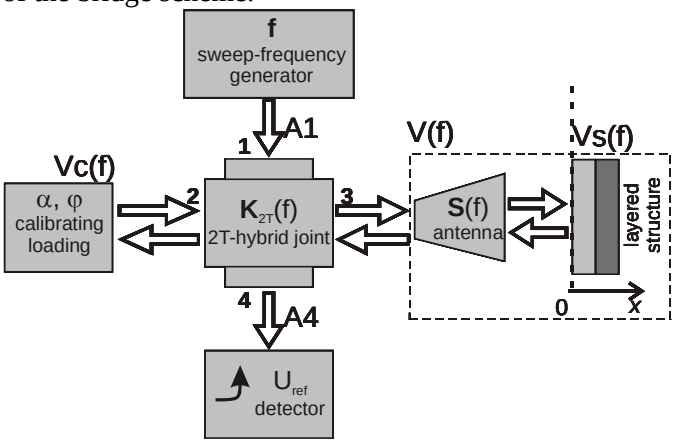

Fig. 1. Schematic model of test bench:
f is sweep frequency generator;
U_{ref} is detector of the signal from reflected wave;
V_c is the CRF of calibrated loading;
$\mathbf{K}_{2T}$ is a matrix of scattering of the double T-bridge;
V(f) is the CRF of loading under measurement;
S(f) is antenna;
$V_s(f)$ is the CRF of the flat-layered environment in free space

Detected voltage of the incident and reflected waves are proportional to the power of the signal in the UHF tract U ~ P ~ $|A|^2$. It has been shown the unbalance signal is determined by the relation:

$$D\left(\dot{V},\dot{V}_c(\alpha,\varphi),\dot{k}_0,\dot{k}_1,\dot{k}_2,\dot{k}_3\right)=\frac{U_{ref}}{U_{inc}}=\left|\dot{k}_0+\dot{k}_1\cdot\frac{V-V_c}{(1-\dot{k}_3\cdot V)\cdot(1-\dot{k}_3\cdot V_c)-\dot{k}_2\cdot V\cdot V_c}\right|^2, \quad (1)$$

where $k_0(f)$,.. $k_3(f)$ are complex factors, that depend on the geometry of the 2T-joint and frequency. They describe properties of interferometer and can be determined on the basis of data of natural experiment.

The relation between the measured CRF V(f) and CRF of the flat-layered environment $V_s(f)$ can be written as

$$V=S_1+\frac{S_2V_S}{1-S_3V_S},\ \text{or}\ \ V_S=\frac{S_1-V}{S_1S_3-S_2-S_3V}, \quad (2)$$

where S_1,..,S_3 are complex factors, determined through elements of the antenna scattering matrix. The CRF

of flat-layered environment depends on thickness of layers and electrophysical parameters of materials, it can be written as

$$V_s=V_s(f,h_1,..,h_{M-1},\varepsilon_1,..,\varepsilon_M,\mathrm{tg}\delta_1,...,\mathrm{tg}\delta_M). \quad (3)$$

Parameters of bridge scheme and antenna are determined at the stage of calibration and are known, which has been described in the previous report. So, one can write the generalized model of the output signal of the bridge scheme

$$D_{th}=D_{th}(f, \mathbf{p}), \quad (4)$$

where **p** is vector of unknown (sought) parameters of layered environment, f is a frequency.

In the previous report we have shown that on the basis of the frequency dependence of the CRF of the structure $V_S^{ex}(f_i)$ its parameters have been determined. We shall show below that with the use of scalar signal $D_{ex}(f)$ one can also determine parameters of the structure.

The inversed problem (IP) for testing of environment is to determine the vector of sought parameters of flat-layered environment **p***. We can write the target function by the measured frequency dependence $D_{ex}(f)$ and model of the signal of bridge scheme. The IP is solved by the method of functional minimization

$$\mathbf{p}^* = \inf_{\mathbf{p}\in\mathbf{P}} F_D(\mathbf{p}),\ F_D(\mathbf{p}) = \sum_{i=1}^{N_f} \left| D_{ex}(f_i) - D_{th}(f_i,\mathbf{p}) \right|^2, \quad (5)$$

where N_f is the number of probing frequencies.

Fig. 2 illustrates the shape of measured signal for free space and dielectric plate (plexiglass 10.5 mm).

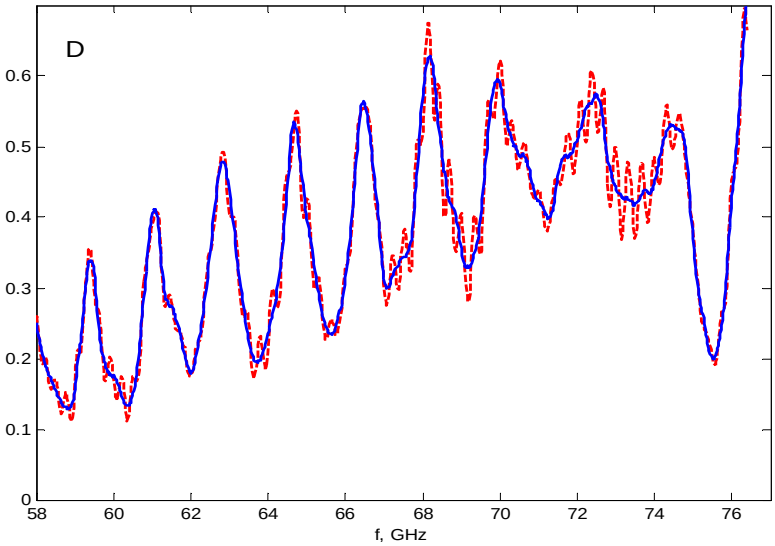

a)

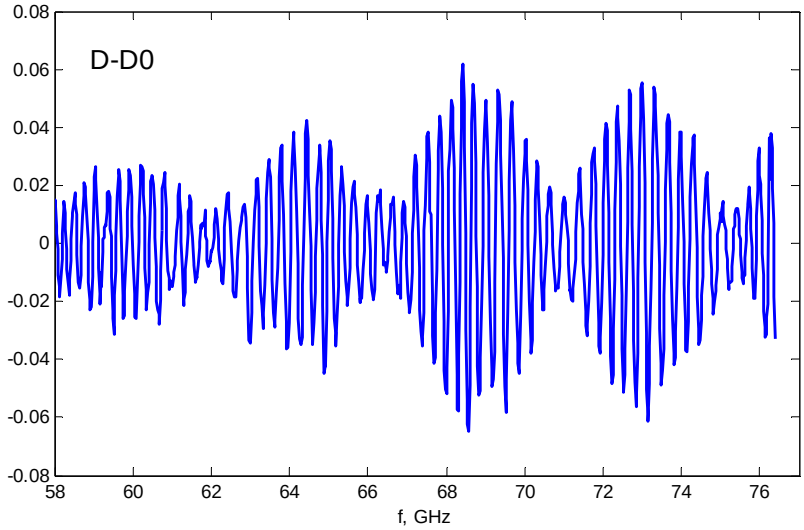

b)

Fig. 2. Output signal from bridge scheme for free space (—) and dielectric plate (- - - -) (a) and difference of these signals (b).

As can be seen from the figure, the signal gas large dynamic range and is rather rapidly changing. This is related to the fact that shoulders of the bridge are loaded to the structures of different length. One can see also that the signal is sensitive to the structure in free space, however it is difficult to analyze it in such a form. Therefore further on we'll consider difference signal $D_{ex}(f)= D_{ex}(f) – D_{ex0}(f)$, where $D_{ex0}(f)$ is the signal for free space (Fig. 2b).

Fig. 3 presents the dependence of the D(f) signal on parameters of layered structure, the solid line shows the signal from the structure without defects – two plexiglass plates without the air gap, the dashed line is a signal for "flawed" structure, the air gap between plates is about 0.25 mm. As can be seen from the figure, the signal is sensitive to changes of structure parameters.

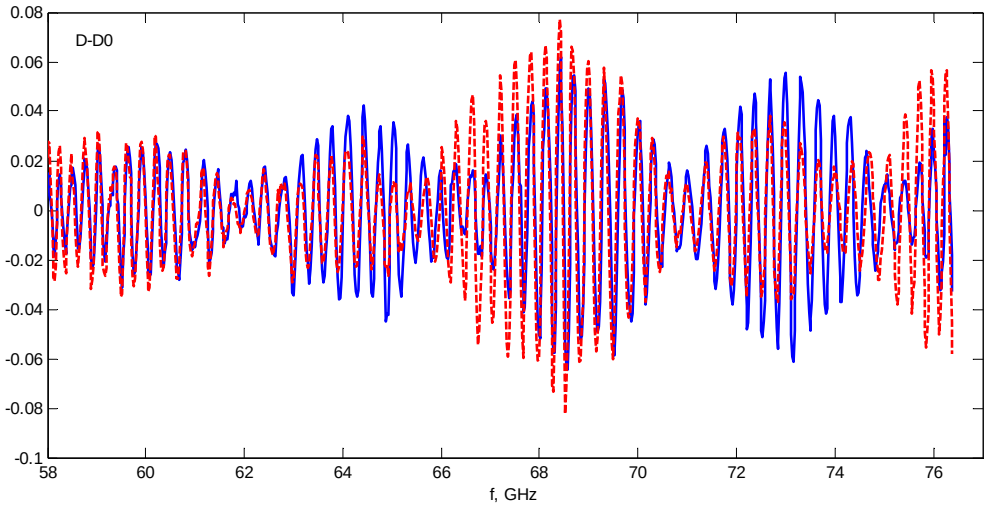

Fig. 3. Sensitivity of the D signal to the availability of air gap between two dielectric plates 10.5 mm: (——) without air gap, (- - - -) gap 0.25 mm.

Let consider now the result of modeling. Fig. 4 presents the measured and modeled signals D(f) for dielectric plate made of plexiglass. Dependence is provided in larger scale of frequency.

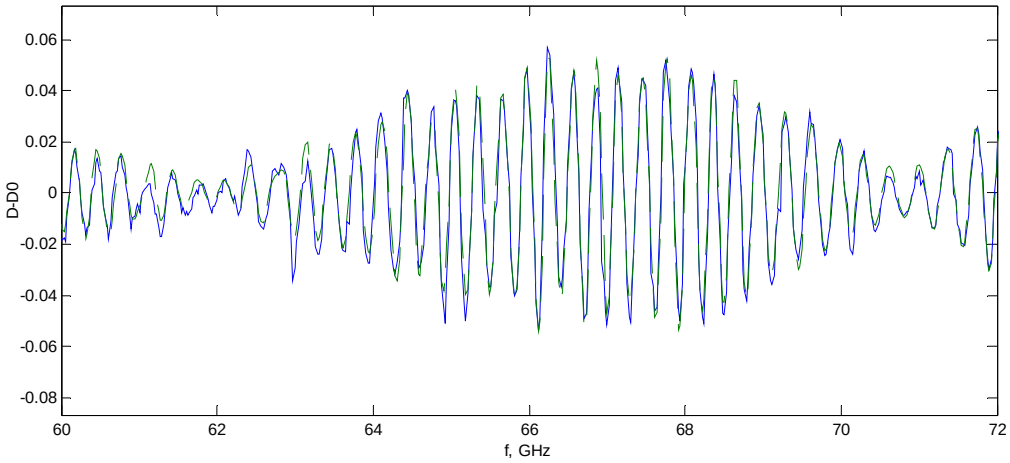

Fig. 4. The D(f)–D_0(f) signal for dielectric plate; (——) experiment, (- - -) numeric model.

In order to compare results of the solution of the IP let consider the same model structure, as they were in the previous chapter, namely plexiglass dielectric plate and two plates with air gap.

In order to determine parameters of the material (plexiglass) the CRF of one plate has been measured. Proceeding from the solution of IP we have determined the following structure parameters: plate position h_1*=–0.358 mm, thickness h_2*=10.461 mm, and electrophysical parameters ε_2*=2,624, $tg\delta_2$*=6,71×10^{-3}The thickness of the plate was controlled as well with the help of micrometer. In the measurement point in is h_2=10,46 ±0,005 mm.

Dielectric plate with an air gap was described by the model of 4-layer environment: air layer between zero plane and dielectric of h_1 thickness; the second and the fourth layers of dielectric with parameters h_2, h_4, $\varepsilon_2=\varepsilon_4$, $tg\delta_2=tg\delta_4$ and the third air layer – gap h_3.

The inverse problem of probing of air gap in plate was solved in the following statement. Let consider parameters of material (plexiglass) and gap (air) to be preset. On the basis of measured frequency dependences of CRF we were to determine positions and thicknesses of all layers of structure, i.e. the vector of the sought parameters **p***=(h_1, h_2, h_3, h_4).

Table 1 presents results of the solution of the IP on determination of thickness of individual layers for the plate and for two plates with an air gap. For comparison, we provide thicknesses determined from the CRF of structure (F_{Vs}) and by the proposed method from the signal of bridge and target function F_D (5). It can be seen from the table, the IP can be successfully solved on the basis of scalar signal of the bridge D(f). Deviations from solutions of IP by the F_{Vs} are within measurement error.

Table 1. Comparison of IP results obtained by the use of CRF V_s(f) and by output signal D(f)

		1 plate		2 plates with an air gap	
Number of layer	h, mm	F_{Vs} h*, mm	F_D h*, mm	F_{Vs} h*, mm	F_D h*, mm
h_1*, mm		-0.358	-0.373	-0.4852	-0.48516
h_2*, mm	10.46	10.461	10.458	10.464	10.464
h_3*, mm				0.2701	0.27013
h_4*, mm	10.41			10.414	10.414

2. Functional scheme of the device for radio-wave NDT

Let consider the functional scheme of the devise for radio-wave non-destructive testing which is

being developed (see Fig. 5). The device contains the following modules:

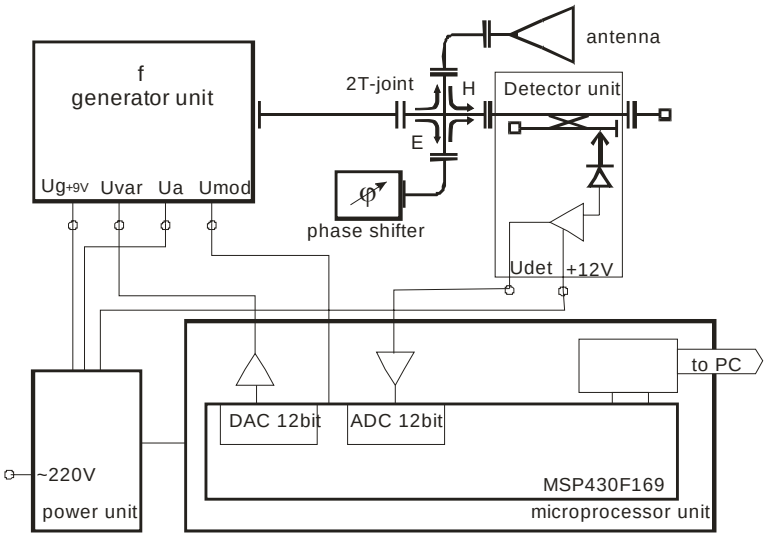

Fig. 5. Functional scheme of the device of radio-wave NDT.

UHF tract in the generator block, bridge scheme, detector block, etalon and calibrated loadings, and measuring-receiving antenna. Generator serves for generation of oscillatory e.m. wave in the 92…99 GHz frequency range. The work of the generator block has been reviewed in details in the previous report.

Block of control and digital processing of information is created on the basis of single-crystal microcontroller MSP430F169. The block includes as well the input cascade for measurement of the signal of detector section; synthesizer of controlled voltage to control the frequency of generator; interface for connection with the PC.

The microcontroller includes as well the programmed ROM for storage of the program codes and working constants, RAM, universal anisochronous receiver-transmitter.

The scheme of digital control over generator frequency is realized on the basis of 12-digit digital-to-analog converter, measurement of analog information is performed by 12-digit ADC, and the input cascade has as well an amplifier with gain constant controlled through the digital-to-analog converter. The appearance of the module is shown in Fig. 6. Principal electric scheme of the module is presented in Fig. 7.

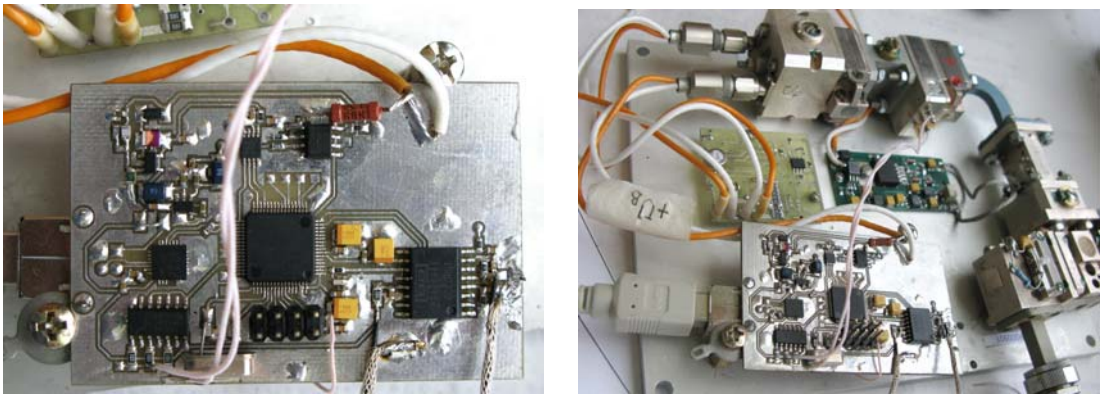

Fig. 6. Block of control and digital processing on the model of the NDT device.

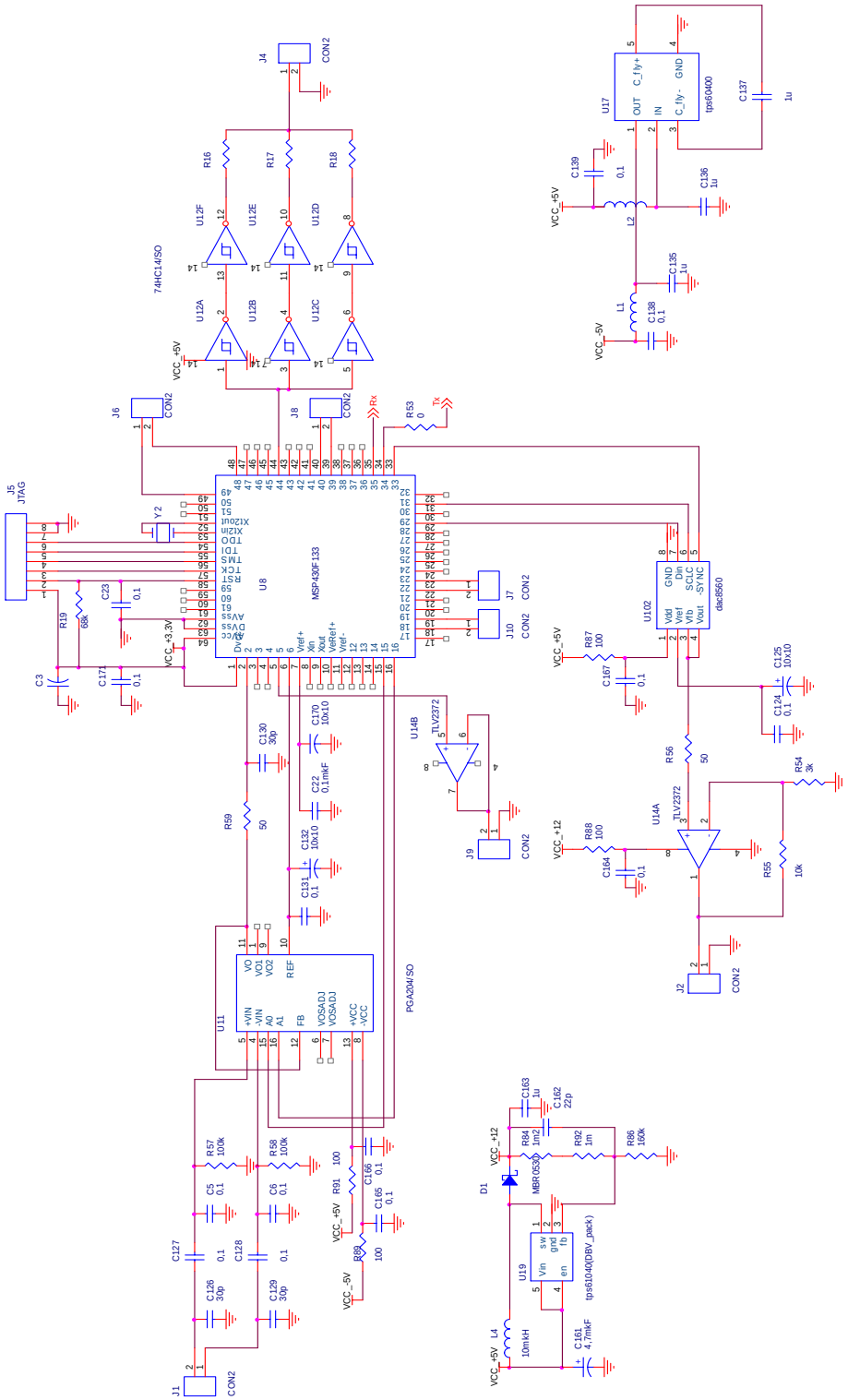

Fig. 7. Principal electric scheme of the block of control and digital processing of information.

The outer feeding block serves to produce feeding voltage, necessary for the work of generator block and block for control and digital processing.

During the reported period the generator block, block of control and digital processing and detector section, as well as the first version of software for microcontroller and programs for data processing on PC have been developed and tested. During the next quarter we plan to finish the elaboration of feeding

block, manufacture calibrated loadings and finalize the development of software for the device.

3. Experimental study of detector block

Detector block is a directed coupler on crossed wave-conductors, the main channel of which is loaded on the non-reflecting (coordinated) loading, in the side channel there is detector section based on diode with Schottky barrier. Directed coupler and coordinated loading serve to coordinate output channel of the bridge scheme with detector block for avoiding the reflected wave in the bridge scheme.

Detecting diode is positioned in the section of waveguide video bandwidth with 1.2×2.4 mm cross-section, in the body of detector section there is as well the amplifier of video signal, fed by +12 V voltage. Detector section serves to detect UHF signals in the 90…120 GHz range both constant and amplitude-modulated, frequency band of amplification of the detected signal is 0.03…300 kHz. Fig. 8 presents the appearance of detector section and detector block assembled. Fig. 9 illustrates the principal electric scheme of detector section.

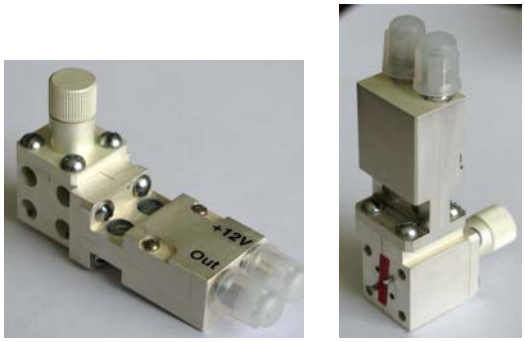

Fig. 8. The assembled detector block.

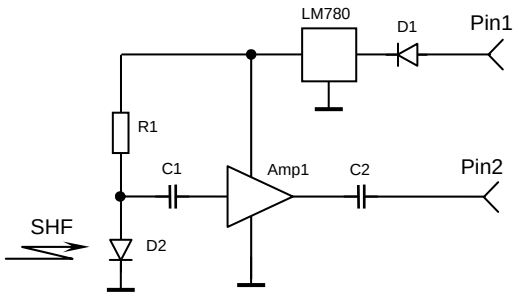

Fig. 9. Principal scheme of the UHF detector: D2 is Schottky diode, Amp1 is operational amplifier OP27, Pin2 is CP50-751 connector

Main technical characteristics of the detector section:

Range of working frequencies, GHz 78 … 100
Transformation coefficient, V/W > 10 000
Video bandwidth, Hz $1 – 1 \cdot 10^3$
Feeding voltage, V 12 … 15
Weight, g, not more than 60
Temperature of environment, °C from 0 to +50
Relative humidity at 25 °C, % 80 max.

Complex testing of detector section have been performed. Fig. 10 shows it frequency and dynamic characteristics. Dynamic characteristic is monotonous and close to the linear one. Frequency dependence of transformation factor should be taken into account during processing of the measured signal.

Fig. 11 shows frequency dependence of elements of scattering matrix of the directed coupler. It can be seen from the coefficient of transmission from input arm to detector section S31 is lower than -15 dB, and cross coupling is lower than –25 dB in the whole frequency range

Let now consider parameters of the ready-assembled detector block. The main requirements to detector block are sufficient sensitivity of detector and amplifier, as well as maximum reflection factor to damp down the reflected wave in the bridge scheme. Fig. 12 illustrates frequency dependence of transformation coefficient of the detector block. It has certain heterogeneity in frequency because of interaction of incident and reflected waves of the main and branched-off channels. In Fig. 13 we can see the reflection factor S_{11} and coefficient of standing wave (VSWR) of detector block. In the whole frequency range it is smaller than –20 dB, and has substantial heterogeneity in frequency. This can be attributed to superposition of waves reflected from the detector and from coordinated loading in the main channel of directed coupler.

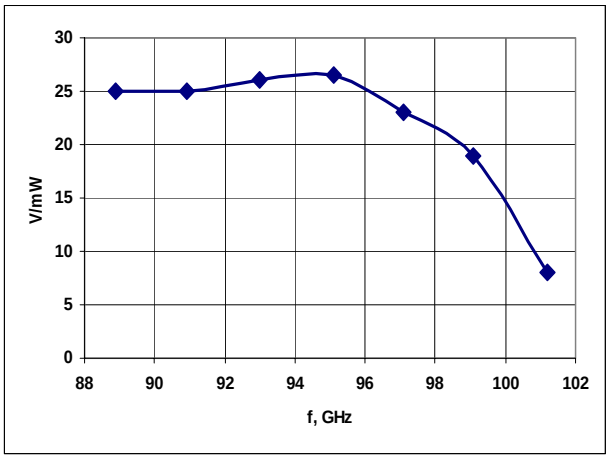

Fig. 10a. Frequency characteristics of detector section, P_{in}=10 W power.

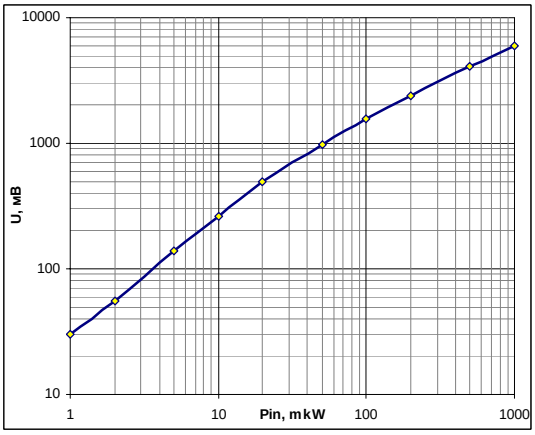

Fig. 10b. Dependence of output voltage on the incident power of UHF field at 95 GHz frequency.

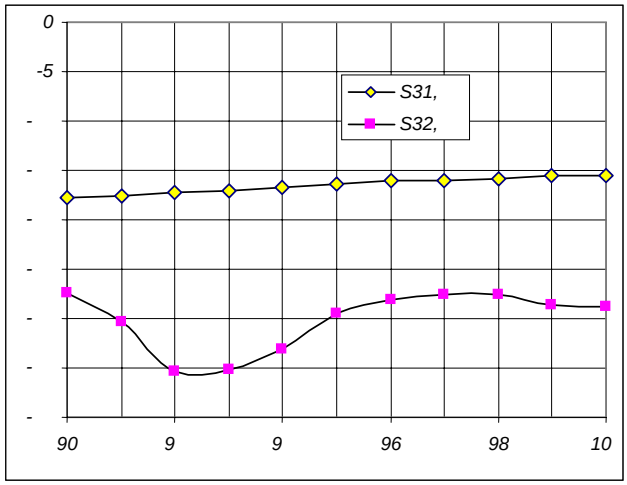

f, GHz

Fig. 11. Coefficient of transmission and cross coupling of channels of directed coupler.

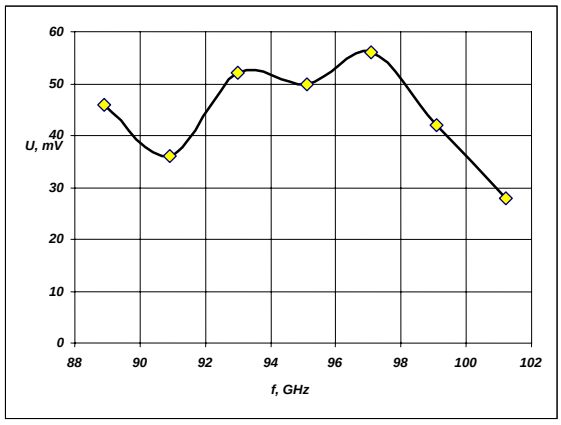

Fig. 12. Frequency dependence of the output voltage of detector block at the input power of Pin=100 W.

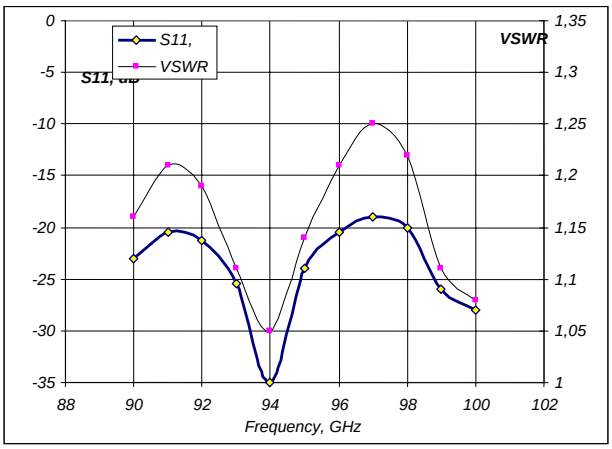

Fig. 13. Frequency dependence of the reflection factor and the factor of standing wave of the detector block.

The output voltage does not have noticeable valleys in the working range of frequencies, and the

signal reflected from detector block will extinct not less than in 100 times in comparison with the incident one. Let draw a conclusion that the detector block is manufactured at high quality and can be used to detect the output signal of the bridge scheme.

4. Development of software for controlling module of digital processing of information and programs for exchange with PC

Software for single-crystal microcontroller is the background-prompt system, which fulfills the following tasks:

1. Connection with PC, receiving constants for the work of the system. Work regimes for detector diode, starting and ending frequency and the scanning step, time of delay and time of data collection during scanning are programmed from the PC. Constants can be stored in the nonvolatile random-access memory and loaded when power supply is switched on.

2. Adjustment of generator frequency according to the measurement program.

3. Measurement of signal from quadratic detector proportional to the power of the UHF field in detector section, control of variable amplification coefficient of the input cascade, digital demodulation of the measured signal.

4. Data transmission to the PC for further processing.

Microcontroller manufactured by Texas Instruments Incorporated MSP430F169 has embedded 12-digit ADC (workability of 200 000 symbols per second) and digital-to-analog converter. Microcontroller with the help of digital-to-analog converter carries out direct control of the measurement scheme, with the help of ADC conducts measurements (gets signal from primary transformer and makes it demodulation) and transmits the measured data to the PC. The microcontroller is connected to the PC by the USB interface. In the ROM of microcontroller there is software developed under the IAR Systems. The software for the PC is developed in the Delphi 7 shell. For the work with the USB-port from the Delphi 7 shell the additional TXComm component and the driver of the virtual COM-port have been used. The TXComm component provides high-level communication with the microcontroller through the virtual COM-port thanking to built-in realization of protocol of data exchange through the port. In particular, there are realized procedures of opening and closing of the port, writing and reading from it, tracing the status of port, controlling the readiness signal, work with buffer.

Software of the PC contains the following procedures:

StartCommPort – start of work with microcontroller;

StopCommPort – end of work with microcontroller;

SetCommPort(b:byte;D:word) – transfer of the package of data to mictocontroller;

XComm1Data(Sender: TObject; const Received: Cardinal), i

GetData(Received:Word; Var wA1,wA2:Word) – getting data from mictocontroller.

Data exchange protocol from the PC to the microcontroller foresees package transmission of data. Each package from the PC contains three bytes: the first one is the attribute of the command and its number, and the next two are data bytes. To control the measuring scheme from PC the following input parameters are transferred to microcontroller:

1. Starting code of digital-to-analog converter corresponding to the starting frequency of the UHF generator;
2. End code of digital-to-analog converter corresponding to the end frequency of the UHF generator;
3. Change step of the code of digital-to-analog converter corresponding to the step of changes of UHF generator frequency;
4. Time of measurement at each frequency point, its value corresponds to the number of obtained observation for demodulation of the signal from the UHF tract at each frequency point;
5. Amplification factor of the modulated signal before analog-to-digital conversion. Codes 0 to 3 correspond to amplification in 1, 10, 100, 1000 times, respectively.

After receiving input parameters the microcontroller starts working with ADC, digital-to-analog converter and amplifier. Codes corresponding to the frequency of the UHF signal are passed by turns to the

digital-to-analog converter. During measurement time for each frequency point the ADC performs certain number of transformations by groups of 16. Microcontroller carries out summing of each group and operates with them as with individual observations and calculates results of demodulation and initiates their transfer to the PC.

Measurement results are passed by microcontroller in the form of a sequence of four bytes. Two high-order bits correspond to the number of bytes; six low-order bits contain six bits of measurement results.

Algorithm of data exchange between PC and microcontroller

1. Opening of port, in the case if it's impossible, the error message.
2. Signal of readiness to receive data (DTR) with a tag brClear (unreadiness).
3. Cleaning of output buffer of the port.
4. Transmission of scanning parameters to microcontroller, they consist of 7 packages of 3-byte length (3 variable of the Byte type). The first byte corresponds to the name of parameter, two the next two bytes contain its value, composed from 16-digit number of the Word type.

The starting code of the digital-to-analog converter, ending code of digital-to-analog converter and a step of code change of digital-to-analog converter, delay time for collecting measurement result and amplification factor are set by 16-digit numbers. The available values of amplification factor are 1, 10, 100, and 1000.

Correspondence of the value of the first byte and the name of the parameter:

3 –starting code of digital-to-analog converter (two bytes);
4 – end code of digital-to-analog converter (two bytes);
5 – changing step of digital-to-analog converter code (two bytes);
6 – time of delay for storage of measurement result (two bytes);
7 – amplification factor (two bytes)

5. Cleaning of input buffer of the port.
6. Delay.
7. Sending the signal of readiness to receive data (DTR) with tag brSet (ready).
8. Waiting for data receiving.
9. Microcontroller receives measured data from 12-digit ADC, results of measurements are 16-digit numbers, each of which is the sum of 16 observations at certain frequency point. To pass results into the port, 4-byte packages are formed (2 bits in each byte correspond to its number) and subsequently passed to the port.
10. PC traces the state of the port and if there are not less than four bytes it chooses 4 bytes and checks there sequence by the control sum.
11. If the control sum mismatches, data are shifted until reaching the needed sequence.
12. Upon matching of control sum from received four bytes, a 16-diit number is formed, which is the result of measurements.
13. Measurements results are transmitted to the video monitor and saved in a file.
14. After finishing of measurement the port is closed.

5. Conclusions

A new method for control of parameters of layered dielectric environment without need of readjustment of phase-twister during measurement and calculation of environment CRF has been proposed. This allows substantially simplify the design of the device, shorten the measurement time and improve work operability of the NDT system. The testing of this method revealed that its accuracy and resolution are not worse than those in the method, based on the determination of CRF.

The works on modernization of the NDT device have been continued. The detector block has been manufactured and tested. The module of control and digital processing of measured information and software for the device to control the generator, measure and detect signal of detector and transfer of information to the PC have been elaborated.

VIII. VERIFICATION OF THE RESULTS OBTAINED

1. Finishing of development of the radio-wave NDT device and software

During the last quarter the design, calibration and testing of the NDT device for flat-layered dielectric structures have been finished. Fig. 1a presents the appearabnce of the device in the body during run of experiment. In the figure there are also power unit, horn aerial, sample holders, cables for connection with power unit and PC.

Fig. 1b presents UHF tract of the device from the bridge circuit side. In the centre of the photo there is a doubled T-bridge, which is joined to the calibrated direct reading phase changer (in the left), and horn aerial (in the right) and detector section of the input shoulder of the bridge (at the top). The doubled T-bridge contains in its body 90° turns of wave-conductors of cross-arms, this allowed що дозволило вивести flanges of wave conductors for attaching reference loads onto the side panel of the device without additional adapters. The detector section is connected to the microprocessor by coaxial screened cables with plug-and-sockets.

Calibrated phase changer (Fig. 2) is designed as a piston, moving along wave-conductor channel under the action of spring-loaded micrometer screw, this allowing control the movement with 0.1 mm precision. Knowing wavelength in the wave-conductor one can find the phase change angle of the reflected wave.

The power unit (PU) for the device has been designed and manufactured (Fig. 1a). It serves for formation of supply voltage for generator and microprocessor blocks and for detector section. The power unit is connected to the device by multiple-core cable with a header. PU is fed from mains system by ~220V AC.

Fig. 4 presents the appearance of the main user interface window during measurements. The user can set frequency range of measurement, number of frequency readings, and data acquisition at each frequency and see real time measurement results of the output signal. There exists the possibility to save calibration curves and output normalized data to the screen. Measurements results are stored in text format for further use and treatment.

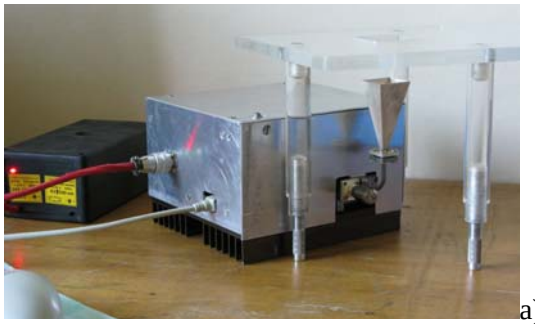

a)

b) 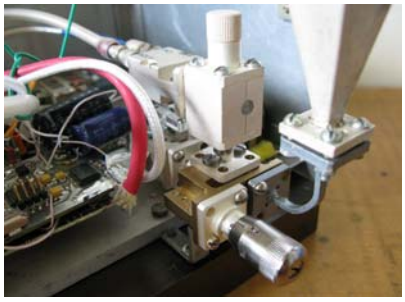

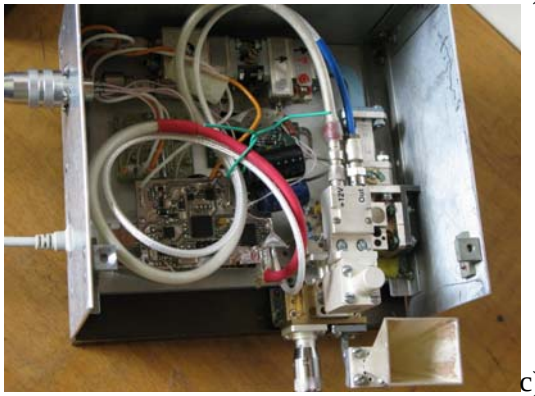

c)

Fig. 1. Appearance of the NDT device for flat-layered dielectric materials:
a) device during the measurement;
b) bridge circuit of the device;
c) appearance of the device without upper cover of the body.

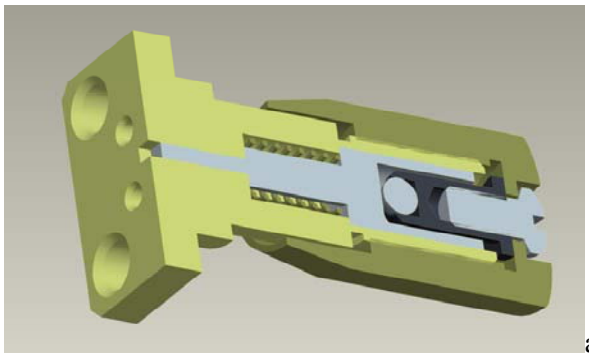
a)
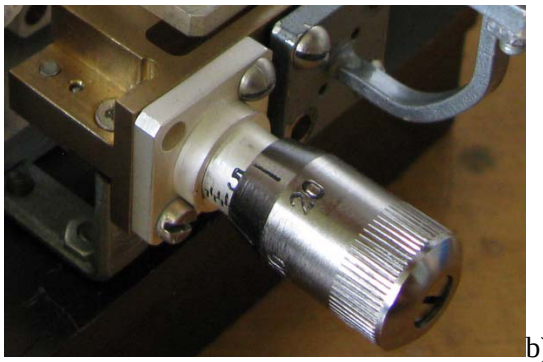
b)

Fig. 2. Direct reading phase changer, cross-section (a) and appearance (b).

Fig. 3 provides the functional scheme of the device.

Table 1. Supply voltage of the NDT device

Supply voltage, V, max current, A	Purpose
9 V, 1.5A	Supply Gunn oscillator
6 V, 1.0A	Supply power amplifier
12 V, 0.5A	Supply detector section
24 V, 0.5A	Supply module for controlling varactor diode voltage

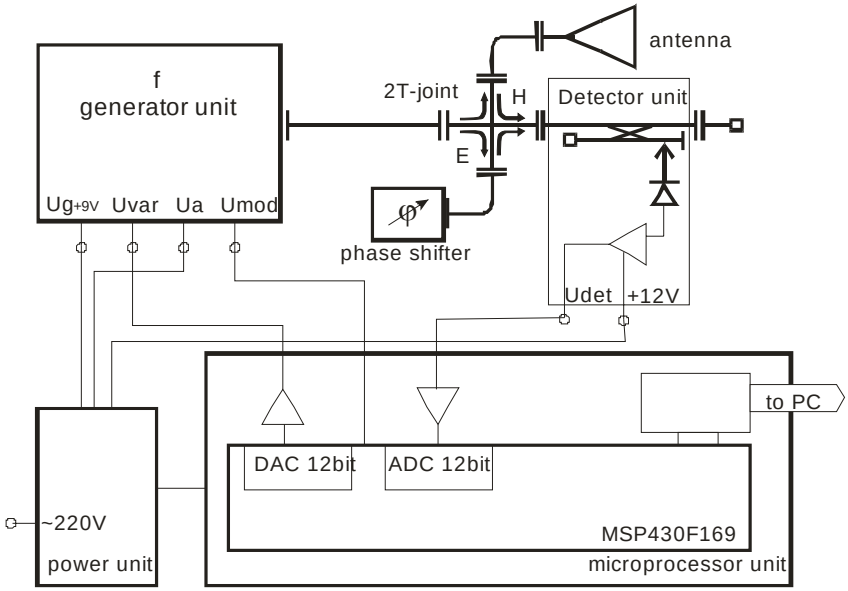

Fig. 3. Functional scheme of the radio-wave NDT device.

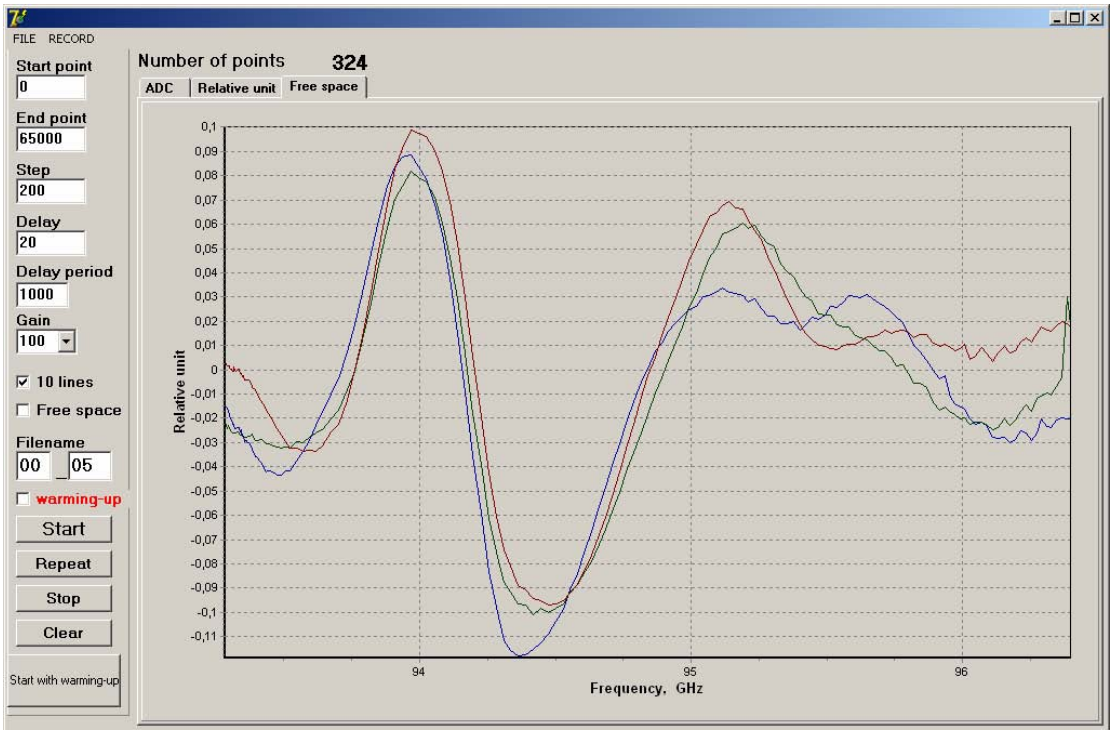

Fig. 4. Work of the device software.

2. Calibration of generator block by frequency and extinction

In order to control the generator frequency the microprocessor block forms a code for 16-digit digital-analogue converter (DAC), the voltage from the DAC is passed to the amplifier with constant coefficient and then – to varactor diode. In order to calibrate the device by frequency the dependence of voltage of varactor diode U_{var} on the control code has been measured with the help of digital voltmeter. Measurement results are presented in Fig. 5. It can be seen from the figure that the voltage on the varactor starting from 1.9 V changes linearly and does not fall below this point due to scheme protection of varactor diode against current overloading. Generation frequency varies in the 93 – 98.5 GHz range nonlinearly because of dependence of generation frequency on controlling voltage U_{var}. Further on we shall consider frequency dependences of measured parameters.

Dynamic and frequency characteristics of generator block and detector section have been stidied. Fig. 6 illustrates frequency dependence of signal of generator, received at the output of detector section after digital demodulation. Detector section is joined to the generator block. As can be seen from the figure, the power if signal strongly depends on frequency and has a maximum in the middle of the range and quickly decays in high frequency range. This occurs because of complex frequency characteristics of generator block, in particular strong frequency dependence of transmission coefficient is revealed by frequency multiplier. As a result the error in measurements in upper frequency sub-range will be increased because of low power of measured signal, which leads to decrease of capacity of ADT and temperature instability of measurements. Frequency point at 97.3 GHz should be omitted from consideration since there characteristics of generator change very quickly and in vicinity of that point there could appear large measurements errors.

Fig. 7 shows dependence of demodulated signal of detector section on power of incident signal. Measurements were conducted in all frequencies of the range with the help of polarisation attenuator. It can be seen from the figure that dynamic characteristics of measuring tract are close to the linear one.

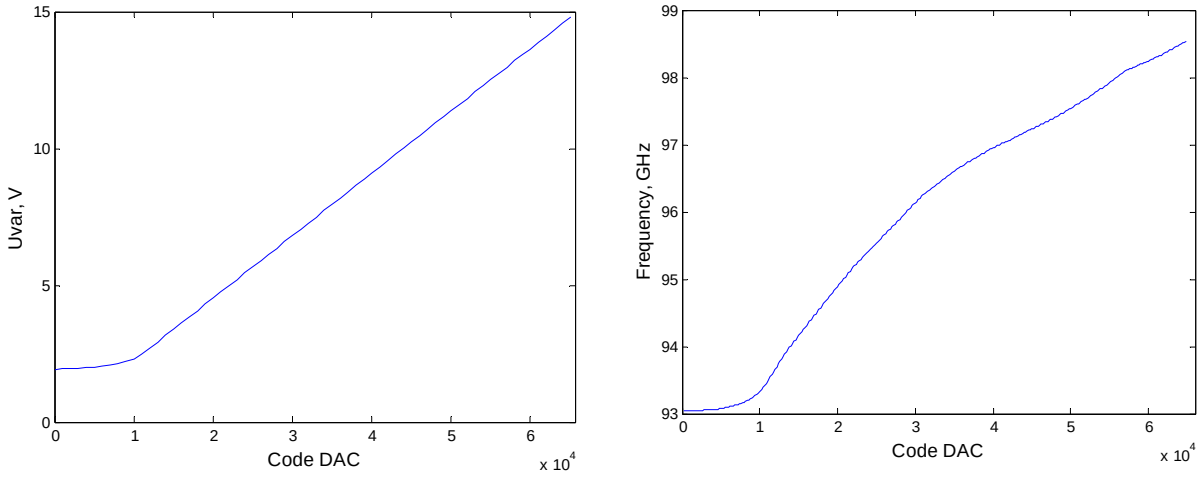

Fig. 5. Calibration of the device by frequency, dependence of voltage on varactor (a) and frequency (б) on the DAT code.

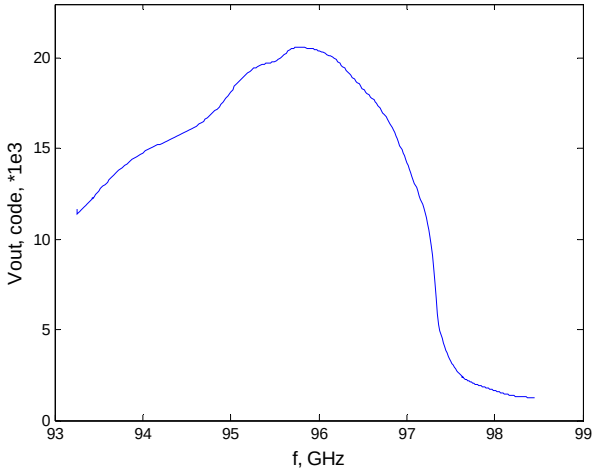

Fig. 6. Dependence of output signal of detector on frequency.

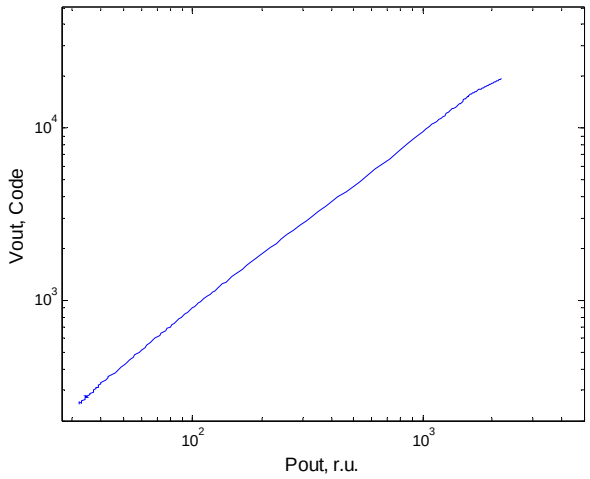

Fig. 7. Dependence of output signal of detector on signal power.

.Further on the measured output signal of bridge circuit we shall note as D and present it in relative units or decibels in dependence on frequency.

3. Calibration of the bridge circuit

In order to calibrate bridge circuit parameters of 2T-bridge should be defined. The scheme of the model is presented in Fig. 8. According to this model the detected output signal of the bridge circuit (un-balance signal) is determined by form:

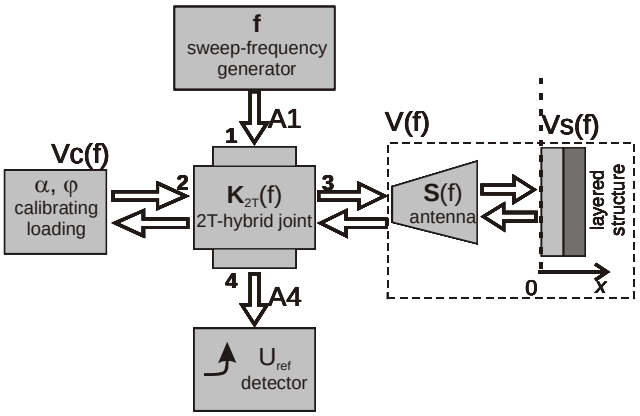

Fig. 8. Schematic model of test bench:
f – generator of oscillating frequency;
U_{ref} – detector of signal of reflected wave;
V_c – CRF of calibrated load;
$\mathbf{K}_{2T}$ – dispersion matrix of the double T-bridge;
V(f) – CRF of load under measurement;
S(f) – aerial;
V_s(f) – CRF of flat-layered environment in free space

$$D(V,V_c,k_0,...,k_3)=\left|k_0+k_1\cdot\frac{V-V_c}{(1-k_3\cdot V)\cdot(1-k_3\cdot V_c)-k_2\cdot V\cdot V_c}\right|^2, \quad (1)$$

where k_0(f),.. k_3(f) are complex coefficient dependent on geometry of 2T-bridge and frequency. They describe properties of interferometer and can be determined on the basis of natural experiment results.

Calibration of measuring scheme includes measurement of parameters of bridge circuit k_0(f),.. k_3(f) for all frequencies of the range. To do so, the calibrated phase changes are joined to cross-arms of the bridge and the dependence of signal D on the phase of calibrated load for all frequencies is measured. Value of the phase depende of the choice of reference plane – zero position of the scale of phase changer. The scale position s_{sh} = 0 mm has been chosen as zero plane відліку. Distance between neighbouring position of phase changer was s_{sh} = 0.2 mm. Phase of the CRF of reference load $_{sh}$ was determined through the length of the wave in wave-conductor $_a$ by formula

$$\varphi_{sh}=2\pi\frac{2s_{sh}}{\lambda_a}+\ _0, \text{ [rad]}. \quad (2)$$

where s_{sh} is the position of phase changer scale; $_0$ is phase incursion corresponding to zero plane, this parameter is dependent on frequency and is determined together with parameters of bridge circuit.

Coefficients of mathematic model of the bridge are determined by the following objective function

$$F_1(\dot{k}_0,..,\dot{k}_3)=\sum_{i=1}^{N_\varphi}\left(D_i-D(\dot{V}_{et},\dot{V}_c(\alpha_i,\varphi_i),\dot{k}_0,...,\dot{k}_3)\right)^2, \quad (3)$$

where D_i are measured values of unbalance signal of the set of calibrated loads V_c(,) and known reference load V_{et}; N is the number of fixed position of the phase of calibrated load. Optimum values of model coefficients are determined by the minimum of the objective function:

$$(\dot{k}_0,...,\dot{k}_3)^*=\inf_{|k_0|<1}F_1(\dot{k}_0,...,\dot{k}_3). \quad (4)$$

Fig. 9 shows experimental dependences of unbalance signal for different position of the calibrated phase changer. Number of the curve corresponds to the piston shift by 0.2 mm. These dependences were used for identification of parameters of bridge circuit. Fig. 10 provides frequency dependences for complex parameters of the bridge circuit k_0(f),.. k_3(f) and for zero phase.

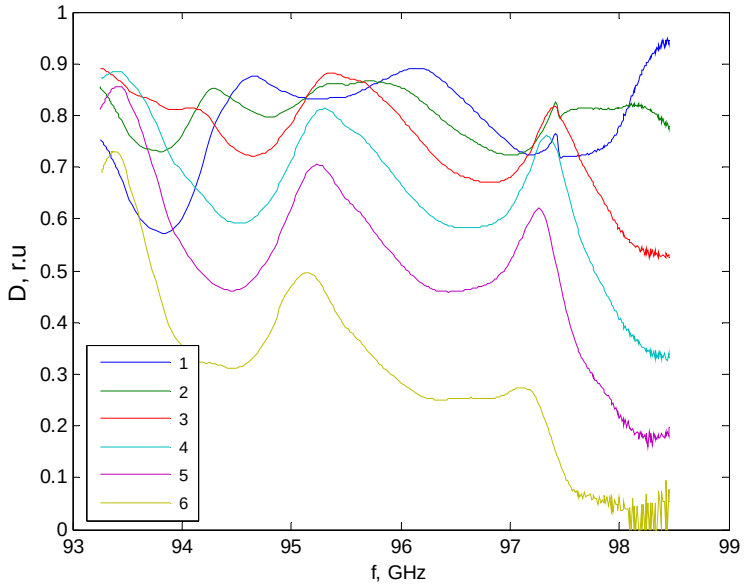

Fig. 9. Frequency dependence of unbalance signal for different positions of phase changer. Number of curve corresponds to the piston shift by 0.2 mm.

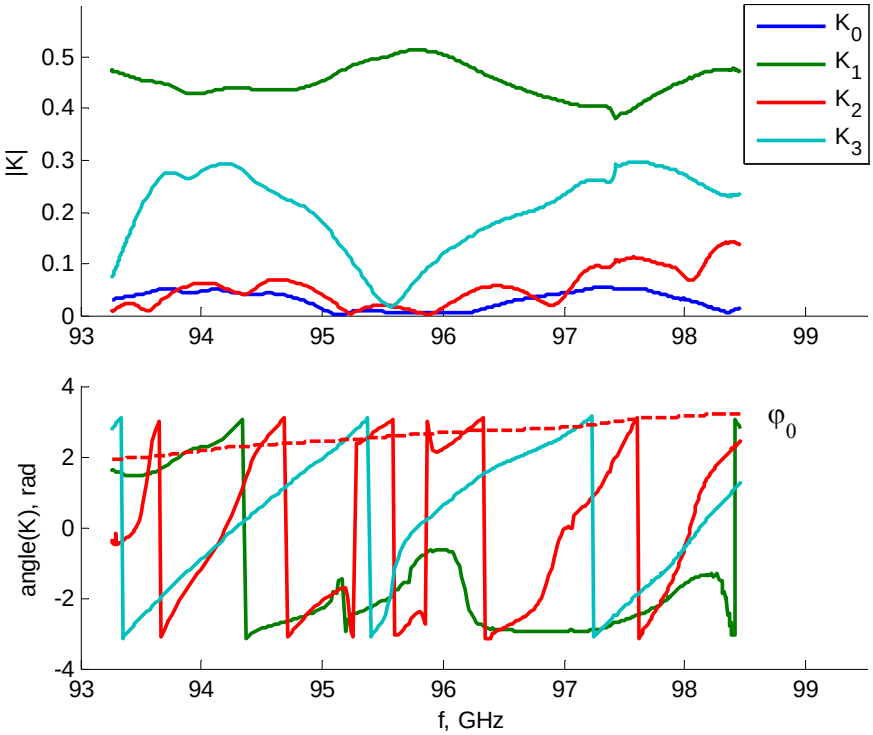

Fig. 10. Frequency dependences of complex coefficients of the bridge circuit model k_i and position of zero phase $_0$.

CRF of unknown load is determined on the basis of frequency dependences of signal D at different positions of calibrated load V_c:

$$V^* = \inf_{|V|<1} F_2(V), \quad \text{where } F_2(V) = \sum_i \left(D_i - D\left(V, V_c(\alpha, \varphi_i), k_0, .., k_3\right)\right)^2. \tag{5}$$

Fig. 11 shows CRF of reference load under different positions of piston, determined by formula (2)

with the use of obtained values of model parameters. It can be seen from the figure that module of CRF is close to 1, phase changes linearly with frequency and corresponds to theoretical phase incursion by formula (2).

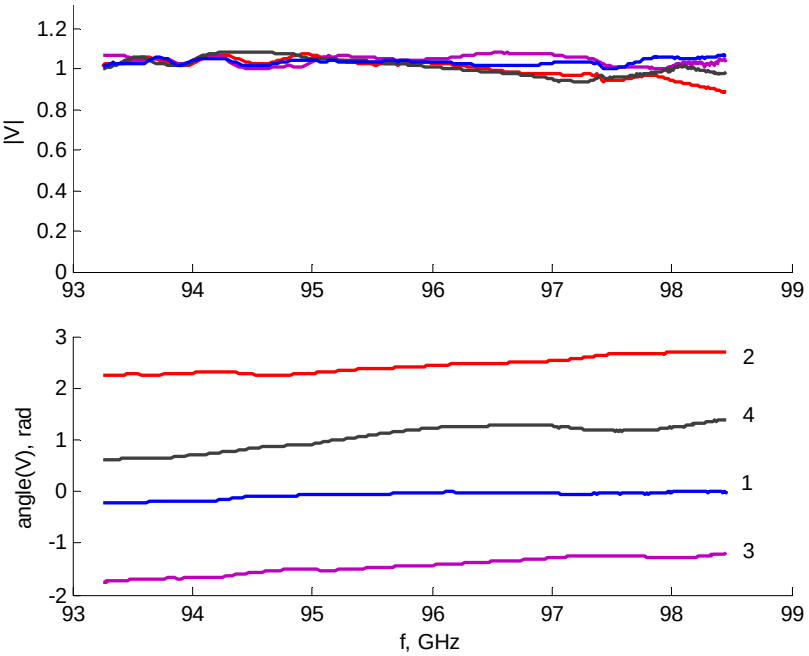

Fig. 11. Measured CRF of reference direct reading phase changer. Number of the curve corresponds to the piston shift by 0.8 mm.

4. Measurement of CRF of loads in free space. Determination of parameters for the model of emitter-receiver aerial

Let now address to measurements of structures in free space. We have joined a pyramidal horn aerial to the lateral shoulder of the bridge through a wave-conducting adapter with 90° turn (see Fig. 1a). Aerial parameters are the following: length from orifice to aperture is 42 mm, aperture 25×30 mm. samples for measurements were placed on the special table.

The CRF of aerial has been measured when it was loaded to free space and metal screen, placed at different distances from aperture. (see Fig. 12).

Relation between measured CRF V(f) and CRF of flat-layered environment V_s(f) can be written as

$$V = S_1 + \frac{S_2 V_S}{1 - S_3 V_S}, \text{ or } V_S = \frac{S_1 - V}{S_1 S_3 - S_2 - S_3 V}, \tag{6}$$

where S_1,..,S_3 are complex coefficients, determined through elements of aerial dispersion matrix and cam be determined experimentally.

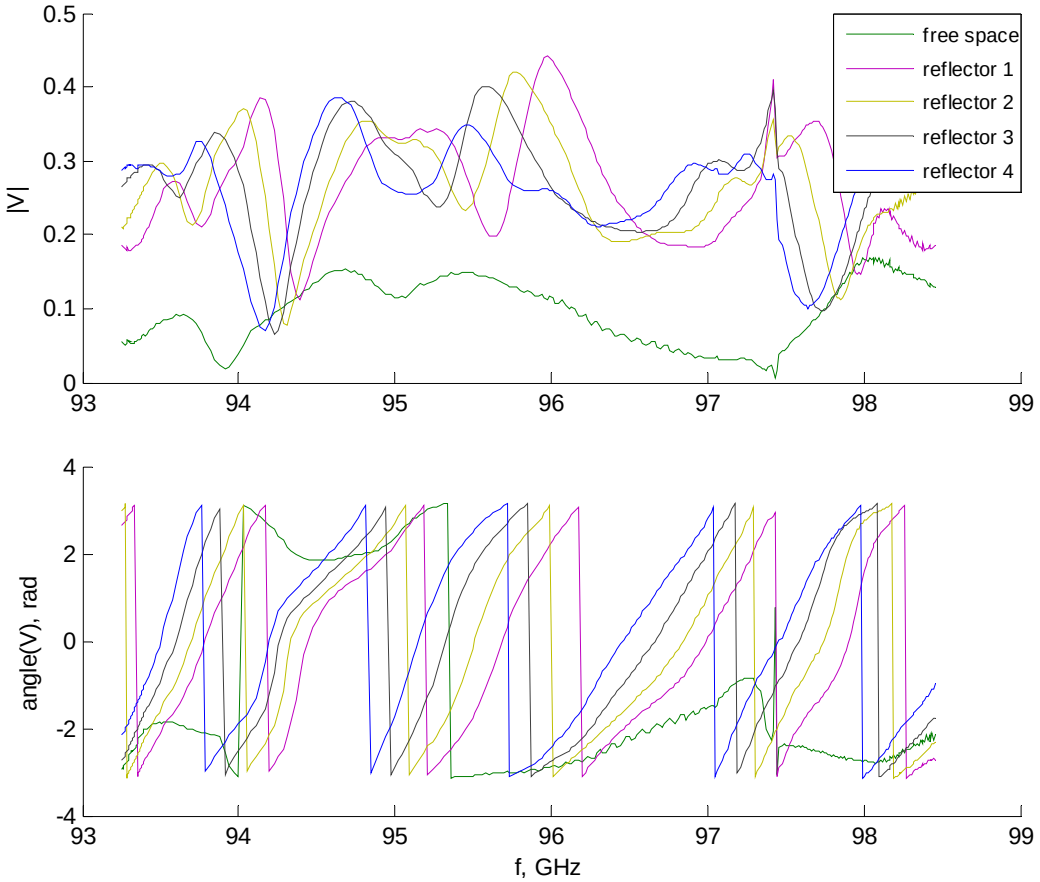

Fig. 12. CRF of aerial with free space and a the screen. Number of the screen corresponds to a shift of metal sheet by 0.2 mm along the aerial axis.

In order to determine parameters of the aerial a flat metal screen has been used as a reference load in free space $V_{set}(f, x)$. Its position was changed in the range x=0…20 mm from zero plane with a x=0,2 mm step. Distance from aerial aperture to zero plane was 35 mm.

It has been assumed for metal screen that

$$|V_{set\ th}| = 1,\ \arg(V_{set\ th}) = 2 \cdot 2\pi x/\lambda_0 + \quad , \tag{7}$$

where x is position of the screen in relation to zero plane, $_0$ is length of electromagnetic wave in vacuum.

Complex coefficients $S_1(f),..,S_3(f)$ for each frequency can be determined using the experimentally measured values of $V_{et}(f, x)$ and theoretical CRF values of reference load $V_{set\ th}(f, x)$.

$$(S_1, S_2, S_3)^* = \inf_{|S_i|<1} F_3(S_1, S_2, S_3), \quad F_3(S_1, S_2, S_3) = \sum_{i=0}^{Nx} \left| V_{et}(x_i) - V(S_1, S_2, S_3, V_{set\ th}(x_i)) \right|^2 \tag{8}$$

where x_i=i x. Figs. 13 and 14 present frequency dependences for $S_1(f),..,S_3(f)$ coefficients of the aerial model and CRF of reference load recalculated for free space according to the $V_s(f)$ model of aerial (6).

Let study sensitivity of measured signal to parameters of layered structure.. Let carry out measurement of signal D for two dielectric plates made of plexiglass with 10.5 mm thickness, between which there was formed a slit of 0 to 0.6 mm thickness. Such a structure models foliation in dielectric material. Fig. 15 shows dependence of difference signal D – D_{fs} (where D_{fs} is a signal for free space) on frequency for different values of slit between plates. It can be seen from the figure that signal is sensitive to changes in thickness of foliation.

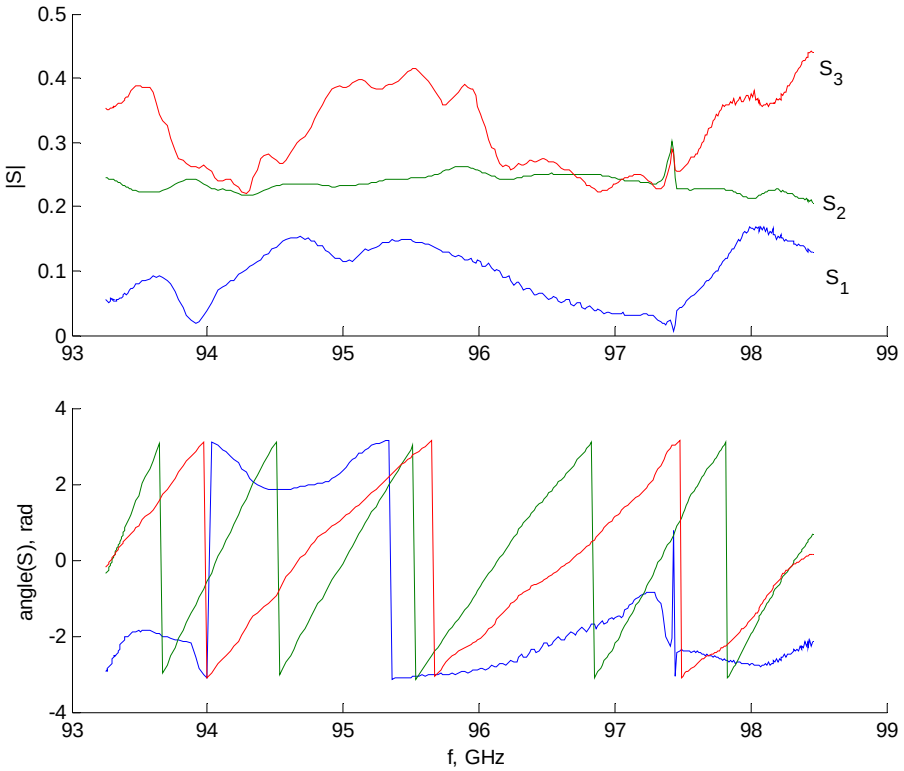

Fig. 13. Frequency dependence of the model of horn aerial.

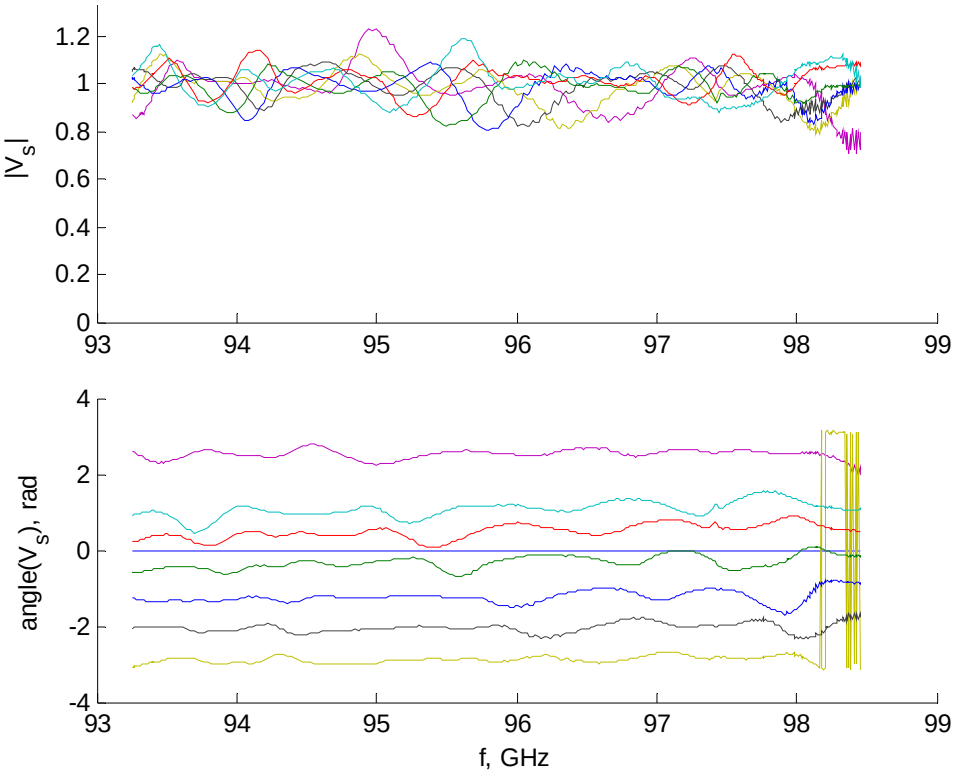

Fig. 14. Measured CRF of metal screen, 0.2 mm shift.

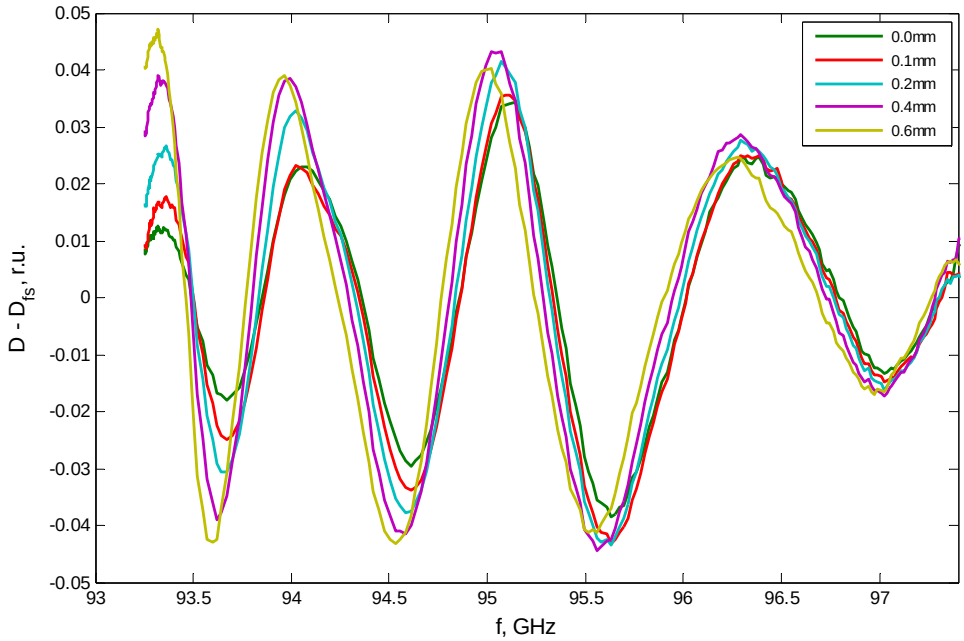

Fig. 15. Frequency dependence of unbalance signal for different thickness of foliation in dielectric plate.

Similarly the experiment for dielectric plate with metal support has been carried out. Slit between dielectric and metal plate models foliation between dielectric layer and metal base. It can be seen from Fig. 16 that the measured signal is sensitive to the thickness of foliation and it can be used for diagnostics of similar structures.

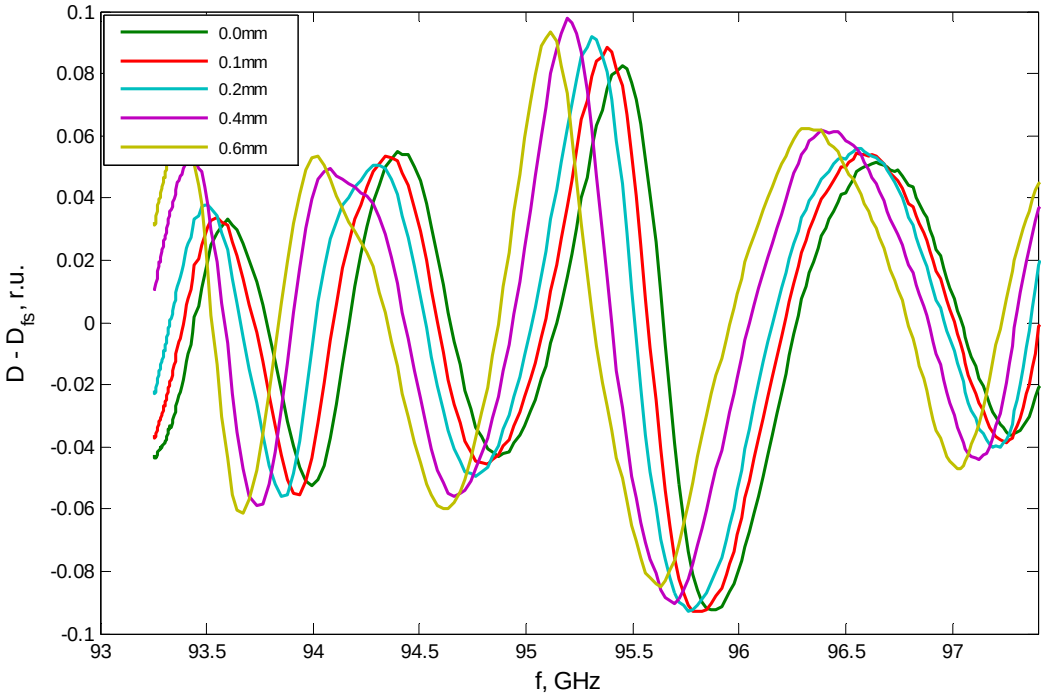

Fig. 16. Frequency dependence of unbalance signal for different thicknesses of foliation between dielectric plate and metal substrate.

5. Technical specifications of the radio-wave NDT device for flat-layered dielectric structures

Frequency range of measurement, GHz	93.2…. 98.5
Power of generator module, mW	8
Frequency of modulations, Hz	1000
Unevenness of generator along the range, dB	12
Transformation coefficient of detector, V/W	> 10 000
Band of video transmission, Hz	$1 – 1•10^3$
Max. number of frequency readings	65000
Error of frequency setting, %	<0.02
Dynamic range of measurement of signal, dB	0… –40
Time for settling the measurement regime, min	20
Output interface	USB
Dimensions (without aerial and PU), mm	150×170×90
Weight (without aerial and PU), kg	1.5
Power supply	~220V, 50W
Environment temperature, °C	from +0 to +50
Relative dampness at 25°C, %	80 max.

6. Conclusions

The designing of the radio-wave NDT device for dielectric structures has been finished. The calibration of the device by frequency and extinction has been performed. The parameters of the models of bridge circuit and aerial for measuring the CRF of structures. The models are shown to describe adequately the probing process of tested structures. The dependence of measuring signal on foliation parameters of dielectric structures.

Frequency range, sensitivity, measurement precision, models of measuring system and interaction of probing field with dielectric flat-layered environment, as well as methods for solution of inverse problems would allow solving a wide range of practical problems of non-destructive testing.